A STUDY OF TOOL WEAR IN TURNING OF PURE ALUMINUM AND DRILLING OF CFRP/TI STACKS

By

Xin Wang

A DISSERTATION

Submitted to
Michigan State University
in partial fulfillment of the requirements
for the degree of

DOCTOR OF PHILOSOPHY

Mechanical Engineering

2012

ABSTRACT

A STUDY OF TOOL WEAR IN TURNING OF PURE ALUMINUM AND DRILLING OF CFRP/TI STACKS

By

Xin Wang

Tool wear in turning of pure aluminum and drilling of carbon fiber reinforced plastics (CFRP)/titanium (Ti) stacks was investigated due to their importance in modern manufacturing. Although pure aluminum is a ductile metal while CFRP contains brittle carbon fibers, there exist also few important similarities which impact tool wear. For instance, neither work material contains inclusions harder than the tool material. Thus, in both cases, the abrasive wear mechanism, which comes from the hard inclusion abrading the tool surface, cannot explain the tool wear. Thus, selecting a tool material solely based on higher hardness does not always provide a longer tool life. This study presents a new explanation for tool wear with these work materials based on our experiments.

Fine and coarse grain tungsten carbide-cobalt tools were used for turning commercially pure aluminum. Two types of tool wear were observed on both grades of tools. The first type of wear was due to carbide grain pullout from the surface by adhesion. The abrasion by the pull-out grains was the second type of wear observed. Larger flank wear was observed on the fine grain carbide than the coarse grain carbide despite the higher hardness of the fine grain carbide. The increase in tool wear was explained by the higher probability of a finer carbide grain being pulled out of the matrix compared to a coarser carbide grain.

The evolution of Built up edge (BUE) in aluminum turning was studied. It was shown that the BUE decreased after the cobalt binder on the surface of the tool was removed by wear.

The influence of oxidation in the formation of BUE is also discussed.

In the CFRP/Ti stack drilling study, three types of experiments were carried out: CFRP-only drilling, titanium-only drilling and combined CFRP/Ti stack drilling. The tool wear were investigated on uncoated WC-Co drills, diamond coated drills, $AlMgB_{14}$ (BAM) coated drills and nano-composite coated drills. There were two significant findings in the CFRP-only drilling study. First, edge rounding was found to be the main tool wear mode for all types of drills. A hypothesis was developed to explain the cause of edge rounding wear in CFRP machining. In metal machining, the wear on the cutting edge is normally prevented by a stagnation zone. However, the fracture-based chip formation in cutting CFRP prevented the formation of a stagnation zone. Rapid wear rounds off the cutting edge. Second, the tool wear measurements in the CFRP drilling experiment did not match the abrasive wear resistance of the drills. Instead, the results from tribo-meter tests correlated well with the tool wear in the CFRP drilling. Therefore, it is believed that tribo-meter testing can be used to rank suitable tool materials for CFRP drilling without carrying out extensive drilling experiments.

In Ti-only drilling, edge chipping and coating flake off were the dominant wear types. The diamond coating, which is effective in drilling CFRP-only, flaked off due to Coefficient of Thermal Expansion (CTE) mismatch and graphitization.

Finally, it was found that CFRP/Ti stack drilling was mainly a combination of the gradual wear in CFRP drilling and the coating flaking off and edge chipping in Ti drilling. Study of the individual work materials provided understanding of the combined wear mechanisms. This allows for future improvement of tools used in the machining of CFRP/Ti stack drilling.

ACKNOWLEDGMENTS

My first debt of gratitude must go to my advisor, Dr. Patrick Kwon. He patiently provided the vision, encouragement and advice necessary for me to proceed through the doctoral program and complete my dissertation. I also wish to thank my committee members, Dr. Liu, Dr. Feeny and Dr. Lai for their support, guidance and availability.

Appreciation for financial assistance and general guidance during the course of my studies goes to Los Alamos National Laboratory and the Boeing Company. A special thanks to Mr. Lars at Franhoufer CCL USA and Dr. Kim at Washington State University for their generousness in making equipment available for use.

I want to thank Dr. Tim, Kyunghee Park, Sun Li and Jorge Olortegui-Yume for their unflagging encouragement and their service as a role model to me as a junior member of academia. A special acknowledgement is due to my co-worker David Schrock for his enlightening advice and help in improving my scientific and writing skills. Furthermore, I am appreciative of my co-workers Trung Nguyen and Wang Mingang for assistance with conducting some of the experiments contained in this work. Thanks also to Sirisak Tooptong and Matt Lempke for stimulating discussion and general support as friends and co-workers.

Most importantly, I wish to thank my parents, Wang Changsong and Wang Weiguang. Their love provided my inspiration and was my driving force. I owe them everything and wish I could show them just how much I love and appreciate them.

Table of Contents

LIST OF FIGURES

LIST OF TABLES

KEY TO ABBREVIATIONS

ALE: Arbitrary Lagrangian Eulerian

BUE: Built up edge

CER: Cutting Edge Rounding

CFRP: Carbon Fiber Reinforced Plastic

CIM: Computer Integrated Manufacturing

CLSM: Confocal Laser Scanning Microscopy

CTE: Coefficient of Thermal Expansion

EDS or EDX: Energy Dispersive X-ray Spectroscopy

FEM: Finite Element Method

FRP: Fiber Reinforced Plastic

GFRP: Glass Fiber Reinforced Plastic

HSS: High Speed Steel

KFRP: Kelvar Fiber Reinforced Plastic

OECD: Organization for Economic Cooperation and Development

RHS/RHC: Right Hand Spiral, Right Hand Cut

SEM: Scanning Electron Microscopy

TEM: Transmission Electron Microscopy

Ti: Titanium Alloy Ti-6Al-4V

Chapter 1. Introduction

1.1. The motivation to study tool wear

Manufacturing is one of the most important segments of the economy. The cost breakdown of typical machining in the industry is shown in Figure 1-1 [1]. Tool wear contributed significantly not only in the final cost, but also productivity. Selecting a right tool material to achieve a longer tool life increases the productivity and reduces the cost.

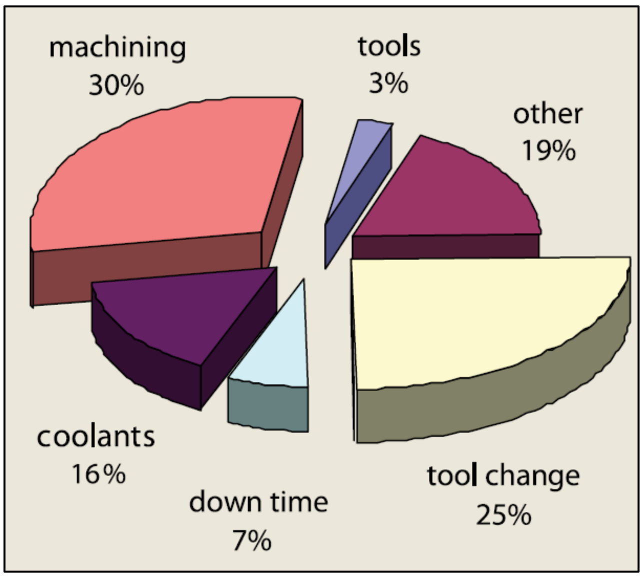

Figure 1-1, Typical end user manufacturing costs [1] (For interpretation of the references to color in this and all other figures, the reader is referred to the electronic version of this dissertation.)

Computer Integrated Manufacturing (CIM), which greatly reduce the labor cost by eliminating the operators [1], are widely used in the industry. However, without an operator, it is hard to know when to change the tool. If a severe worn cutting tool is used in the machining, the final product cannot meet not only the final surface finish but also the required tolerance [2].

Sometimes, to provide the wear information about cutting tool, continuous measurements based on the work piece surface roughness are used. However, the cost and complication associated with continuous measurements limit the use in most cases, and therefore the cutting tool is simply changed at the conventionally predicted tool life. A better understanding of wear mechanisms will allow us more accurately predictions of tool life. This will help the CIMS to achieve higher productivity and lower cost, without a major investment.

Tool wear in machining steel has been studied thoroughly in the past and is relatively well understood [5]. The flank wear on a cutting tool is mainly caused by abrasive wear. It has been shown that the hard cementite (Fe_3C) phase in the steel abrades the cutting tool flank surface [5]. On the other hand, crater wear on the rake surface of the tool is mainly caused by the combination of dissolution wear and abrasive wear mechanisms [4]. The tool material dissolves into the work material and generates a crater on the tool rake surface. The crater wear weakens the cutting edge and can easily lead to chipping.

Coating technology has widely contributed to reduce tool wear in machining. Producing a special coating on the cutting tool substrate has been shown to greatly increase tool life in machining a variety of work materials. The coatings have a wide variety of thermal and mechanical properties, selecting an appropriate coating can reduce the tool wear of different wear mechanisms. The coatings with high hot hardness, such as TiAlN and TiCN, are used to reduce abrasive wear, while the coatings with have good chemical stability and low solubility in the work material, such as Al_2O_3 in steel machining, reduce the diffusion and dissolution wear. In steel machining, the TiAlN and Al_2O_3 multilayer coatings increase substantially the tool life compared with uncoated carbide tools [4].

However, the successful coatings in steel machining have not been successful in machining other work materials, such as titanium, aluminum, and Carbon Fiber Reinforce Plastic (CFRP) [7]. The dominant tool wear mechanisms in machining these materials are not clearly understood. Understanding the wear mechanisms will help in choosing a better coating to reduce the tool wear and achieve better performance, thereby increasing productivity.

Due to the high strength-to-weight ratio and good corrosion resistance, aluminum and its alloys are wildly used in many applications such as automobiles and airplanes. Aluminum and its alloys are not considered to be difficult-to-machine materials. However, in a soft unalloyed state, the ductility of aluminum introduces a significant adhesion problem, in aluminum machining [9].

The carbon fiber reinforced plastic (CFRP) / titanium (Ti) is widely used in aerospace structural applications. At the same time, both CFRP and Ti are difficult to machine materials. In CFRP machining, severe wear caused by the fibers make the tool cutting edge dull [11]. In Ti machining, high cutting temperatures due to the low thermal conductivity of Ti cause severe diffusion and/or dissolution tool wear [7]. The CFRP/Ti stack is a hybrid structure, drilling the composite CFRP/Ti stack in one shot is difficult due to the dissimilar thermo-mechanical properties of the CFRP and Ti, which significantly decrease tool life [12].

In this thesis, tool wear in turning commercially pure aluminum and drilling CFRP/Ti hybrid stack were studied.

1.2. The principle wear mechanisms

Wear is the material removal from the interacting surfaces as a result of mechanical action or combined with other actions [19]. Wear has first been categorized into four separate types, namely adhesive wear, abrasive wear, corrosive wear and fatigue wear in 1969 by the Organization for Economic Cooperation and Development (OECD) [13]. Since then, diffusion wear and dissolution wear were discovered in high temperature applications such as high speed machining [14, 15]. When the researchers analyze practical wear problems, they have to consider each type of wear mechanism separately, and decide which wear mechanisms are operative and which wear mechanism dominate in regards to total tool wear.

1.2.1. Adhesive wear

Adhesive wear is one of the most complicated wear mechanisms. Although the study on this topic has started in the very beginning of 20^{th} century, its fundamental mechanism is still not well understood today. In this section, a very simplified description of adhesive wear will be introduced first, and a review on adhesive wear work will be introduced later.

1.2.1.1. A simplified description of adhesive wear

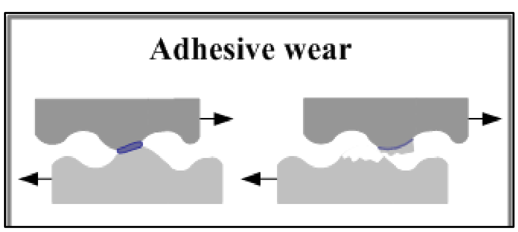

Figure 1-2, The adhesive wear

Two sliding surfaces are in contact with each other at only a small fraction of the apparent area between them [16], as in Figure 1-2. Even if the surfaces are quite smooth, when seen in a highly magnified view, each surface is characterized by microscopic asperities which make contacts with their counterparts. Since the load is transmitted only by those contact points, the stresses involved can be very high, leading to plastic deformation and adhesion. As the two surfaces slide pass each other, the bonding between two asperities fails and leads to the breakage of the bond junctions. The bonding junction is sometimes stronger than either or both of the interacting materials. When this bonding is broken, wear particle is generated and may transfer from one surface to another. Most of the time, the wear particle comes from the weaker (softer) surface. However, the harder surface sometimes wears down, even if it is much harder than the opposing surface. For example, when steel slides on Teflon, the study showed that steel wear particles are found on the Teflon surface [17]. One of the major challenges in studying adhesive wear is to explain why the adhesive wear can never be completely eliminated. This question has never been answered.

1.2.1.2. A literature review of adhesive wear

The first quantitative expression for adhesive wear is the Holm-Archard relationship [18], which is an empirical equation, and is still used in many engineering applications today. The Holm-Archard relationship is shown in equation (1-1)

$$\mathrm{V} = \frac{kLx}{3p} \qquad (1\text{-}1)$$

where V is the wear volume lost, k is the wear coefficient, L is the normal force, x is the sliding distance, and p is the hardness of the softer material.

The normal force (load) and sliding distance are all proportional to the number of the junction breaked in the sliding. Note that the surface asperities will deform to carry the applied load. Hence, the intimate contact area (junction) will inversely proportional to the yield stress, which is proportional to the hardness of the softer material. Therefore, the wear volume is proportional to the normal force and sliding distance but inversely proportional to the hardness of the softer material.

All of the parameters in the Holm-Archard equation can be determined except the wear coefficient k. The wear coefficient k relates the probability of forming a wear particle to the breaking of a junction between two surfaces. It is hard to determine the exact value of the wear coefficient k from the basic material properties of the contacting materials. Some studies collected the values of k applicable to various sliding situations and others made certain appropriate generalizations [18]. For example, it has been found that hexagonal metals with large c/a ratios (like cobalt and rhenium) give very low values of k [20]. However, no research has yet been able to integrate these empirical observations and determine k under specified circumstances.

Rabinowicz [17] divided the adhesive wear by wear coefficient k and wear particle size into three regimes: the severe wear regime, the moderate wear regime, and the burnishing regime. Severe wear occurs when clean or poorly lubricated metal pairs slide over each other. The wear particle size is in the range of 20-200 μm, and the wear coefficient is in the range of 10^{-2}-10^{-4}. Moderate wear occurs when adhesion strength between two surfaces is relatively lower, such as ceramic-ceramic pair. In this case, the wear particle size is in the range 2-20μm, and the wear coefficient is in the range of 10^{-4}-10^{-6}. Finally, the burnishing regime happens when the adhesion strength between two surfaces is extremely low, as in well lubricated or highly incompatible surfaces with low load. In this case, no sizeable wear particles are observed, and the surfaces take on a burnished appearance. The wear coefficients are typically in the range of

10^{-6}-10^{-8}. The adhesion between two solid surfaces will be greatly reduced with air or liquid between them [21]. The well lubricated condition means low adhesion between two surfaces. Thus, severe wear happens in high adhesion, moderate wear happens in normal adhesion and low load, and burnishing wear happens in low adhesion and low load.

1.2.1.3. Sliding Wear

In the study of adhesive wear, many authors found that other mechanisms such as oxidation, delamination and fatigue will also greatly influence the adhesive wear rate at some tribological conditions [21]. Rigney et al. believed the label 'adhesive wear' is inappropriate when referring to the wear generated in sliding between two surfaces [21]. Although adhesive action is involved in wear generated in sliding, it was stated that using the label 'Adhesive wear' may cause research bias in the direction of an adhesion mechanism, neglecting other important mechanisms such as oxidation and fatigue. He preferred to use the term 'sliding wear' to describe wear generated in the sliding process to emphasis other mechanisms which may also influence the wear rate. Therefore, in some papers 'sliding wear' is used instead of 'adhesive wear'.

1.2.2. Abrasive wear

Abrasive wear is understood relatively well today. Abrasive wear occurs when a hard rough surface slides on top of a softer surface [24]. In tool wear, abrasive wear is the removal of tool material by hard abrasive phases in the work material. Cementite (Fe_3C) is one such hard abrasive phase in steel. The abrasive action will scratch and gouge the surface to form and remove wear particles. The abrasive wear usually generates longitudinal groove marks in the direction of relative motion [16].

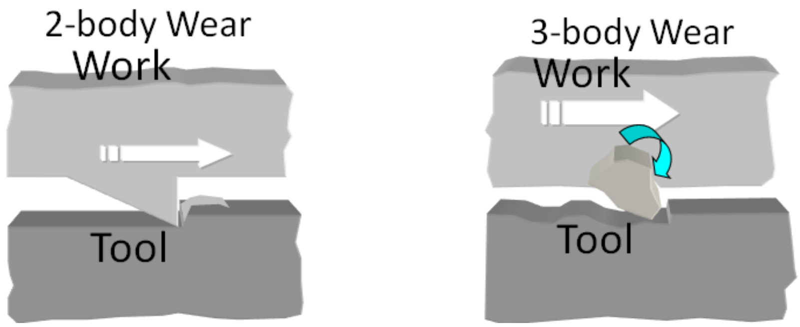

Figure 1-3, The 2-body abrasive wear (a) and 3-body abrasive wear (b)

Depending on the morphology of the abrasive phases, there are two types of abrasive wear: two-body abrasive wear and three-body abrasive wear. As in Figure 1-3 (a), the two-body wear happens with only two interacting bodies involved in the tribological process. In this case the wear of the softer tool material is caused by the harder asperities from work material plowing on surface. The wear volume of two-body abrasive wear can be calculated from Equation (1-2)

$$V = \frac{\tan\theta L x}{\pi p} \qquad (1\text{-}2)$$

where tan θ is the tangent of the average effective roughness angle θ for the hard surface, L is the load, x is the sliding distance, and p is the hardness of the softer material. If the hardness of the asperities is softer than the counter surface, the abrasive wear will be greatly reduced [23].

Three-body abrasive wear is caused by hard particles (grit) trapped between the rubbing surfaces as in Figure 1-3 (b). The particles may be either free or partially embedded into one of the mating materials. The wear volume of the three-body abrasive wear is described in (1-3),

$$V_{3-body} = \frac{xL\tan\theta}{3P_t} \qquad \frac{P_t}{P_a} < 0.8$$

$$V_{3-body} = \frac{xL\tan\theta}{5.3P_t}\left(\frac{P_t}{P_a}\right)^{-2.5} \qquad 0.8 < \frac{P_t}{P_a} < 1.25 \tag{1-3}$$

$$V_{3-body} = \frac{xL\tan\theta}{2.43P_t}\left(\frac{P_t}{P_a}\right)^{-6} \qquad \frac{P_t}{P_a} > 1.25$$

When the hardness ratio between the surface and the trapped particles is higher than 1.25, the three-body abrasive wear will decrease drastically [24].

1.2.3. Diffusion wear

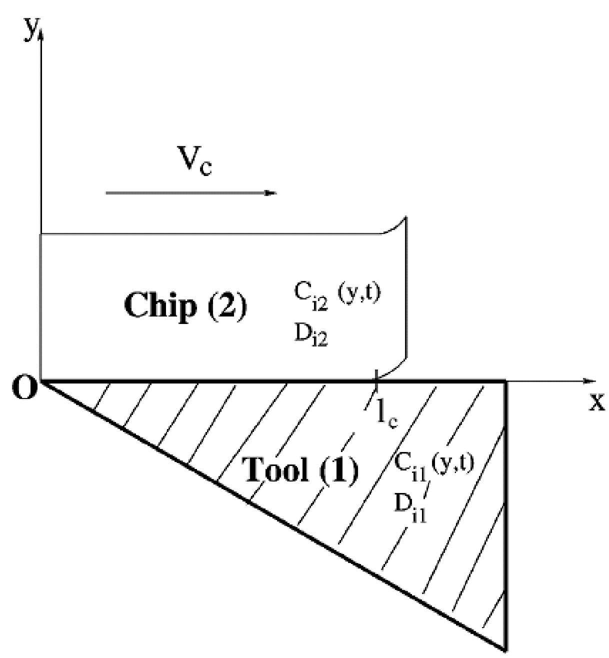

Figure 1-4, Schematic view of the tool-chip contact [25]

Diffusion wear were first reported by Loladze [14], who showed that at conventional cutting speed, tool wear is mainly due to abrasion and adhesion, but at higher speeds is dominated by diffusion processes. Diffusion wear is a process of atomic transfer between two surfaces due to the significant gradients of chemical species and of high temperature in this zone. The Molinari-Nouari model of diffusion wear is shown in Figure 1-4 [25].

Molinari and Nouari [25] assumed that the concentration gradient in the x-direction is small with respect to the gradient in the y-direction in the chip. The effect of material convection due to the sliding of the chip along the tool with velocity V_c is taken into account. It is also assumed that the diffusion process is strongly controlled by the tool–chip interface temperature Θ which depends on x. The basic equations of the diffusion model are,

$$\frac{\partial C_{i1}}{\partial t} = D_{i1} \frac{\partial^2 C_{i1}}{\partial y^2} \qquad (1\text{-}4)$$

By assigning the index 1 to the tool and 2 to the chip, the diffusion equations in the tool and in the chip are given by

$$\frac{\partial C_{i2}}{\partial t} = D_{i2} \frac{\partial^2 C_{i2}}{\partial y^2} - V_c \frac{\partial C_{i2}}{\partial x} \qquad (1\text{-}5)$$

Where t is time, D_{i1} and D_{i2} are the diffusion coefficients of the species i in the tool and chip, respectively. Diffusion is a thermally activated process, with temperature dependence of the diffusion coefficient governed by the Arrhenius' law:

$$D_i = D_{0i} e^{-Q_i/R\theta} \qquad (1\text{-}6)$$

D_{0i} is the frequency factor, Q_i is the activation energy, R is the gas constant and Θ is the absolute temperature. The diffusion wear increases rapidly as temperature increases.

1.2.4. Dissolution wear

In the machining, the high temperature at the interface between the tool and the workpiece may increase the solubility of the tool material in the workpiece. The tool material dissolves into the chip material and form solid solution. Dissolution wear was first been proposed by Kramer [5].

A chemical equilibrium is introduced to interpret the solubility of a tool material within the work piece in equation (1-7).

$$\Delta G_{\text{decomposition of tool}} = \Delta G_{\text{dissolution of tool components into work}} \tag{1-7}$$

The left hand side of the Equation (1-7) is the Gibbs free energy needed to decompose one unit of tool material. The right hand side of the Equation (1-7) is the Gibbs free energy that generated when the decomposed tool material dissolve into the work material. Equation (1-7) should be achieved when the dissolution system reach the equilibrium. The solubility can be derived by

$$C_{A_xB_y} = \exp[-\frac{1}{x}\left(\frac{\Delta G_{A_xB_y} - x\Delta G_A^{Xs} - y\Delta G_B^{Xs} - yRT\ln\frac{y}{x}}{(x+y)RT}\right)] \tag{1-8}$$

where $C_{A_xB_y}$ is the chemical solubility of the coating material in the work piece (mole fraction). $\Delta G_{A_xB_y}$ is the free energy of formation of the coating material. ΔG_A^{Xs} is the relative partial molar excess free energy of solution of component A of the tool material in the work piece material. ΔG_B^{Xs} is the excess free energy of solution of component B. R is the universal gas constant, and the T is the absolute temperature.

This quantitative equation has successfully been used to identify certain nitrides and oxides for their dissolution-wear resistance at high-temperatures in steel machining [4]. However, there have problems when apply this equation to predict the dissolution wear in the titanium machining [7].

1.2.5. Fatigue wear

In materials science, fatigue is the progressive and localized structure damage that occurs when a material is subjected to cyclic loading. In this case, the nominal maximum stress values are less than the ultimate tensile stress limit, and may be below the yield stress limit of the material [16].

Fatigue only occurs if the repeated stress is above a certain threshold, which leads to form crack. Fatigue cracks start at the material surface and spread to the subsurface regions. The cracks may connect to each other, resulting in separation and delamination of the material pieces. The shape of the structure will significantly affect the fatigue life. For example, sharp corners will lead to elevated local stresses where fatigue cracks can initiate.

1.3. The tool wear phenomena in the machining

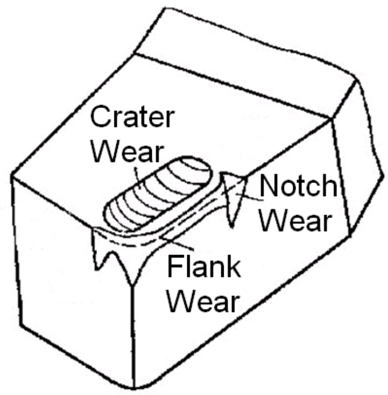

Figure 1-5, The common place of flank wear , crater wear and notch wear in the cutting tool [16]

There are several types of tool wear in machining, Figure 1-5 shows the locations of flank wear, crater wear (rake face wear) and notch wear on the cutting tool [16].

1.3.1. Flank wear

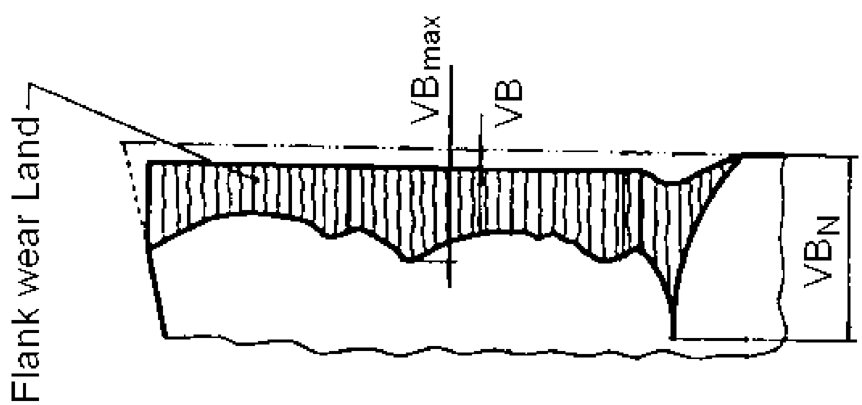

Figure 1-6, Typical flank wear [16]

Wear on the flank (relief) face is called 'flank wear' and results in the formation of a wear land. As in Figure 1-6, the wear land formation is not always uniform along cutting edges of the tool. Flank wear most commonly results from the abrasion on the cutting edge against the machined surface [16]. Flank wear of cutting tools is often selected as the tool life criterion. Flank wear can be measured by using the average or maximum wear land size, defined as VB and VB_{max}.

1.3.2. Crater wear

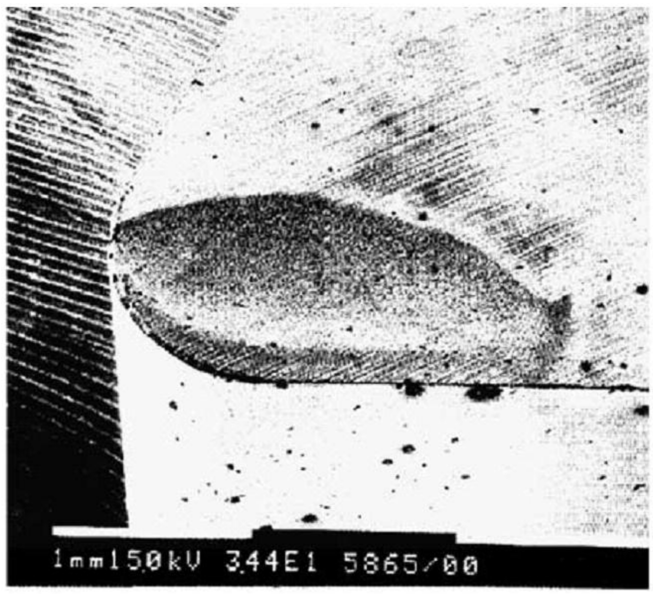

Figure 1-7, Crater wear [26]

The crater wear happened on the rake surface of the tool near the cutting edge, as in Figure 1-7. It will weaken the cutting edge. The crater depth K_T is the most commonly used parameter in quantifying the crater wear. The crater wear is believed to be caused by diffusion and/or dissolution wear at high cutting speed [16].

1.3.3. Notch wear

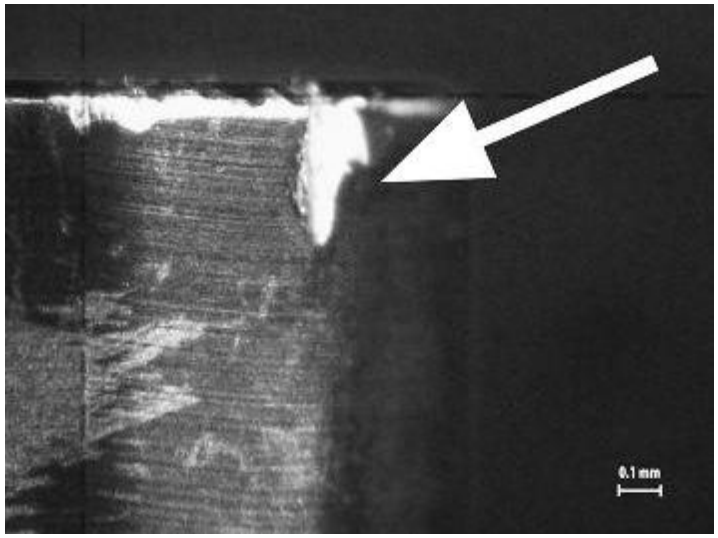

Figure 1-8, Notch wear [27]

Notch wear is a special type of combined flank and rake face wear which occurs adjacent to the point where the major cutting edge intersects the work surface, as in Figure 1-8. The gashing (or grooving, gouging) at the outer edge of the wear land is an indication of a hard or abrasive skin on the work material.

1.3.4. Built up edge

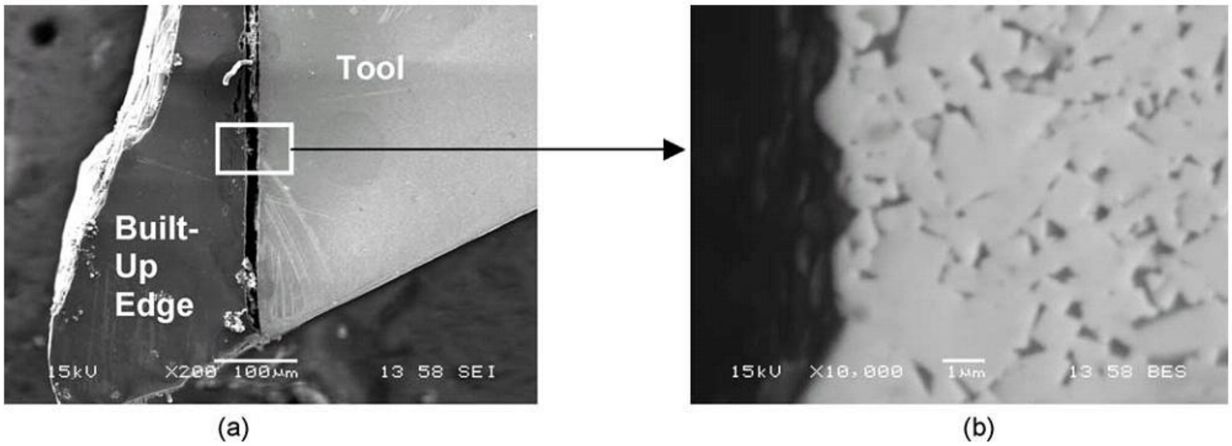

Figure 1-9, Built up edge [28]

Built up edge is the work piece material adhering or seizure on the cutting tool surface, as in Figure 1-9. It changes the cutting edge geometry. If the built up edge is not stable, it will cause unacceptable surface finish of the work piece. When the built up edge is removed from the cutting tool surface it may take pieces of tool material with it and cause tool failure. Built up edge is one of the most important issues in the ductile and soft material machining.

1.3.5. Thermal Crack

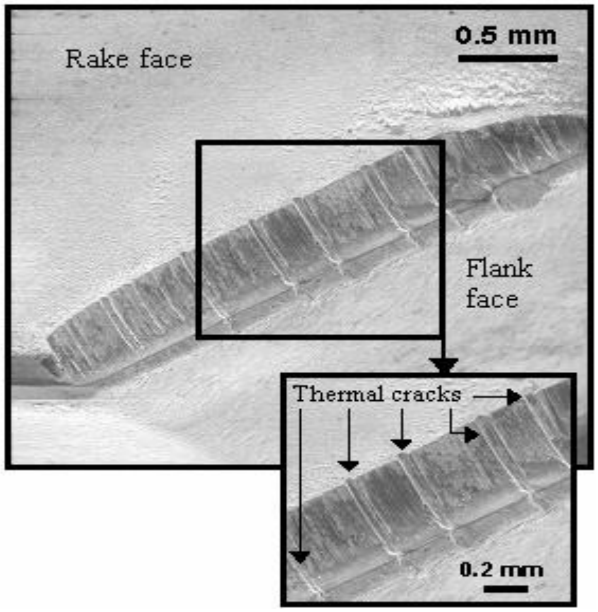

Figure 1-10, Thermal crack [29]

Thermal crack happens in a interrupted cutting condition. The cyclic change of the temperature and traction on the tool surface leads to cyclic expansion and contraction of surface layers of cutting tools. Finally, the fatigue cracks are generated on the cutting tool, which is shown in Figure 1-10.

Chapter 2. Tool wear in turning of pure aluminum

2.1. Introduction of aluminum machining

Aluminum and its alloys have high strength to weight ratios and good corrosion resistance. It has been widely used in many applications such as in aerospace and transportation. Although aluminum and its alloys are relatively softer compared to ferrous materials, there still have many unresolved issues in aluminum machining. Aluminum and its alloys are very ductile and tend to adhere on most types of cutting tool materials to form built up edge (BUE). The BUE generated during machining is usually unstable. It is removed frequently with the chip, which can cause poor surface finish on the work piece material and additional wear on the cutting tool.

2.1.1. Dry machining of aluminum

Coolant used in aluminum machining can reduce the BUE formation [30] and the cutting temperature. However, dry machining of aluminum and its alloys has several advantages for the manufacturing industry. Based on the typical manufacturing costs for metal cutting shown in Figure 1-1, the cost of the coolant is five times more than the cost of the cutting tool. At the same time, coolants used in metal cutting have been a focus of intense regulatory scrutiny during the last 20 years. Dry machining can both reduce the cost of coolant and help to solve the environmental and health problems. In many types of metal machining, eliminating coolant increase the temperature on the cutting tool, often leading to rapid tool failure. However, the temperature in conventional machining of the soft aluminum and its alloy usually stays low [31], which make dry machining of these alloys achievable. In this study, the tool wear in dry aluminum turning was investigated.

2.2. Literature survey on tool wear in aluminum machining

Depending on alloys, different problems are prevalent in machining. Some aluminum alloys used for casting, such as Al-12%Si, contain large amounts of free silicon particles which cause severe abrasive wear in machining [32]. Diamond and diamond coated cutting tools with high hardness and chemical inertness is used to machine aluminum alloy, which results in a long tool life and a good surface finish [32]. However, diamond and diamond coated tools are much more expensive than other coated or uncoated carbide tools. Coatings with high hardness, such as TiAlN, TiCN, and TiN, which were extremely successful in machining ferrous materials, have not worked well in machining aluminum alloys [8]. One problem reported with coated tools is the formation of built up edge (BUE). BUE often results in bad surface finish or the delamination of the coating material as the BUE is periodically removed during machining [8].

In machining of aluminum alloys without major hard inclusions, the abrasive wear is minimal. The adhesion and diffusion wear mechanisms become more important to the tool wear [31]. Nouari et al. concluded that, when machining aluminum at a low cutting speed, the tool wear is mainly due to the formation of built up edge (BUE) or of a thinner formation known as a built up layer (BUL). These BUE or BUL may detach periodically, removing the tool material. At a high cutting speed, unlike machining of other metals such as steel and titanium, no diffusion of tool material into the aluminum work material has been found. Instead, it has been reported that the diffusion of aluminum into the cobalt binder weakens the binder phase. This may ultimately cause the tool failure. A certain amount of oxygen elements have been found in the BUE and BUL near the tool surface, which shows the existence of metal oxide formation during machining [31].

Hu and Chou analyzed the cutting tool flank wear land in turning aluminum alloy Al6061. The layer of work material adhered on the tool had good etching resistant, showed high oxygen concentrations, and had higher hardness compared with the original work material [34].

Rivero et al. carried out dry drilling experiments on aluminum alloys A7075. They concluded that the tool wear was mainly due to detach of the work piece material which adhered on the tool. The formation of large sized burrs was also a reported problem [8].

Chattopadhyay et al. studied the wettability of pure aluminum on uncoated carbide tools in a vacuum. The surfaces of the carbide tools were etched by different chemical solutions to change the Co concentration. The average wetting angle of pure aluminum on WC-6%Co was found to be 95°. The wetting angle on the surfaces of tools with WC-20% Co and WC-3% Co were found to be approximately 45° and 160°, respectively. These results showed that the aluminum tended to adhere more on the cobalt than the WC [33].

Despite a large amount of knowledge accumulated, the tool wear in pure aluminum machining is still not fully understood. It is commonly agreed that the tool wear generated from the removal of BUE is due to adhesive wear. However, there is still a lack of a clear understanding of how this process happens in aluminum machining.

Adhesive wear was one of the oldest and most complicated topics in tribology. The mechanism of adhesive wear is still not very clear. It is commonly believed that the adhesive wear mechanism involves not only mechanical factors but also chemical factors. One of the most important chemical factors in the dry machining process is the interaction of the work material and the tool material with oxygen, the formation of oxide layers. Rowe and Smart [35] found that the cutting forces were 50% higher in a vacuum than in air when machining 0.15% carbon steel.

They explained that the oxide layer formed and contaminated the contact surface, which prevented the metal-to-metal contact and reduced the adhesion force. However, it was found that the presence of oxygen in machining of other types of metal does not always reduce the adhesion and cutting force. Williams [36] found that the cutting force is lower in a vacuum than in air when machining aluminum and copper with high speed steel (HSS) tools. A smaller amount of aluminum adhesion was present on cutting tools in the vacuum environment than in air. The large aluminum adhesion formed in the air increased the cutting force and the friction coefficient. At the same times, Williams found that machining carried out in argon and nitrogen yielded similar results to machining in the vacuum.

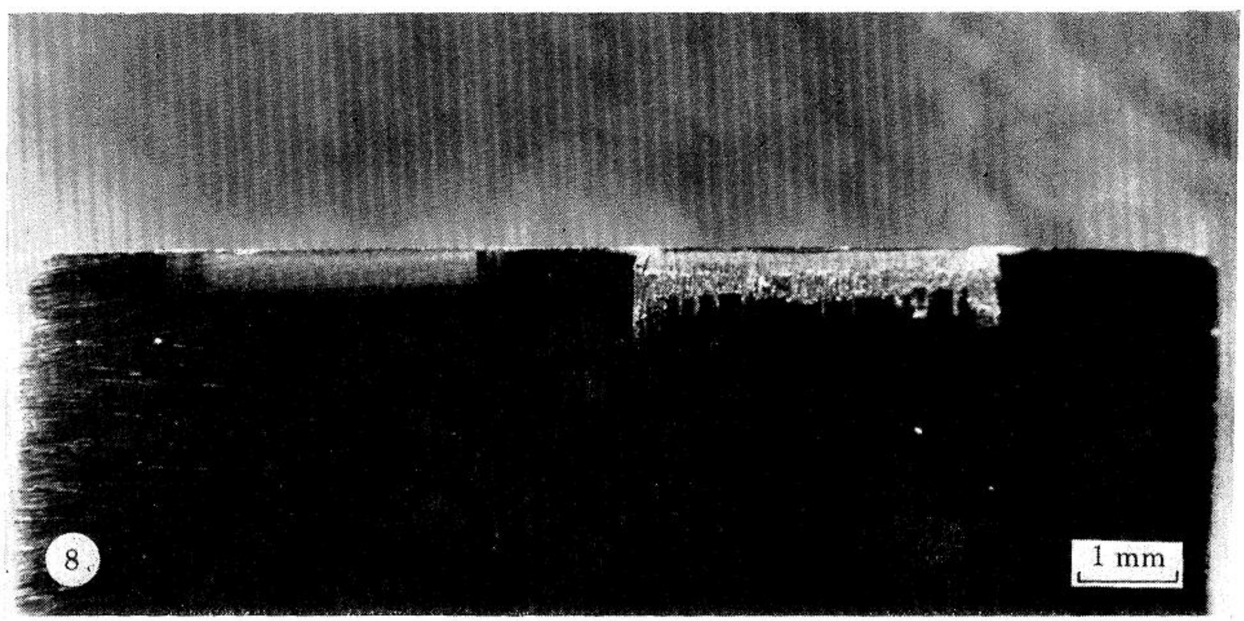

Figure 2-1, Rake face of high speed steel cutting tool, after machining aluminum in vacuum (left) and in air (right) [36]

Considering the BUE formation theory, Iwata et al. [37] suggested that the ‘‘adhesive shearing force’’ at the tool–chip interface governs BUE formation and disappearance. Pepper [38] explained the difference between machining aluminum in vacuum and in air was due to the formation of an adsorbed film between the tool and the work material which increased adhesion strength. Adsorbed film is a complex oxide layer, of spinal structure such as $FeAl_2O_4$ [39]. Pepper [39] also suggested that it is only the formation of monolayers of oxide or initial stages of oxidation that leads to increase friction.

Doyle and Horne [40] used sapphire (Al_2O_3) tools to machine aluminum in a vacuum and air (Figure 2-1) [36]. Cutting force was still lower in the vacuum than in air. Since the Al_2O_3 will not react with sapphire (Al_2O_3) to form a spinel, they suggested that the high adhesion may come from the initial stages of oxidation. When the clean aluminum metal surfaces were exposed to sufficient oxygen to form a monolayer of oxide, an increase in friction was observed.

In addition, the oxide film formed on the work material may influence the BUE formation in mechanical ways. Doyle and Horne [40] observed that the formation of BUE in aluminum machining was not just one of detaching a section of chip material which then acts as an obstruction to the flow of the chip. Rather, it is one of gradual build-up of chip material, where metal is continuously being attached and detached at the sliding interface. Takeyama and Ono [41] proposed two separate steps in built-up-edge formation. First, the work material adheres on the tool. This is the origination nucleus of a built-up-edge. Second, the adhered metal grows from further sliding contact. They emphasized the role of the hardenability of a work material in BUE formation. BUE must be harder than the work material to cause the separation of contact to occur inside of the work material (chip) rather than inside of the BUE. This leads to an increase in the BUE. Based on metallurgical analyses, Williams and Rollason [42] suggested that a second metallurgical phase in a work material is necessary before a large

BUE can form.

A BUE with higher shear strength allows material separation to occur more frequently inside of the chip instead of inside of the BUE. This increases the amount of BUE [43, 44]. Therefore, a shearing strength enhanced BUE, for example one that contains Al_2O_3, allows the volume of BUE to increase. The role of oxidation will also be considered in the study.

The main focus of this research was to understand the tool wear mechanisms and the built up edge formation in dry turning of commercially pure aluminum. The uncoated WC-Co cutting tool, which was the most commonly used tool in industry for aluminum machining, has been chosen as the focus for the research.

2.3. Dry turning of commercially pure aluminum experiment setup

2.3.1. Cutting tool and work material

Two grades of WC-Co inserts with different grain sizes but identical tool geometry were used in the experiment. The inserts were provided by Valenite Inc. (Madison Heights, Michigan). The fine grain carbide (US10) had a grain size of between 0.2-1 μm and the coarse grain carbide (UK20) had a grain size between 1-4 μm. The inserts are 55º diamond shape, mounted on a tool holder which gives a 5º rake angle and 6º relief angle. The work material used in the experiment was commercially pure aluminum (Al1100) with annealed heat treatment, whose composition is Al>99.0%, Si<0.3%, Fe<0.5 and trace of Cu, Mg, and Zn. The size of the aluminum round bar has the diameter of 101.6mm and the length of 762mm. The cutting conditions in the experiment were fixed, the cutting speed at 68 meter/ minutes, the depth of cut at 0.254mm, and the feed rate of 0.0762mm/rev.

Table 2-1, Two grades of carbide tools used in turning experiments

Insert grade (WC-Co)	Fine Grain (US10)	Coarse Grain (UK20)
Geometry	DNMM150404	DNMM150404
Composition	6.8% cobalt + 3.0% (TaC, NbC) + rest WC	6.0% Cobalt + rest WC
Grain size	0.2 -1mm	1 - 4mm
Hardness	92.6 Ra	91.6 Ra

2.3.2. Tool wear test

Both fine grain and coarse grain carbide inserts were used for dry turning. Total cutting time was 9 hours to study the tool wear evolution. After every 3 hours of machining, the turning process was interrupted to measure the flank wear on the insert with a confocal laser scanning microscopy (CLSM). To examine the wear land, 5% NaOH solution is used to dissolve the aluminum adhesion on the tool. Wavelet filtering was used to eliminate the noise and artifacts inherent to the height encoded image obtained by CLSM [45].

A JEOL 6400 SEM Scanning Electron Microscope (SEM) was used to provide the high magnification pictures of the wear pattern. Energy Dispersive X-Ray Spectrometer (EDX) element mapping provided an understanding of the changes in the material composition of the surface.

2.4. Experiment results and analysis

2.4.1. Delamination of tool material in physical detach the BUE

To study the adhesion between the carbide tool and adhered aluminum, the BUE was detached by hand several times after a short machining time. In each case, a large volume of the tool material was delaminated from the tool rake surface, seen in Figure 2-2(b). The adhesive strength between tool and adhesion was strong enough to cause delamination of the carbide tool. This phenomenal has been previously reported when the carbide tool has been physically separated from other adhered metals [46, 47].

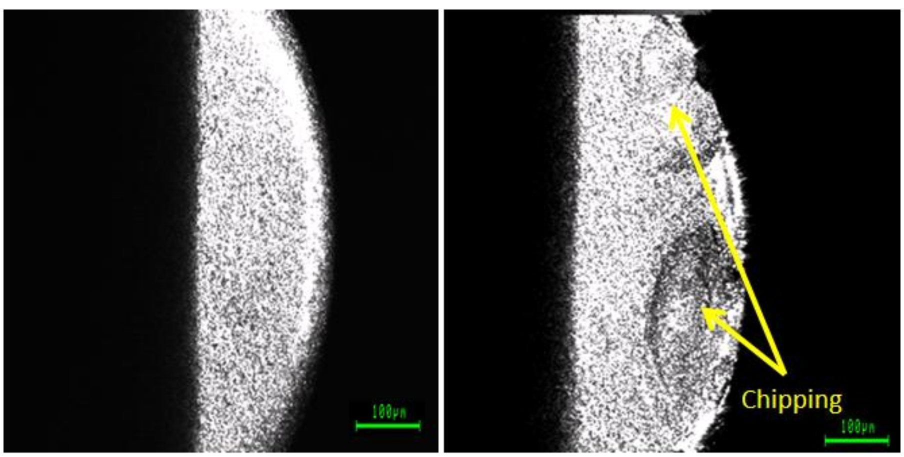

Figure 2-2, (a) Rake surface of the tool before machining, (b) Chipping on the surface after BUE has been physical removed.

During the turning experiment, the detachment of such a large volume of tool material was not common as the cutting tool surface mainly loaded with compressive stress rather than tensile stress. However, the relative sliding between tool and work material generates tensile stress at adhesion junction, breaking the junctions. This may have directly fractured or removed carbide grains from the surface.

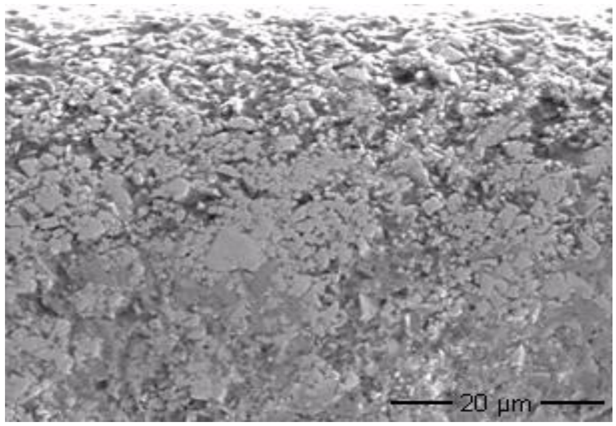

Figure 2-3, Cutting edge and flank surface of unworn coarse grain carbide

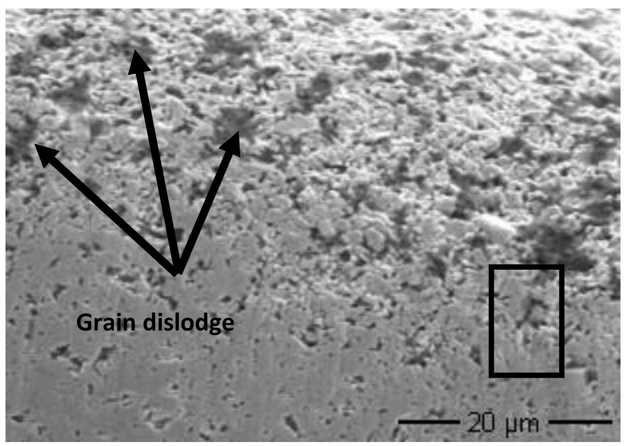

Figure 2-4, Cutting edge and flank surface of coarse grain carbide, after 9 hours machining

The cutting edge and flank surface of an unworn and a worn coarse grain carbide tool are shown in Figure 2-3 and Figure 2-4, respectively. The arrows in Figure 2-4 point out some cavities left behind after carbide grains has been pulled out. In the direction of material flow, some grooves were observed in the downstream of the cavities marked by the rectangle. This demonstrates abrasion of the tool surface due to the pulled-out WC grains.

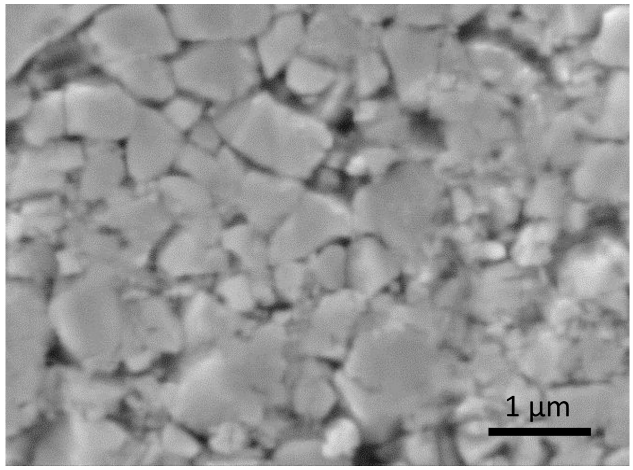

Figure 2-5, Flank surface of new fine grain carbide

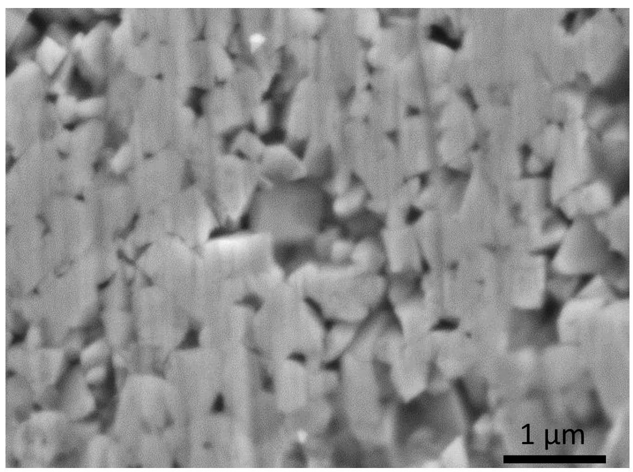

Figure 2-6, Flank surface of fine grain carbide, after 9 hours machining

Figure 2-5 and Figure 2-6 show the new and worn flank surface of the fine grain carbide. As the carbide grains are dislodged and abrade the surface, one can observe in Figure 2-6 the grain pulled out from the surface as well as the grooves generated by the pulled-out grains.

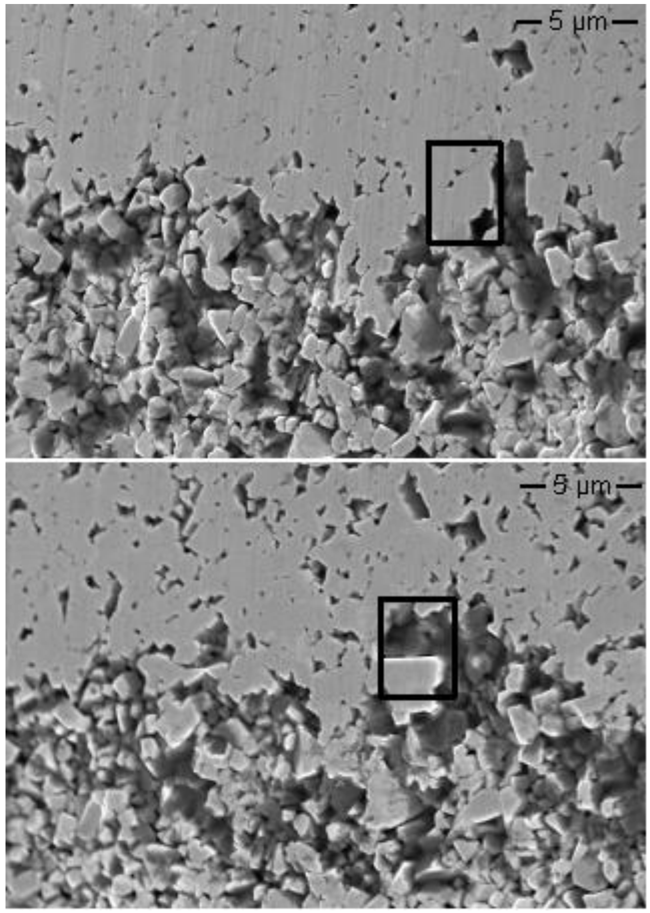

Figure 2-7, Upper (a) and bottom (b) are captured at the same location of a coarse grain insert after 9 and 9.5 hours machining.

Figure 2-7(a) and (b) were captured the change on the flank surface after machining for 9 and 9.5 hours, respectively, on the exactly same location on the coarse grade carbide. A carbide grain has been fractured and pulled out and the boxes on Figure 2-7 (a) and (b) were used to show the location.

2.4.2. Flank wear evolution

Figure 2-8 and Figure 2-9 shows the confocal images of the flank surface of the fine and coarse grain carbide inserts after 0 hour, 3 hours, 6 hours, and 9 hours, respectively. Figure 2-10 shows the SEM images of the flank surface after machining 9 hours. Figure 2-11 shows the time history of the flank wear on both grades of carbide. As evident, fine grain carbides (US10) exhibit more flank wear than coarse grain carbides (UK20).

Figure 2-12 shows the height information of the cutting edge of fine and coarse grain carbide before and after 9 hours of machining. The CLSM image data have been filtered to reduce noise using the wavelet transform. The wear volume was measured using the confocal images by subtracting the worn 9 hour profile of the tool from the original 0 hour profile of the tool and subsequently multiplying a unit length. The flank wear volume of the fine and the coarse grain carbide insert was 124.07 μm^2 and 69.56 μm^2 respectively. The fine grade carbide had about 78% more wear than the coarse grade carbide insert. The flank wear depths on both types of inserts were very small (<5μm).

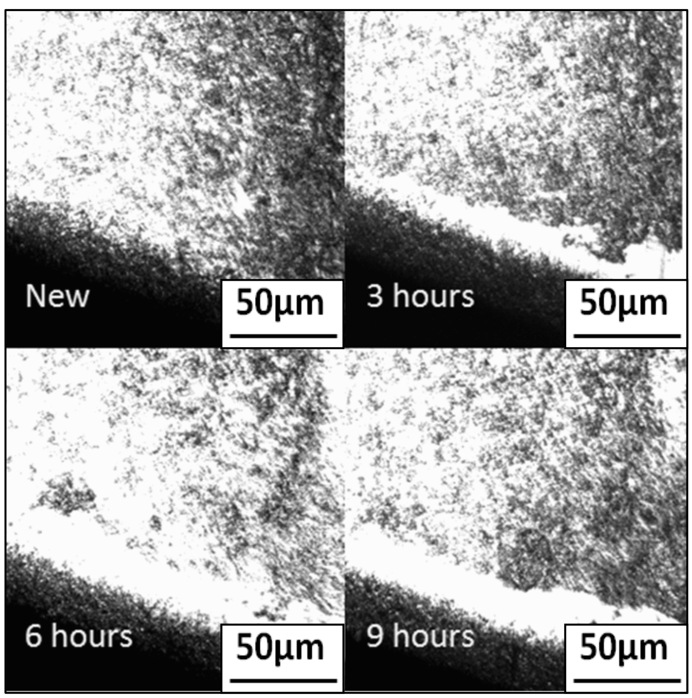

Figure 2-8, Flank surface of fine grain carbide (US10) after machining 0 hour, 3 hours, 6 hours and 9 hours

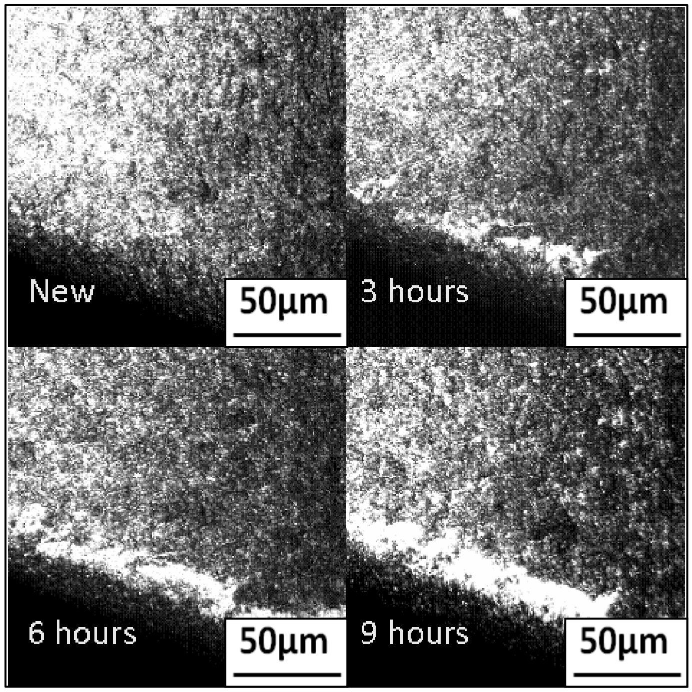

Figure 2-9, Flank surface of coarse grain carbide (UK20) after machining 0 hour, 3 hours, 6 hours and 9 hours

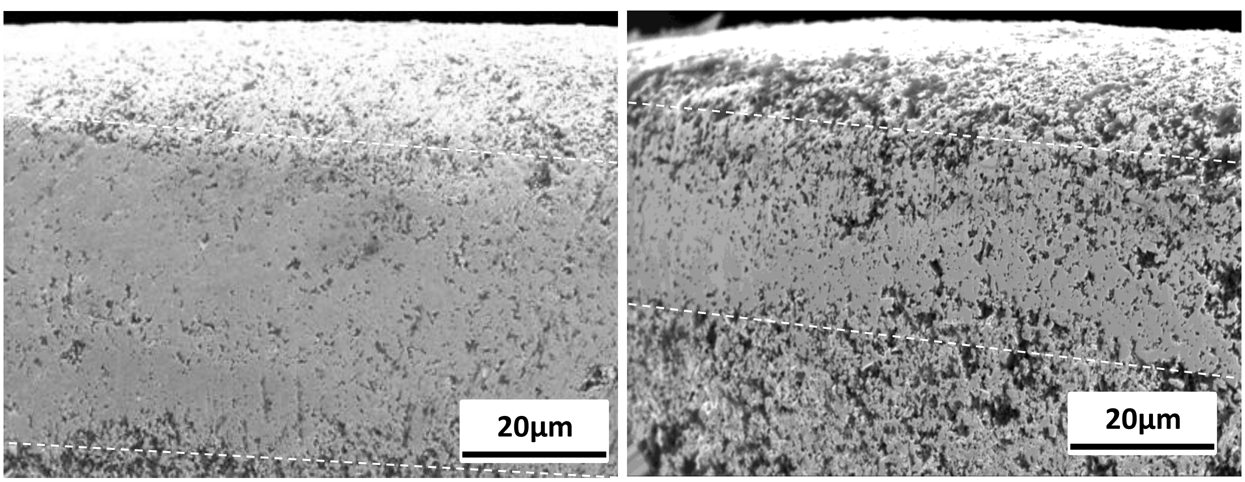

Figure 2-10, SEM pictures of the cutting edge of fine (left) and coarse (right) grain carbide insert after 9 hours machining

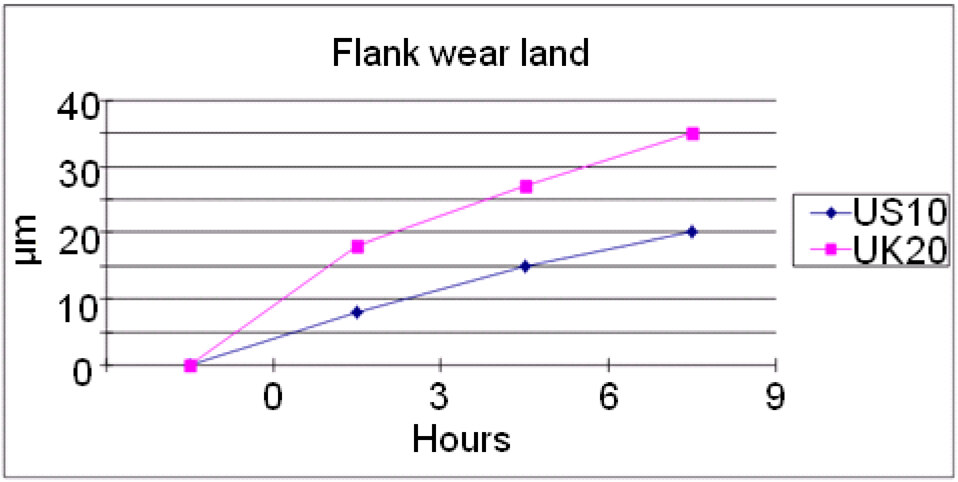

Figure 2-11, Flank wear versus cutting time for fine (US10) and coarse grain (US20) carbides

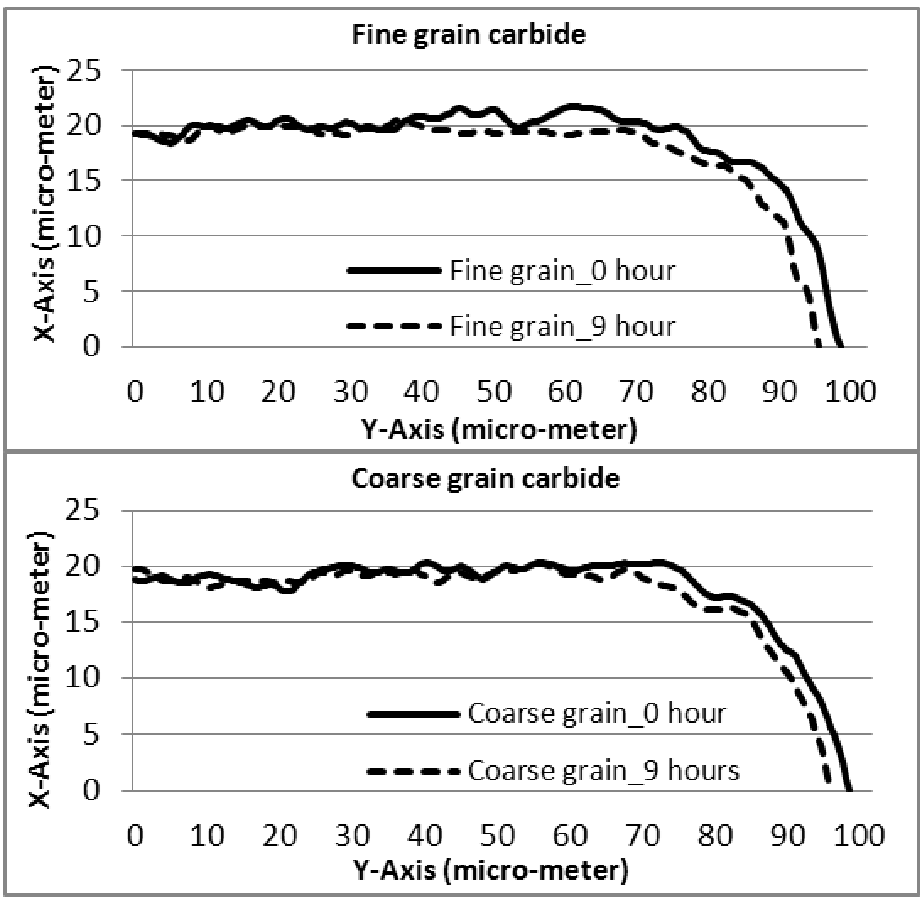

Figure 2-12, Height information of the flank surface of fine and coarse grain carbide before and after 9 hours machining

2.5. Determining the tool wear mechanism

In machining other work materials, the flank wear is mainly caused by hard phases from the work material abrading the tool surface. This abrasion wear is very sensitive to the hardness of the tool and the hard phases in the work materials [23, 24] as shown in Chapter 1.2.2.

The predicted relative abrasive wear from 2-body and 3-body abrasive wear equations are shown in Table 2-2. The fine grade carbide had higher hardness compared to the coarse grade carbide, which typically would reduce abrasive wear [48]. However, in our experiments, flank wear was more extensive on the harder fine grade carbides than on the softer coarse grade carbides. Therefore, the abrasive wear mechanism cannot solely be used to explain these flank wear results.

The aluminum work material used in our experiment was commercially pure aluminum without hard inclusions, which indicated to us that the abrasive wear was not caused by the work material. However, the carbide grains that were dislodged from the tool cutting edge or flank surface could have abraded the tool as they were carried by the flowing chip. The grooves downstream of the location of the dislodged grain, shown in Figure 2-4, proved that the dislodged carbide grains do abrade the tool surface, and likely account for part of the overall flank wear. A similar wear mechanism for carbide tools has been reported in machining of other work materials [49].

Observation of the worn tools demonstrated that it is easier for the smaller WC grains to be pulled out by adhesion than for the larger grains. This is shown in Figure 2-6 and Figure 2-7. On the fine grade carbide insert, many of the carbide grains on the flank surface were entirely uprooted. Compared to the coarse grade carbide in Figure 2-7, most of the holes were generated by a small, fractured carbide grain that was pulled out from the surface rather than removal of an entire grain. The dislodged carbide grains accelerated the tool wear by not only their removal but also their abrasive action during sliding.

Shetty [50] and Ingelstrom [51] found that the fracture path in WC-Co mainly exists the cobalt binder phase. The mean free path of cobalt in the coarse grain carbide is larger than in the fine grain carbide. This helps to more evenly distribute the stress, and prevent stress concentrations, which may cause fracture. Therefore, the coarse grain carbide has better bulk fracture toughness than the fine grain carbide [50, 51]. Consequently, the crack growth is more prevalent in the fine grain carbide, which increases the frequency of the grain pull-out. Thus, the finer carbide grains are easier to be pulled out, which explaining the increased flank wear on the fine grade carbide insert.

Jia and Fisher studied the grain size effect on abrasive wear [48] and sliding wear [52] of WC/Co material. In tribo-testing, the authors found that when the abrasive particles were from the counter surface, the abrasive wear rate of WC/Co material was increased with increased WC/Co grain size. The explanation given was that the large grained carbide has lower hardness. However, when there were not hard inclusions in the counter surface, the wear rate of WC/Co material decreased with an increase the WC/Co grain size. It was found that the wear of the carbide tool included the dislodged tungsten carbide grains, which subsequently abraded the WC/Co surface. This is not exactly same as, but very similar to the tool wear of our pure aluminum machining. This type of wear usually has been referred to as “sliding wear” rather than conventional abrasive wear. The relative sliding wear rate of the fine and coarse grain carbides in our study is shown in Table 2-2. These wear rates were derived from interpolated data from [52].

Table 2-2, Relative flank wear rate from experiment results, theoretical 2-body, 3-body abrasive wear equation and WC/Co cutting tool sliding wear reference [84]

	Hardness	Experiment results (relative wear rate)	2-body abrasive wear	3-body abrasive wear	Sliding wear of WC/Co
Fine grade	92.6 Ra	1.78	0.989	0.947	2.3
Coarse grade	91.6 Ra	1	1	1	1

Comparing the relative wear rate results for pure aluminum machining with the predicted 2-body wear rate, 3-body wear rate, and sliding wear rate, it was shown that the sliding wear rate most closely matched the experimental wear rate. This supports our hypothesis that the wear rate for machining pure aluminum is not due to the conventional abrasive wear.

2.6. Micro-fracture on the tool nose

After 9 hours of machining, a micro-scale fracture was observed on the tool nose of the fine grain carbide (Figure 2-13: left) while no fracture was observed with the coarse grain carbide (Figure 2-13: right). This may due to the fact that the fine grain carbide has better fracture toughness than the coarse grain carbide [50, 51].

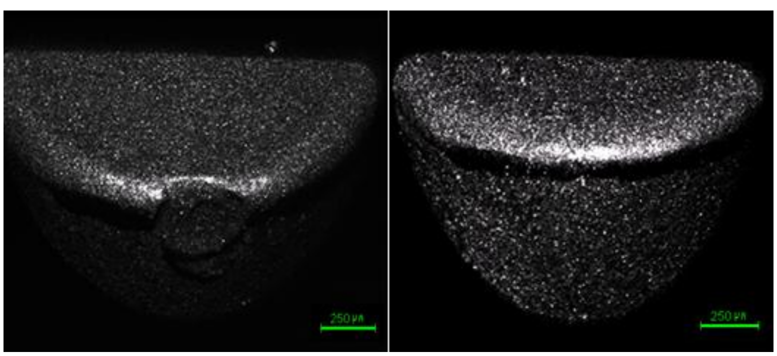

Figure 2-13, Tool nose of fine grain (left) and coarse grain (right) carbide after 9 hours machining

2.7. FEM simulation of the temperature in pure aluminum machining

In machining, it is very difficult to directly measure the cutting temperature. This difficulty is due to the intimate contact between cutting tool and work material. Thus, finite element simulation is commonly used to obtain the cutting temperature on the tool surface.

For our aluminum machining research, a finite element model in Abaqus 6.9 was developed to determine the cutting temperatures. The cutting tools were designated as mechanically rigid since the deformation of a cutting tool is miniscule compared to that of a work material. However, to estimate the tool temperatures, the tool was modeled as thermally non-rigid with appropriate thermal properties such as heat conductivity and specific heat. The Johnson-Cook constitutive model was used to describe the flow stress. The Johnson-Cook model is described in equation (2-1),

$$\sigma = \left\{A + B\varepsilon^{n}\right\}\left\{1 + C\ln\left(\frac{\dot{\varepsilon}}{\dot{\varepsilon}_0}\right)\right\}\left\{1 - \left(\frac{T - T_r}{T_m - T_r}\right)\right\} \tag{2-1}$$

where σ is the effective flow stress, ε is the effective plastic strain. The equivalent plastic strain rate $\dot{\varepsilon}$ is normalized with a reference strain rate $\dot{\varepsilon}_0$. T_r is room temperature (25C°), T_m is the melting temperature of the material, n is the work hardening exponent and A , B, C are constants. The Arbitrary Lagrangian-Eulerian (ALE) element meshing method was used. The computational ALE mesh inside the domains can move arbitrarily to optimize the shapes of elements, while the mesh on the boundaries and interfaces of the domains can move along with materials to precisely track the boundaries and interfaces of a multi-material system.

Johnson-cook parameters were derived from empirical studies. The parameters used in Al1100 aluminum machining simulation was A=265Mpa, B=426Mpa, n=0.34, C=0.015, m=1

[53]. The simulation used a constant friction coefficient of 0.3. The work material flow into the system was from the left boundary at a speed of 200sfm, which is the same as the cutting speed for our aluminum turning experiment. The work material flow out of the system was from both the right boundary and from the top surface of the chip. It was assumed in the FEM simulation that a continuous chip is formed based on our observation of the chips in the turning experiment. One assumption is that steady state shear deformation zones are formed as Figure 2-14, and that this deformation pattern travels effectively unchanged with the tool tip. This is not exactly true as the thickness of the aluminum chip during turning can frequently change within ±30%. However, the aim was to reduce the simulation time without significantly affecting the temperature results. Therefore, the temperatures from the finite element simulation should only be used as an approximate value.

The FEM simulation temperature field is shown in Figure 2-14. The maximum steady state temperature was only about 283 °C, which is similar to that reported by List et al. [28] cutting an aluminum alloy.

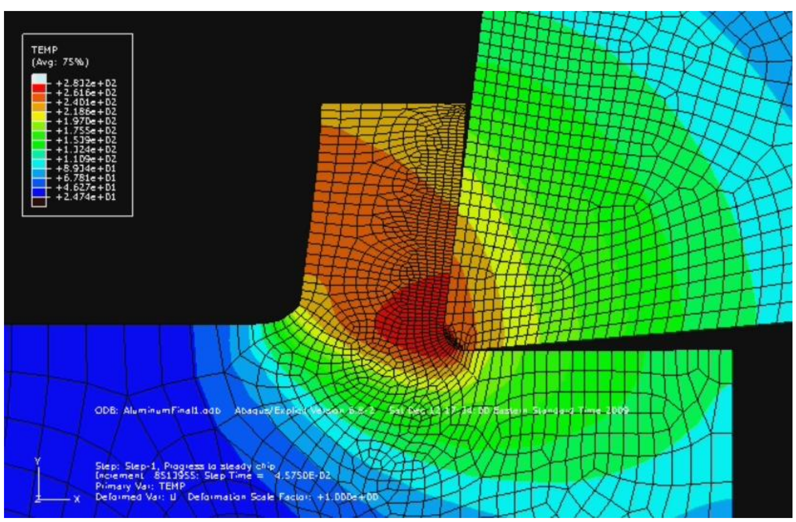

Figure 2-14, Temperature distribution on carbide tool (text is not meant to be readable, but is for visual reference only**)**

2.8. Built up edge test

2.8.1. BUE evolution on the coarse grade carbide inserts

To understand the BUE evolution in the machining, the BUE on the coarse grain carbide tool was measured every half hour with CLSM in the first 2 hours. One additional measurement was made after 9.5 hours of machining. The images of rake and flank surface in BUE measurement were shown in Figure 2-15. The measured volume of BUE was presented in Figure 2-16. There was more BUE after the first half hour of machining than at any of the remaining half hour intervals of the experiment.

Figure 2-17 shows the cobalt and tungsten concentration on the flank surface of the coarse grade carbide insert after 1 hours machining. Less Co was found on the flank wear land than the adjacent area. It indicated that the Co binder phase on the surface was preferentially worn down during the machining. After the Co was worn down, a less amount of BUE was present as the aluminum was less likely to adhere to the WC.

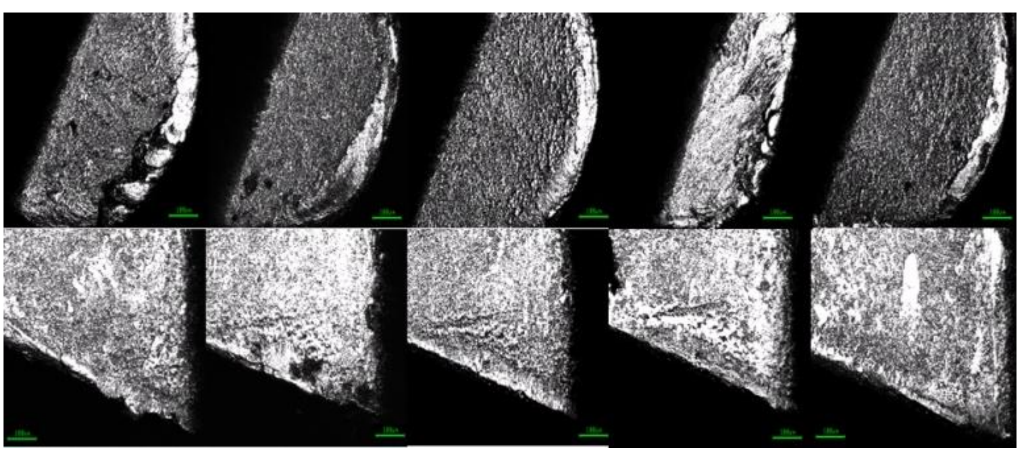

Figure 2-15, BUE on rake and flank surfaces of a coarse grain carbide insert after 0.5, 1, 1.5, 2 and 9.5 hours of machining

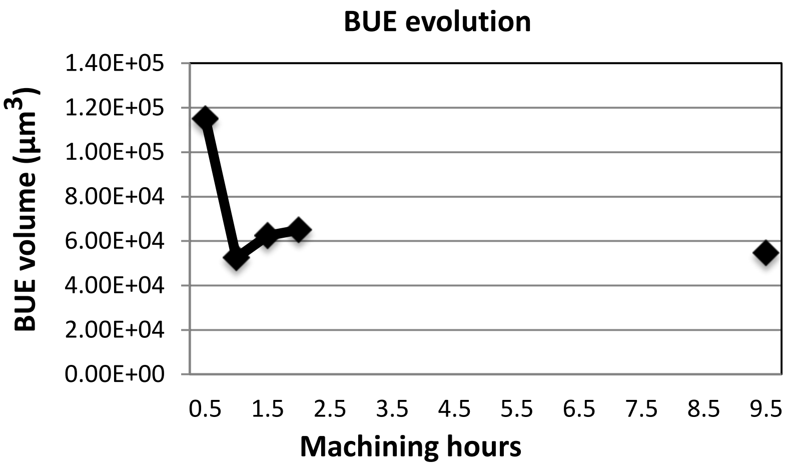

Figure 2-16, The BUE volume on a coarse grain carbide insert after 0.5, 1, 1.5, 2 and 9.5 hours machining

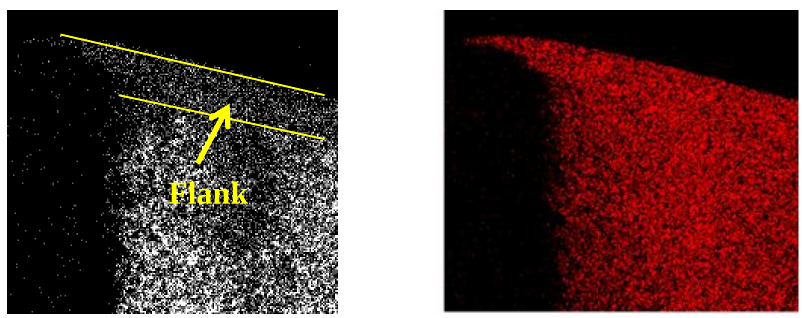

Figure 2-17, EDX pictures of the concentration of cobalt (left) and tungsten (right) on the flank surface of coarse carbide tool, after one hour machining

2.8.2. Chemical composition of the BUE

In the etching process, initially, a solution of 1% NaOH was used to remove the BUE on the surface of the tool. The superficial BUE, thickness of 40um-50um (see Figure 2-18 left) covering the large area of tool rake surface, was dissolved within 5 minutes. However, a very thin adhered layer of 1-4 µm (shown in Figure 2-18 right) was remained on the surface for 2 more hours of etching before being completely removed. This thin layer covered only a small area of the tool rake surface near the cutting edge. This location was characterized by both high temperature and the presence of oxygen from the air during machining.

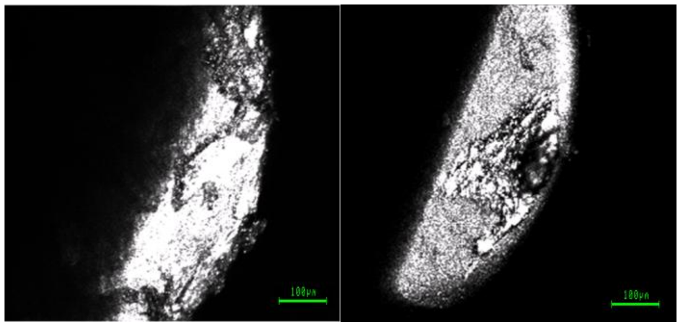

Figure 2-18, Left: The huge BUE before etching and Right: A thin layer after use 1% NaOH etching for 2 hour

Table 2-3 shows the element compositions of the superficial BUE and thin layer detected by EDX at 5000X magnification. The sample and the copper holder were cleaned by Fishione-1020 plasma cleaner for 10 minutes before the EDX measurement. Carbon tape has been excluded during any of the EDX measurements in this paper. Instead, a metal clip has been used to fix the samples.

A higher oxygen concentration was found in the thin layer than superficial BUE. Similar results were also reported in [31, 54]. The thin layer in this work was believed to contain considerable aluminum oxide. The aluminum oxide may increase the BUE by forming complex oxide with cobalt oxide [38] or by enhancing the shearing strength of the BUE [41 - 43].

Table 2-3, Element detected in the superficial BUE and thin layer

Element (at %)	Superficial BUE	Thin layer
Al	77.65	68.48
C	19.54	21.92
O	2.63	9.41
Si	0.18	0.19
W	0	0

An unexpected high carbon concentration was detected in the BUE samples using EDX. This phenomenon has also been reported in [4]. One of the hypotheses was that the carbon comes from the decomposition of the WC, and at the same time the tungsten from the decomposition was worn away by other reasons. However, it is very doubtful that this hypothesis can explain the high carbon concentration which appeared in our EDX measurement. If the 20% carbon concentration measured in the BUE came from the decomposition of the WC, the cutting tool would have severe wear due to the decomposition. However, the cutting tool wear in aluminum machining is extremely small. Also, the temperature in aluminum machining is only about 300°C and the solubility of carbon in aluminum is less than 0.12% below 660°C [55].

In order to explain the high carbon concentration measured on the BUE, additional experimental investigations were carried out. The results showed that the high carbon concentration detected in the BUE samples, most of which possibly came from the “carbon contamination” process.

2.9. Carbon contamination

In order to eliminate as much of the carbon source as possible from the environment, the carbon tap, which is commonly used in SEM to fix the sample, has been replaced by a metal clip in our experiment. Isaballer et al. [56] and Janbroers et al. [57] reported that less carbon was detected during EDX measurements after the samples were cleaned with plasma than after being cleaned with ethanol. This means the residual ethanol, which contains carbon, may affect the carbon concentration detected by the EDX. Therefore, a Fishione-1020 plasma cleaner has been used in our experiment rather than ethanol. One continuous aluminum Al1100 chip has been cut into multiple pieces and used as the samples in the experiment. The compositions of the samples were assumed to be the same.

Table 2-4 and Figure 2-19 present the carbon concentration detected by EDX on the aluminum samples in our experiment after the cleaned samples had been exposed to air for different lengths of time. All the results were measured using consistent SEM parameters. The results show that the carbon concentration detected on the aluminum sample increased with the exposure time to the air. Thus, one of the most important carbon sources was the air, which was really unexpected. The reason that the exposure times of less than 5 minutes could not be reported here was due to the time needed to transfer the sample from the Plasma cleaner into the SEM chamber.

Table 2-4, The carbon concentration detected by EDX on work material (Al1100) after exposed to air for different time

Exposure time	<5mintes	1 hours	2 hours	1 day
Carbon concentration	5.86%	9.12%	11.24%	22.74%

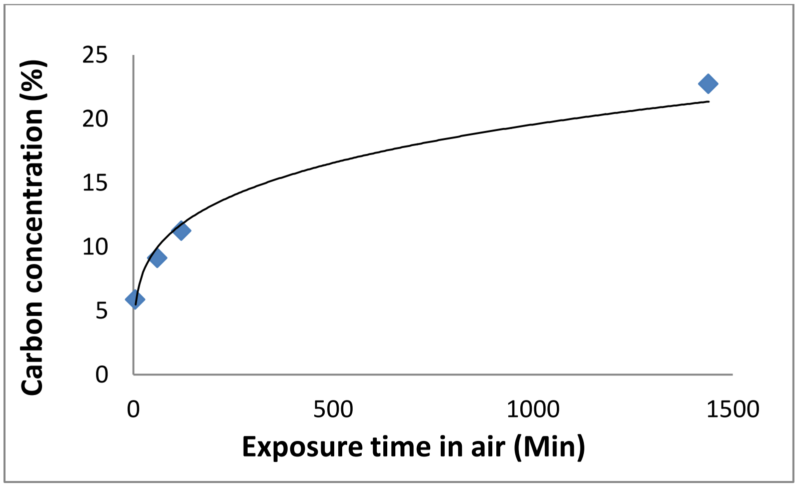

Figure 2-19, Carbon concentration measured on the aluminum chip for different exposure times in air.

Air is mainly composed of nitrogen, oxygen and trace amounts of other gases. The concentration of gas phase hydrocarbons, such as CH_4, in the air is extremely low. However, small organic particles, which float in air, also contain carbon. Therefore, the hypotheses of air providing to the observed carbon concentration was reasonable as indicated in the results. However, an amount in the range of 20% carbon concentration measured on the samples was too high to be explained solely by the carbon in the air. Therefore, a number of additional experiments have been carried out to search for the drastic increase in the carbon concentration measured on the surface. It has been found that the magnification of the SEM during the EDX measurement also affect the carbon concentration measured on the samples.

Figure 2-20 shows the surface of an aluminum chip, which has been element-mapped at 1000X and 5000X magnifications using EDX. The carbon-accumulated areas (black areas) are easily seen. Some carbon particles (black dots) have a diameter bigger than 1 µm. The two small black squares were the irradiation (element detection) areas at 5000X. More carbon was formed in the boundaries of each region.

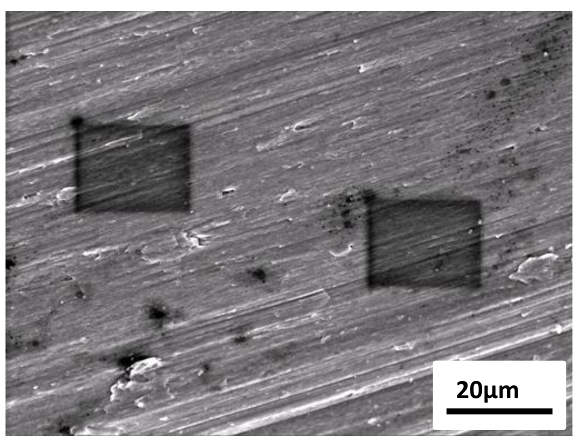

Figure 2-20, Picture of the aluminum chip captured at 1000x after EDX element mapping

The average carbon concentrations detected on the aluminum chip at 200X, 1000X and

5000X magnification are shown in Table 2-5. A greater than 2X difference in carbon concentration between 1000X and 5000X was observed.

Table 2-5, The carbon concentration measured by EDX on an aluminum chip by different magnifications.

Element (at %)	5000X	1000X	200X
Al	74.22	88.33	97.91
C	23.79	9.52	0
O	1.81	2.12	2.27
Si	0.18	0.20	0.21
W	0	0	0

A possible explanation was that the carbon containing compounds inside of the irradiation area of the SEM, where exists high speed electrons, decomposed into carbon compounds very quickly. After the carbon containing compounds inside of the irradiation area decomposed, the remaining carbon containing compounds from the surrounding area could diffuse into the irradiation area, which promoted the accumulation of carbon in the irradiation area. Since all the carbon containing compounds from outside of the irradiation area need to pass through the boundary before entering it, this causes more carbon compounds to form at the boundary. The total output irradiation in SEM was constant at different magnifications. However the irradiation area at a higher magnification was smaller. Thus, the irradiation density at higher magnification was higher. This caused more carbon to accumulate on the surface per unit area at higher magnifications.

Conducting EDX at low magnification was one way to reduce the effect of carbon accumulation. For example, carbon has not been detected at 200X magnification. This means the X-ray feedback generated by the accumulated carbon on the surface did not exceeded the background noise at 200X.

In our BUE element measurement, unfortunately, the aluminum thin layer covers only a small area, and the 5000x was the best magnification for the EDX. Thus, we could not reduce the magnification to lower the irrelevant carbon from air. Fortunately, the detection of carbon does not influence the detection of other elements and could simply be taken out of the experiment results and the tool wear consideration.

From the literature survey, the unexpected high carbon concentration detected by the EDX has been reported by many researchers when measuring various different samples [34, 58-60]. However, in the microscopy field, this phenomenon, which has been called “carbon contamination”, has been known for many years [61]. This was even being exploited to fabricate nano-probes for scanning probe microscopy [62] and nanotips for field emission [63]. Unfortunately, researchers outside of the microscopy field have frequently misunderstood this phenomenon when conducting their experiments. This sometimes causes confusion.

Studies in the microscopy field have shown that the carbon contamination in the TEM or SEM process mainly occurs as a three-step process. First, the hydrocarbon (C_xH_y) molecules from different contamination sources adhere on the sample surface. Second, the adsorbed hydrocarbon molecules decompose under the high-speed electrons in the irradiation area of SEM, which forms amorphous graphite on the sample surface. Finally, the adsorbed hydrocarbon molecules from surrounding areas transfer to the irradiated area by surface diffusion, which supports the continued growth of the amorphous graphite [61].

Because the “carbon contamination” phenomenon is so similar to that observed in our experiments, it is believed that the high carbon concentration detected on our samples is the result of this “carbon contamination” rather than from the decomposition of the carbide tool.

2.10. Summary of tool wear in turning of pure aluminum

The carbide grains pulled out by the adhesion force was observed as one of the important wear mechanism in dry machining of commercially pure aluminum. The dislodged carbide grains abraded the flank surface generating flank wear. The fine grain carbide tool exhibited more flank wear than the coarse grade carbide tool. The initial volume of built up edge from machining aluminum reduced as the surface cobalt was preferentially worn down. Higher oxygen concentration was detected in the bottom layer of the BUE which contacts the tool surface. This layer was believed to contain aluminum oxide, which can increase the adhesion and BUE. It has been found that the high carbon concentration detected on the BUE sample was from carbon contamination rather than from the decomposition of the carbide tool.

Chapter 3. Tool wear in carbon fiber reinforced plastic CFRP drilling

3.1. Introduction of CFRP/Ti stack machining

As introduced in Chapter 1.1, both the carbon fiber reinforced plastic (CFRP) and the titanium (Ti) are promised materials in aerospace structural applications [7, 64]. In a hybrid structure, various materials work together, this is usually better than any of the single materials in it. Titanium provides high ductility, high compressive strength and good corrosion resistance. In the carbon fiber reinforced plastic (CFRP), the carbon fiber provides high hardness and tensile strength, and the plastic provides low density. The hybrid structure of a CFRP/Ti stack provides the advantages of both CFRP and Ti to components. Therefore, CFRP/Ti stack has high tensile strength, low density, high ductility, high compressive strength, and good corrosion resistance.

However, both CFRP and Ti cause severe tool wear in machining. In CFRP machining, dulling of the cutting edge is the main wear phenomena [11]. In Ti machining, severe diffusion and dissolution wear is generated on the tool due to the high temperature [7]. In CFRP/Ti stack drilling, the wear involved not only includes the problems in drilling CFRP and Ti separately, but the combined material also causes additional new problems. Due to the different mechanical and thermal properties of the CFRP and Ti, drilling the composite (CFRP)/Ti stack by one shot generates further more problems [12]. In order to find better solutions to save the cost and time, it is very important to understand the tool wear mechanisms in the CFRP/Ti stack drilling.

In the present work, three types of experiments were carried out: CFRP-only drilling, titanium-only drilling and combined CFRP/Ti stack drilling.

3.2. Literature survey of CFRP machining

Carbon fiber reinforced plastic (CFRP) is a promising material in the aerospace industry, which combines high strength, high stiffness, and low weight. However, due to high hardness and high tensile strength of the carbon fiber, CFRP has been considered a highly abrasive material for machining. The carbon fibers in CFRP can cause rapid tool wear [64-67]. This research attempts to delineate the cause of tool wear in drilling CFRP. Understanding the wear mechanisms in CFRP drilling will allow us to select a right tool material for each application of CFRP drilling.

The fiber reinforced plastic (FRP) materials, such as CFRP, glass fiber reinforced plastic (GFRP) and Kelvar fiber reinforced plastic (KFRP), are highly anisotropic and inhomogeneous materials. The chip formation in FRP machining has been found to be quite different than the chip formation in conventional metal machining [68-71].

Koplev et al. [69] concluded that the chip formation process in CFRP machining consists of a series of brittle fractures and is strongly dependent on the fiber orientation. Arola et al. [70] found that in edge trimming of graphite/epoxy laminates, the chip formation involves fracture and compression induced shear failure. Sakuma and Seto [71] carried a GFRP turning experiment with various fiber orientations of GFRP. They found that the fracture and shear induced chip formation occurred in certain fiber orientations, and can be explained by comparing the shear and tensile strength of the glass fiber.

Generally, fracture dominates the chip formation mechanism in CFRP machining. This is different than the chip formation in conventional metal machining, which is mainly due to shear. Since the fracture does not need as much energy as shear, the cutting force and temperature are much lower in CFRP machining [64, 72] than metal machining. For example, Chen [64] studied temperature in dry turning CFRP. The highest temperature at 200m/min on the tool was approximately 340°C. Liu et al. [72] studied temperature in drilling CFRP. Compressed air was used as the coolant. The highest temperature measured using a thermocouple at the cutting speed of 200m/min was less than 100C°.

The low machining temperature greatly reduced the diffusion and dissolution wear in CFRP machining. The main tool wear mechanism was believed to be the result of mechanical type of wear.

Many investigations [10, 11, 49, 73-75] have been carried out to understand the tool wear in CFRP machining. In addition to edge chipping, it was also reported edge dullness resulted from abrasive actions of the fibers. This wear has been called edge rounding wear or edge recession.

Sakuma et al. [10] investigated the performance of several kinds of tool materials such as carbides, ceramics and cermets in GFRP and CFRP turning. In GFRP turning, the thermal conductivity of a tool material had great influence on tool wear. With the higher thermal conductivity of tool materials, tool wear is expected to decrease. However, the influence of the thermal conductivity of a tool material had not been observed in CFRP machining. Sakuma et al. [10] explained that the carbon fiber had a higher thermal conductivity than the glass fiber, which, with a better heat transfer, machining the CFRP yields low machining temperatures. Therefore, the temperature influence in CFRP machining was not as important as in GFRP machining. The authors attributed the tool wear mechanism in CFRP machining to dislodging of hard tool particles from the tool surface.

Masuda et al. [49] analyzed the failure of uncoated carbide tools when machining sintered carbons such as graphite and amorphous carbon and CFRP materials. They found that tool wear decreased with an increase in carbide grain size despite of the fact that increase carbide grain size will decrease the hardness. Because the abrasive wear should increase with decreasing the tool hardness, it was concluded that traditional abrasive wear could not explain the tool wear in turning carbon materials [49]. They also found that tool wear was increased when increasing the cobalt (Co) content of the tool. The high Co content may improve fracture toughness of the carbide tool, however high content of soft Co promotes the dislodging of carbide grains during CFRP machining. The exposed carbide grains interact much more intensely with the work material as it traverses across the tool surface action. This accelerates crack generation and eventual dislodge in the carbide grains.

Rawat and Attia reported that the abrasive wear of WC drills in CFRP drilling is the result of both hard and soft abrasion modes [73]. In the hard abrasion mode, the tool is directly abraded by its fractured and dislodged grains and powdery chips as in a 3-body abrasive wear condition. The soft abrasion mode is similar to the wear mode described in Masuda et al. [73].

Thrust force is considered to correlate to the observed tool wear. The experimental studies indicated the thrust force is significantly affected by feed rate, cutting speed and tool wear, and an empirical model was developed [74, 75]. In the same drilling condition, thrust force is proportionally related to tool wear [74, 75].

Faraz et al. [11] introduced cutting edge rounding (CER) as an important tool wear criterion in drilling CFRP composite. The correlations between the CER and the drilling loads and the degree of delamination on CFRP are described.

Compared with uncoated carbide tools, the wear mechanisms of coated tools in CFRP machining are not well understood. Only a few studies [49, 76, 77] have conducted tool wear of the coated tools in CFRP machining, which have shown that only diamond coatings improve tool life. However, the wear mechanisms acting on the coated tools have not been studied comprehensively. The factors that determine the wear resistance of coatings in CFRP machining are still not very clear.

Finally, tool wear observed in wood cutting should also be considered. It shows very similar features to tool wear observed in CFRP machining. Although the hardness and tensile strength of wood fibers were much lower than those of the carbon fibers, the primary tool wear in wood machining is still the edge rounding [78]. Therefore, the edge rounding in CFRP machining may not be due to the high abrasiveness of the fibers.

3.3. The influence of the stagnation zone in edge rounding wear

Tool wear in CFRP machining is quite different than that in conventional metal machining. In conventional metal machining, crater and flank wear were the dominant wear types. In contrast, the primary tool wear type is edge rounding when machining CFRP. The best way to understand the edge rounding wear in CFRP machining might be to discuss the reason for not having edge rounding wear in conventional metal machining.

In metal machining, the continuous chip formation is due to shear deformation [68]. The chip and newly generated work material surfaces slide across the rake and flank surfaces of the cutting tool, respectively. Typically, the edge of a cutting tool, however, is covered by the work material. It is known as the stagnation zone, which protects the cutting edge from the excessive mechanical wear.

In the stagnation zone, the work material does not flow as quickly as the work material flow in the rake and the flank surface [79-83]. Depending on the friction and other parameters during machining, the stagnation zone may either contain a "dead metal" that sticks on the top of the cutting edge, never sliding [79-81] or may contain a stagnation point [82-83]. The work material is being separated around the stagnation point either to form chip or to become the new surface of the work piece.

According to Archard wear equation [18] applicable for both abrasive wear and sliding wear [19], the wear volume is proportional to the sliding distance. Therefore, the stagnant zone on cutting edge will protect the edge in machining metals [84]. For example, Schmidt [84] studied the wear in turning hardened steels with a PCBN tool, which has a blunt cutting edge. The cutting edge of the worn PCBN tool, shown in Figure 3-1, has been divided into five zones. Zone 1 and Zone 5 did not have any tribological contact between work material and chip, and did not show any evidence of wear. Zone 2 and zone 4 contacted the chip and machined surface, which are crater and flank wear, respectively. Interestingly, Zone 3 does not exhibit any sign of wear. This was reported as being due to no relative velocity between tool and work material in zone 3, as shown in Figure 3-2 [82].

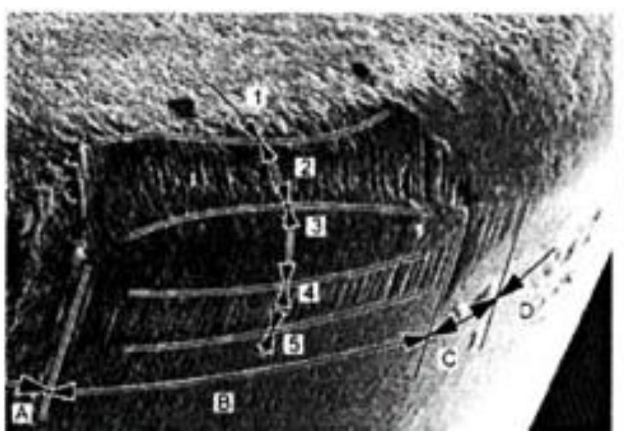

Figure 3-1, Typical wear pattern of a PCBN tool from [84]

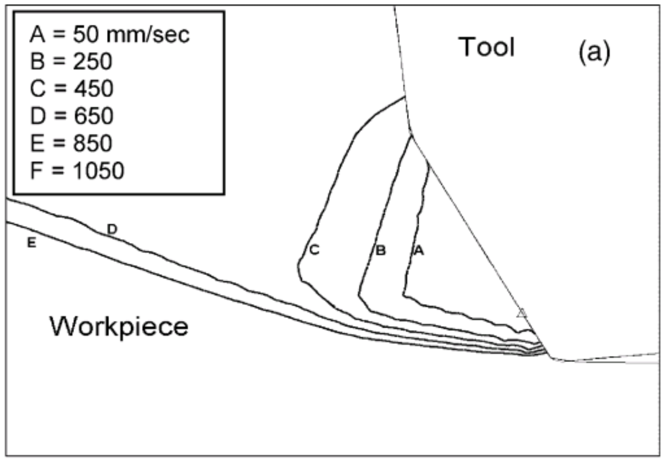

Figure 3-2, Velocity of work material in stagnation zone [82]

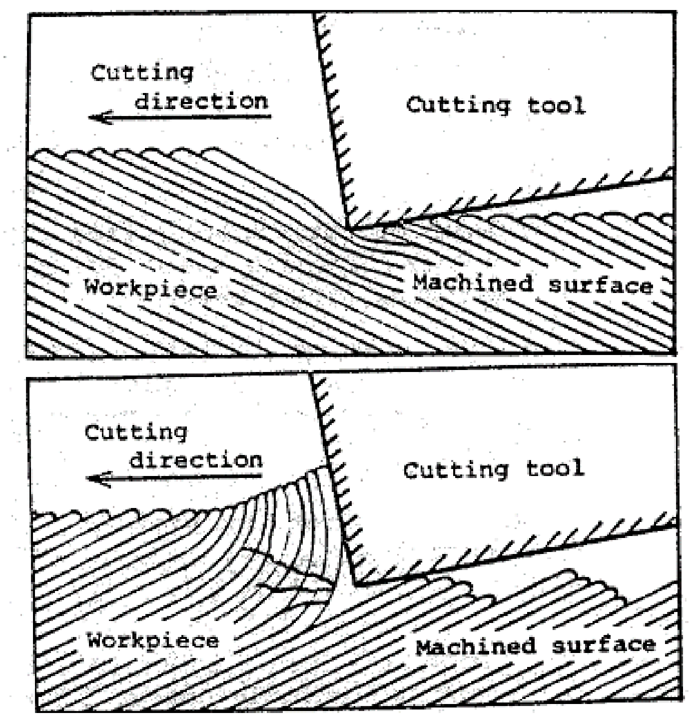

Figure 3-3, chip formation in CFRP machining [10]

The stagnation zone is stable during continuous chip formation, but not stable in other types of chip formation process. In the machining of brittle materials, the chip formation mainly is due to fracture, which generates flank wear and dulling the cutting edge [85]. The chip formation in CFRP machining, shown in Figure 3-3 [10], is dominated by the fracture without any stable stagnant zone. The work material flows around the cutting edge without any disruption, developing into the edge rounding. The protruding shape of the cutting edge makes vulnerable to mechanical wear. After the cutting edge becomes blunt, it cannot efficiently cut the fibers, which increases the cutting force.

3.4. Experimental procedures

3.4.1. Workpiece Material

The CFRP laminates used in the experiment were acquired from the Boeing Company. The composite material consisted multidirectional graphite fibers in an epoxy matrix. The CFRP plate had a total thickness of 7.54 mm with an average ply thickness of 0.1141 mm. The hardness of carbon fiber used in this experiment is reported to be 800-1100Hv.

3.4.2. Uncoated WC-9%Co twist drill and four types of coatings

Uncoated WC-9%Co drill, nano-composite C7 grade (AlTiN grain with Si_3N_4 binder) coated, AlTiN coated, BAM ($AlMgB_{14}$ with TiB_2) coated, and diamond coated WC-9%Co drills were used in this investigation. The BAM coating provided by the Fraunhofer USA is still being refined. It is applied using PVD DC magnetron sputtering, but the exact composition and methods are proprietary to Fraunhofer Inc. There were several studies on the BAM material [86-88]. AlTiN coating was also prepared by Fraunhofer USA. Nano-composite coating and AlTiN coating were prepared by Unimerco, Inc. (Saline, Michigan), and the diamond coated drill was provided by the Boeing Company.

All the drills had the same drill geometry with the outside diameter being 9.525 mm and the flute length being 38.1 mm. The shank diameter was also 9.525 mm and the overall length was 88.9 mm. The drills had the standard configuration with two flutes in a helix angle of 25 degrees and a right hand spiral, right hand cut (RHS/RHC). The drills had a point angle of 135 degrees with a faceted split point per NAS907 P-3. Lastly the base uncoated carbide drill before coating was premium carbide Ultra-Grain® (submicron grain size) with a SmoothGrind® finish. The diamond coating has a thickness of 12.5μm while the nano-composite coating and BAM coating has a thickness of 3.5μm, and AlTiN coating has a thickness of 3μm.

The 2-dimensional profile of cutting edge is measured with confocal microscope as shown in Figure 3-4. The diamond coated drills have a dull edge due to the thick coating. The hardness of coatings and other drill geometries are listed in Table 3-1. The hardness of carbon fiber used in our experiment is 800-1100Hv, which is only half of the hardness of the tungsten carbide.

Table 3-1, Drill geometries and coating hardness and thickness

Tool	Uncoated carbide	Nano-composite	BAM	PCD
Hardness (HV)	2200	3800	5000	8000
Drill diameter (mm)	9.525			
Flute length (mm)	49.15			
Overall length (mm)	100.3			
Web thickness (mm)	0.853			
Major cutting edge length (mm)	5.115			
Point angle°	135			
Helix angle°	28			
Rake angle°	7			
Lip relief angle°	18			
Chisel edge angle°	100			

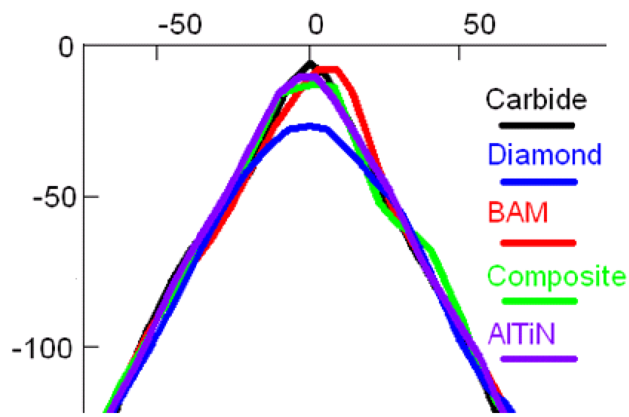

Figure 3-4, Cutting edge 2-D profile of different types of drills (μm)

The drilling experiments were carried out on a 3-axis CNC vertical mill (MiniMill, HAAS, USA). The dynamometer (TRS-1K-OPT-THR, Transducer Techniques, USA) had a fixture mounted on it to hold the CFRP laminates. The CFRP laminates were clamped to the fixture so that the forces generated during drilling is measured by the dynamometer. The measured thrust and torque forces were transmitted to signal amplifiers, then to an A/D board (NI USB-6251, National Instruments NI, USA) and recorded on a personal computer using data acquisition software (LabView 7.1, NI, USA). A spacer plate was put underneath the work material plate. This plate had ½ inch holes in a pattern that matched the holes to be drilled in the work material. Thus, the spacer plate supported the work material during drilling, while also providing a space for the drill to completely pass through the material. The entire experimental step is shown below in Figure 3-5.

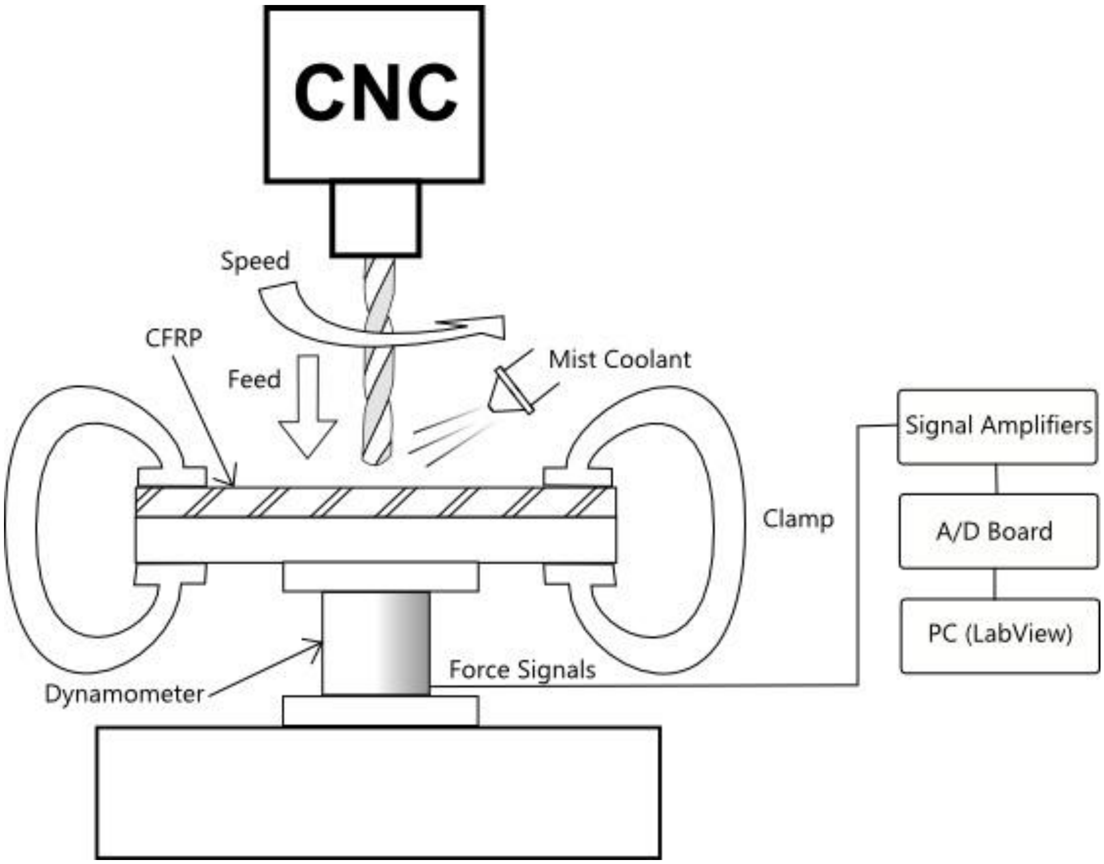

Figure 3-5, Schematics of drilling experimental set up

The drilling experiment condition is fixed for all types of drills; the RPM of 6000 and the feed rate of 0.0762 mm/rev. A water soluble cutting fluid coolant is used in the experiment. The mist coolant has a constant flow rate at 16mL/min. The drilling experiments were conducted until each drill produced 80 holes.

3.4.3. Wear evolution analysis

A number of instrument and techniques is used to measure tool wear. The confocal microscope accurately provides the profile information of the worn cutting edges. In addition, the Scanning Electron Microscope (SEM) is used to provide the high magnification pictures of the wear pattern.

Tool wear is measured after drilling the first 10 holes and subsequently after drilling every 20 holes. The tool wear profiles measured after drilling helps us to observe and analyze the progress of tool edge rounding. The 2-D profile is consistently measured at the location 300 micrometer from outer surface for all drills, shown in Figure 3-6. The wavelet filtering is used to eliminate the noise and artifacts inherent to the height encoded image obtained by the confocal microscope [45].

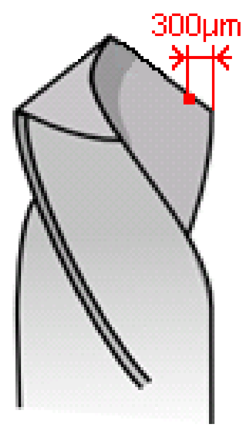

Figure 3-6, Location of the 2-D profile measured

The wear volume (per unit length) for a consistent location on the various drills was measured using the confocal images by subtracting the worn 2D profile of the tool from the original 2D profile of the tool and subsequently multiplying a unit length. The phrase 'wear volume per unit length' will be simplified as 'wear volume' in the following chapters.

Because the coating thickness was known in priory, the coating wear rate of the coated drills was calculated by separating the total wear volume into the wear vol. of the coatings and the carbide substrate. In order to simplify the name of the different types of drills for the different types of drilling conditions, the uncoated, diamond coated, BAM coated, nano-composite coated and AlTiN coated drill were named as "K", "L", "M", "N", "P" respectively, and the CFRP-only, Ti-only and CFRP/Ti stack drilling processes were named as “C”, “T” and “S”, respectively. For example, the uncoated carbide drill in CFRP-only drilling was named “KC”, and the diamond coated drill in Ti-only drilling was named “LT”.

3.5. Results and discussion

3.5.1. Drilling forces

The maximum drilling thrust force and torque as a function of hole number are shown in Figure 3-7. As more holes are made, the thrust force increases due to the wear on the drills. As shown in Figure 3-7(a), the thrust force on the diamond coated-drill slightly increases with the number of holes drilled. The thrust force on other four types of drills steadily increased to more than twice after drilling 80 holes. This comes from the fact that the larger edge rounding occurring on both uncoated and AlTiN coated drills compared with the diamond coated-drill.

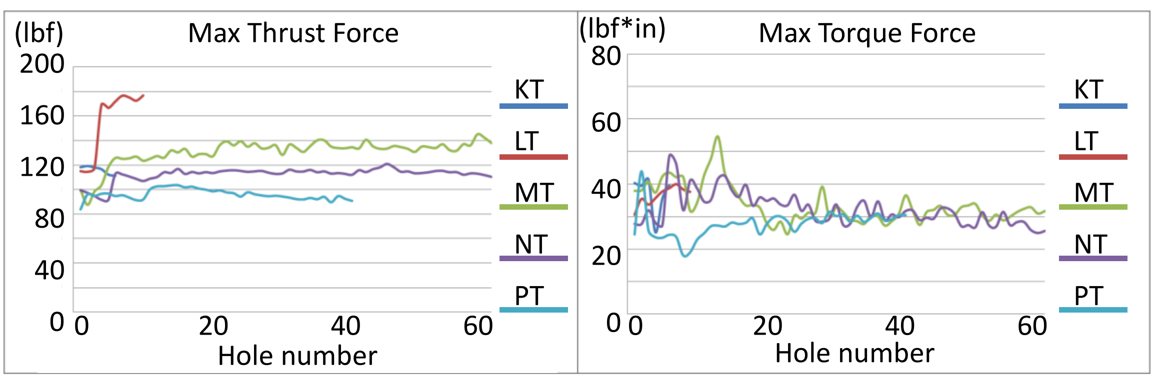

Figure 3-7, Changes in drilling forces vs. hole number

Similar to the thrust force, the torque also increases with hole number due to tool wear. Interestingly, the diamond coated-drill showed that the torque decreased up to hole 50 and subsequently increased, as shown in Figure 3-7(b). This may come from the reduction in friction as the rough surface of the diamond coated drill at the beginning worn down to be smoother. The torque increased as more holes are drilled for other four types of drills.

3.5.2. Tool wear in uncoated WC-Co drill

The progression of tool wear is visible in the SEM images. Figure 3-8 shows a sharp edge of the fresh uncoated drill before drilling. Subsequent images in Figure 3-8 show a rounded tool edge with the increase in hole number. No chipping or micro fracture were observed.

The 2-D profiles from the confocal microscopy of the flank surface of the uncoated carbide drill show that edge rounding is the primarily cause of tool wear. This can be seen in Figure 3-9. The wear volume at different hole numbers are shown in Table 3-2.

Table 3-2, Wear volume on the uncoated and coated drills

Wear vol. (μm^2)	10 holes	20 holes	40 holes	60 holes	80 holes
Uncoated	117.1	257.5	427.4	641.3	846.4
coating	0	0	0	0	0
substrate	117.1	257.5	427.4	641.3	846.4
Diamond	15.0	27.5	48.6	71.5	93.9
coating	15.0	27.5	48.6	71.5	93.9
substrate	0	0	0	0	0
Composite	155.1	359.0	579.8	761.3	983.4
coating	132.6	204.9	257.2	268.1	393.3
substrate	22.5	154.1	322.6	493.2	590.1
BAM	129.6	325.0	616.8	1015.6	1407.0
coating	115.5	222.8	339.9	499.1	599.3
substrate	14.1	102.2	276.9	516.5	807.7
					76 holes
AlTiN	182.3	353.6	599.1	824.0	976.9
coating	133.5	245.5	299.4	405.4	491.6
substrate	48.8	145.7	299.7	418.6	485.3

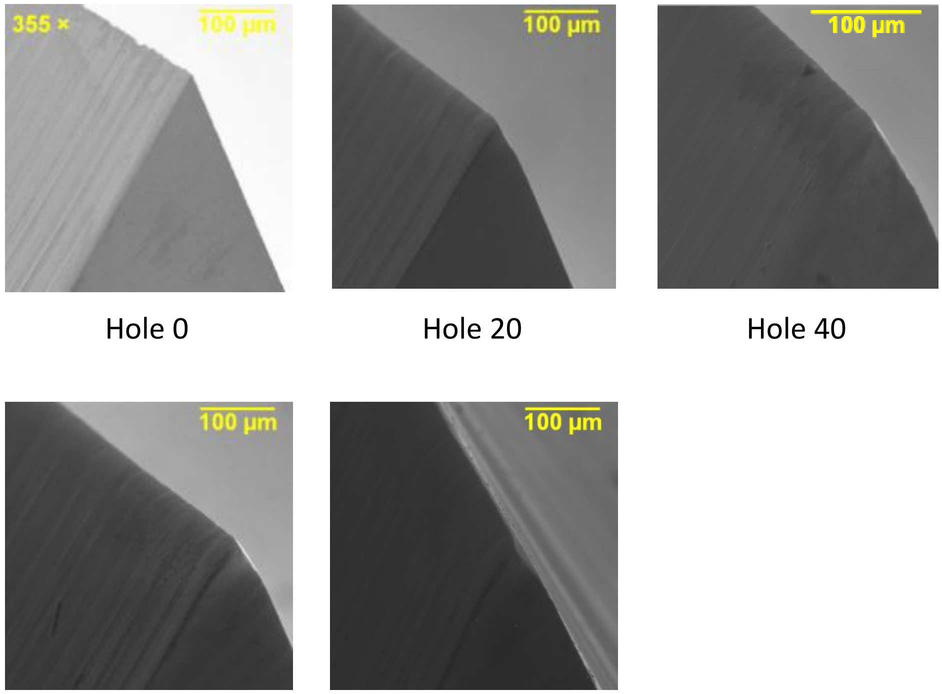

Figure 3-8, SEM pictures of uncoated carbide drill margin

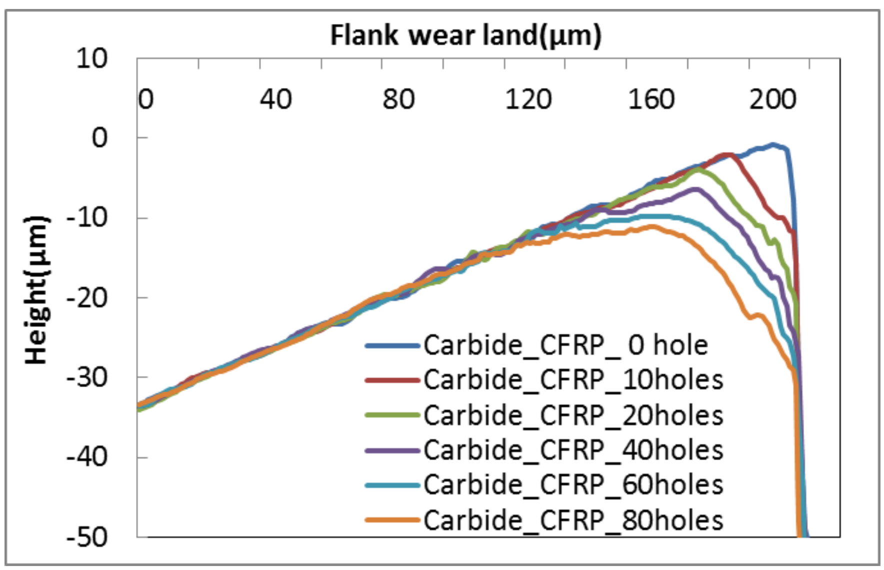

Figure 3-9, The flank surface profile of uncoated carbide drill (µm)

An SEM image of the worn surface of an uncoated carbide drill cutting edge at the magnification of 10,000 is shown in Figure 3-10 and Figure 3-11.

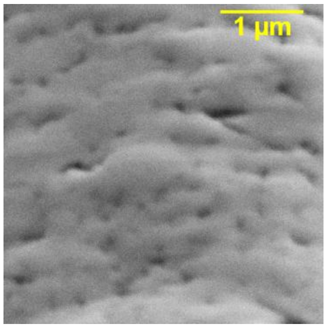

Figure 3-10, The primary appearance of worn uncoated carbide surface

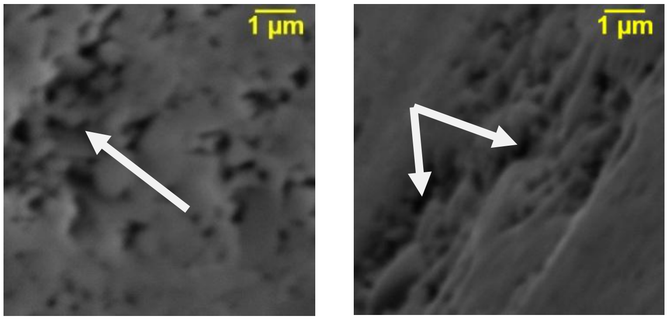

Figure 3-11, Spots (a) rake surface (left) and (b) flank surface (right) showed carbide grain dislodging

It is shown that the black dots indicated the Co binder removals, exposing carbide grains. Carbide grain dislodging was observed on both the flank and the rake surfaces as shown in Figure 3-11 (a) and (b). Soft Co binders were removed during drilling and many carbide grains seemed to be pulled out from the tool surface.

3.5.3. Tool wear in nano-composite coated drill

Figure 3-12 shows the cutting edge of the nano-composite coated drill. The cutting edge became dull and the coating on the flank surface gradually wore as the drilling process progressed.

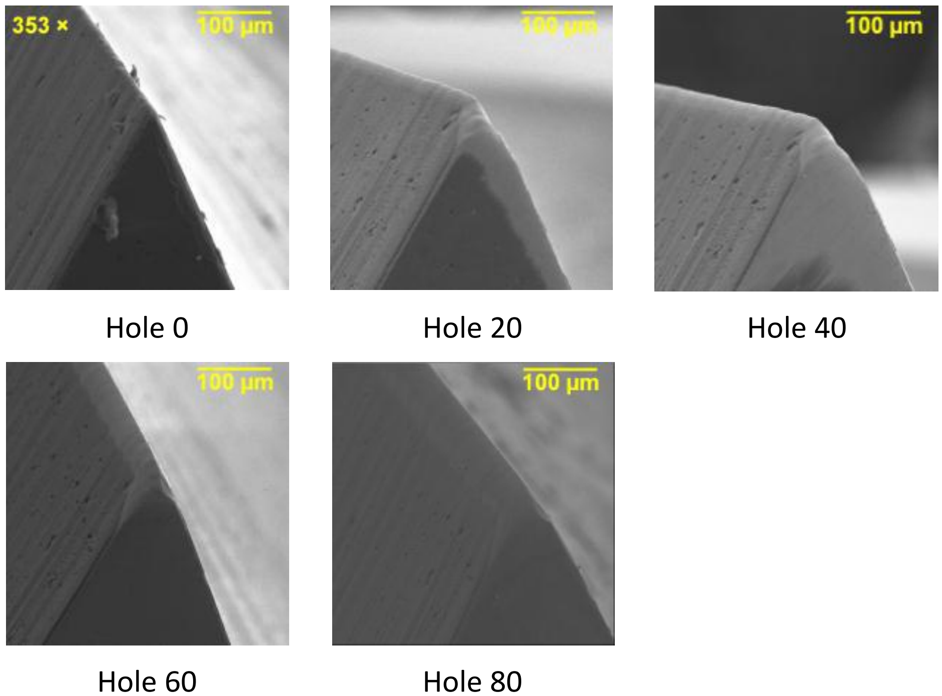

Figure 3-12, SEM pictures of nano-composite drill margin

The cutting edge profile of the nano-composite coated drill is shown in Figure 3-13. Figure 3-14 shows a transition area of a nano-composite coated tool on the flank surface. The carbide substrate was exposed in the upper right of the figure, and the coating remained unworn in the bottom left. The worn surface of the nano-composite coating marked by the arrow between these two regions was flat and has a color gradient. The deeper color was from the nano-composite coating and gradually changed to a whiter color from the carbide substrate. Therefore, the nano-composite coating was gradually worn in the transition area.

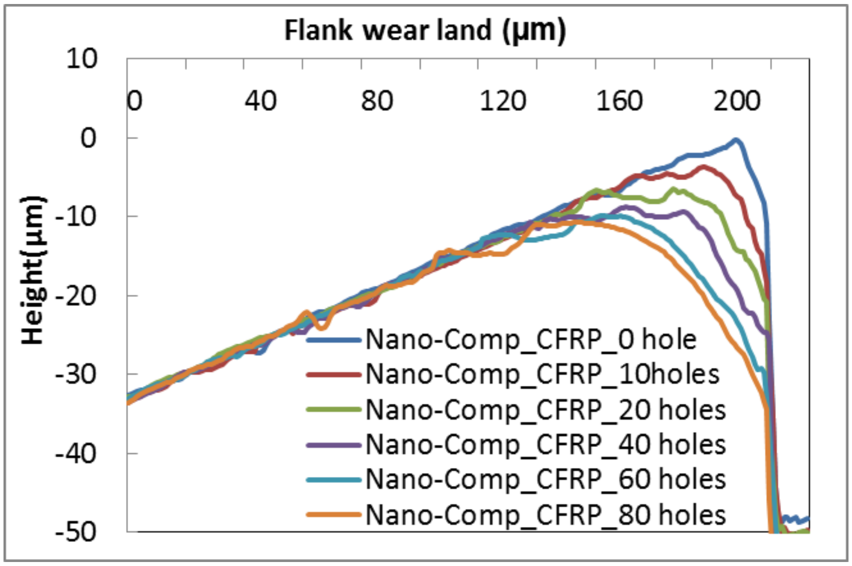

Figure 3-13, The flank surface profile of nano-composite drill (µm)

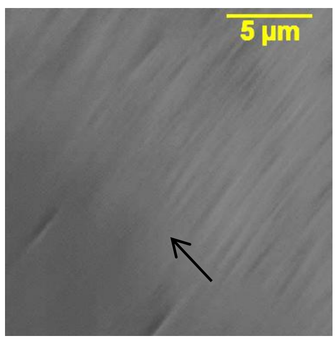

Figure 3-14, The transition area of nano-composite coated tool in the flank surface

The wear volume at different hole numbers are shown in Table 3-2. The nano-composite coating did not alleviate the dulling of the edge. After the thin nano-composite coating was worn down, the tungsten carbide substrate was exposed, which finally caused similar edge rounding wear as seen with the uncoated carbide drills.

3.5.4. Tool wear in BAM coated drill

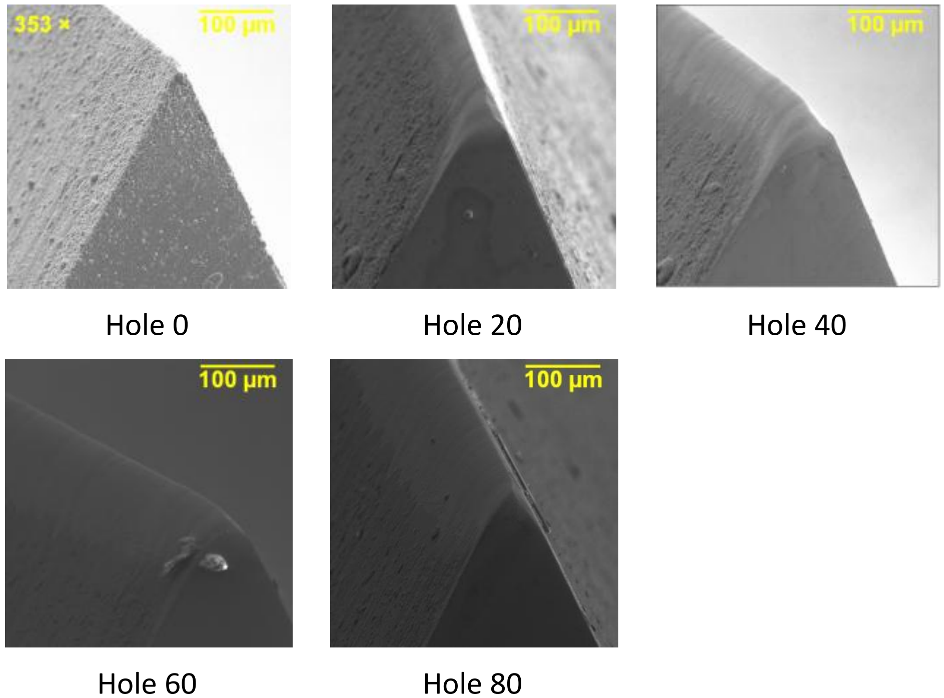

Figure 3-15, SEM pictures of BAM drill margin

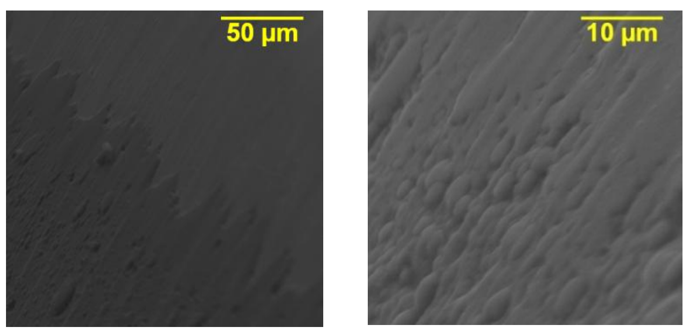

(a) Flank face at 80 holes

(b) BAM coated new surface

Figure 3-16, Flank surface at 80 holes and new surface of BAM coated drill

The BAM coated drills, which are shown in Figure 3-16 (b), have a relatively rough surface compared with the other drills. The average roughness of the profile (Ra) of the BAM coating was about 0.5µm, while the other coatings all have the Ra smaller than 0.1µm.

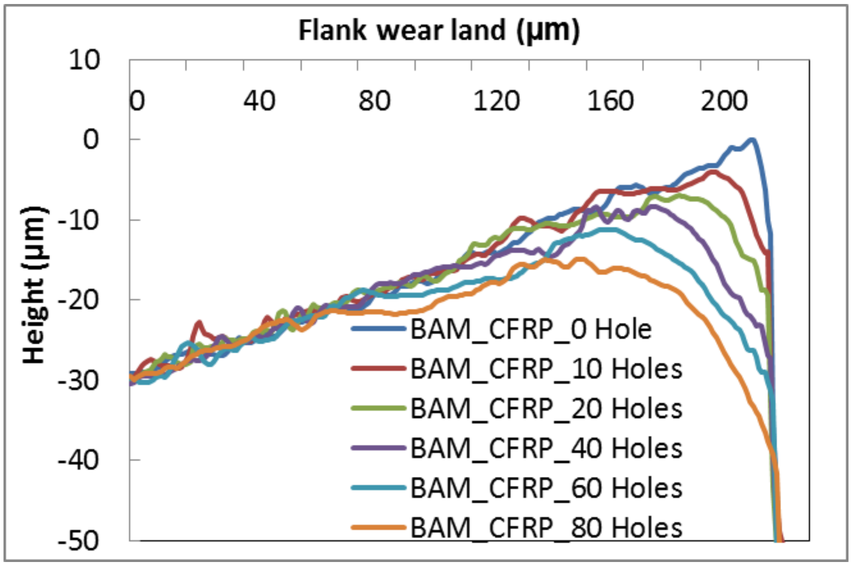

Figure 3-17, The flank surface profile of BAM coated drill (µm)

The thickness of the BAM coating was 3.5µm. Figure 3-17 shows that the BAM coating at the cutting edge was already worn down after the first 10 holes. In addition, the carbide substrate was exposed on the surface. Edge rounding was still the primary wear on the BAM coated drill. The wear were separated in two categories: wear of the carbide substrate and wear of the coating. This was calculated for each of the recorded hole numbers in Table 3-2.

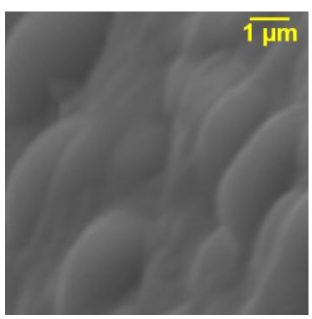

(a) Un-worn area

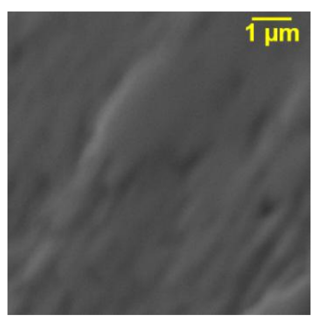

(b) Worn area

Figure 3-18, The unworn and worn area of BAM coating

Figure 3-18 shows the appearance of a typical unworn and worn BAM coating. The roughness on the original, unworn coating was gradually reduced in the machining. The BAM coating, despite its high hardness, wore quicker than the carbide substrate. Therefore, the BAM coating did not protect the carbide substrate from wear. One of the possible reasons for the increased wear was the rougher surface of the BAM coating from the coating process as compared to that of the other drills. The poor surface finish of the BAM coating could be easily attacked by the concentrated stress during machining.

3.5.5. Tool wear in diamond coated drill

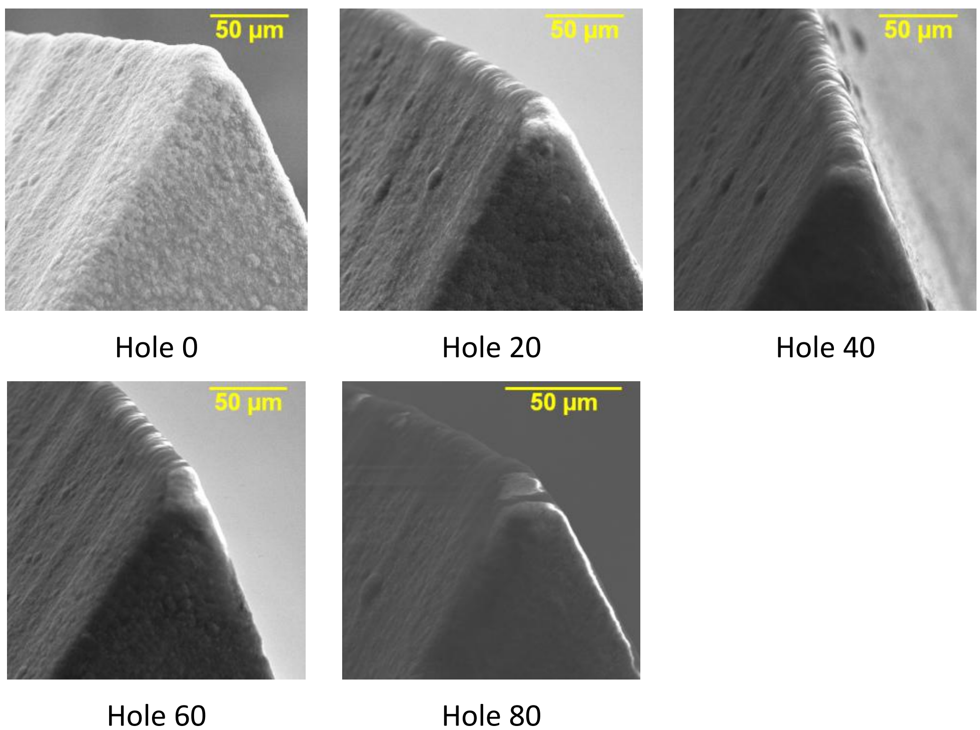

Figure 3-19, SEM pictures of diamond drill margin

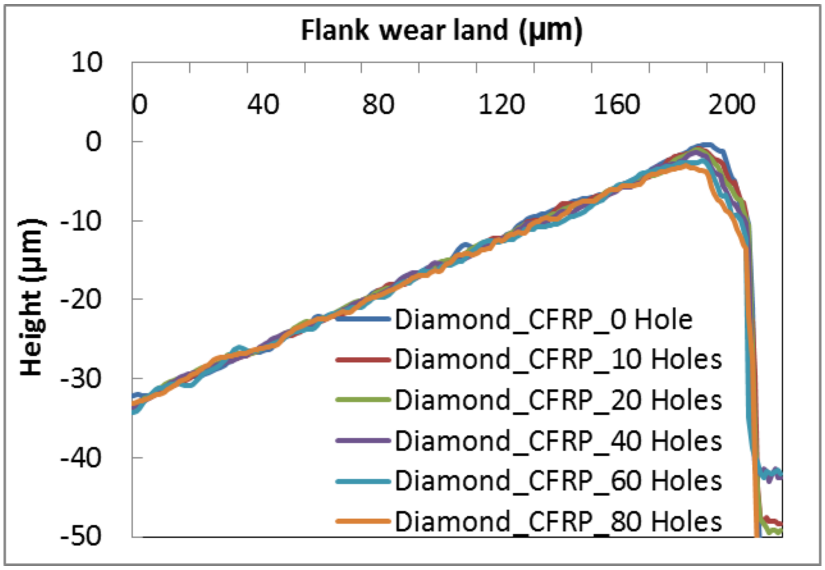

Figure 3-20, The flank surface profile of diamond coated drill (μm)

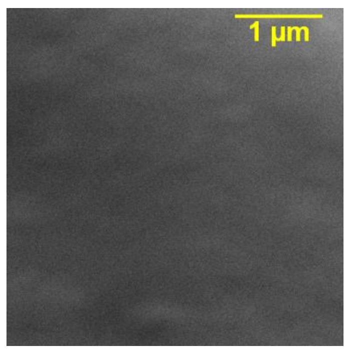

Figure 3-21, The diamond coating on the worn area. The diamond coating had shown a flat surface.

Figure 3-19 and Figure 3-20 show that the cutting edge of the diamond-coating was still sharp even after drilling 80 holes. Although the diamond coating flaked off in some areas after 40 holes, the diamond-coated drill, where the coating remained intact, still represented the best performance among all of the drills tested in this experiment in the areas. The wear volume on the diamond coated drill is shown in Table 3-2. All the wear represents the wear of the diamond coating, because the carbide substrate was not exposed at the measuring cross section at 80 holes. The worn edge surface of the diamond coating was flat, which indicated the minimal gradual wear only occurred. There was no sign of fracture or grain pullouts.

3.6. Tool wear in the AlTiN coated drill

Figure 3-22 shows the cutting edges of the AlTiN coated drill. The cutting edge became dull and the coating on the edge and flank surfaces was gradually worn as the drilling process progressed. There was no sign of flaking or chipping.

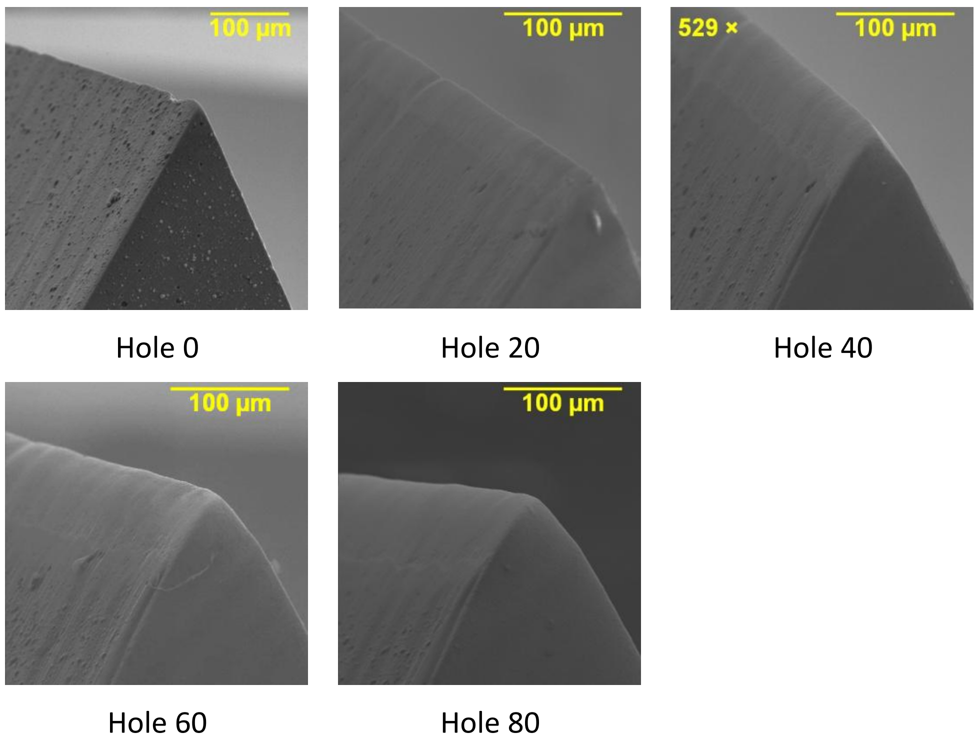

Figure 3-22, SEM pictures of drill margin on the AlTiN coated drill

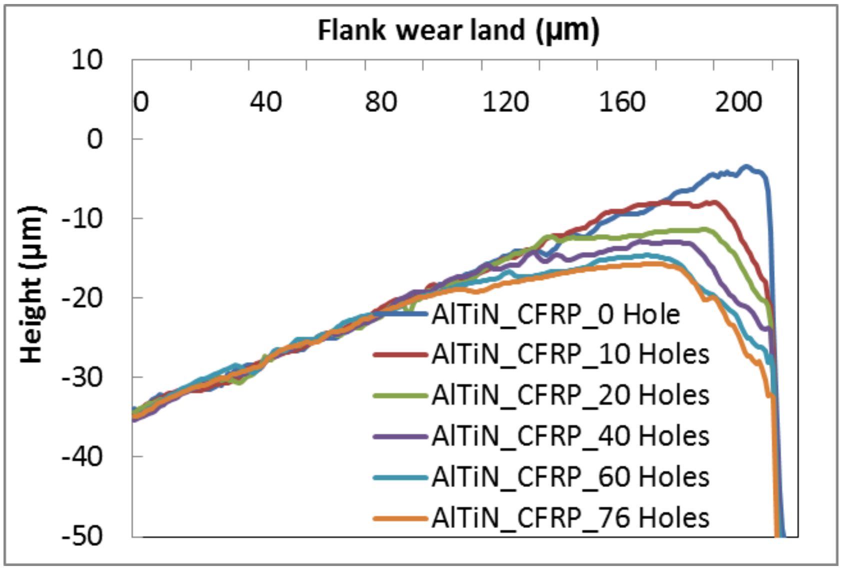

Figure 3-23, The cutting edge profile of AlTiN coated drill(μm)

The cutting edge profiles of the AlTiN coated drill are shown in Figure 3-23. The profiles were measured every 20 holes. The 76th hole profile was measured for AlTiN-coated drill instead of the 80th hole, due to accidental damaged to the drill that was not the results of wear from machining occurred after 76 holes.

It is noted that tool material removal in the flank surface was observed in the AlTiN coated drill. This might be due to the oxidation. Oxidation of the Ti-based coating has been reported as an important wear mechanism [89, 90]. TiO_2 and Al_2O_3 resulted from oxidation of the AlTiN coating are softer than AlTiN. This led to rapid wear of the coating. It was also reported that micro-chipping of the AlTiN coating may generates wear debris, which abrades the coating from subsequent sliding on the AlTiN coating and generate flank wear [90].

3.7. Discussions of tool wear in drilling CFRP

The blunting of the cutting edge occurred on all of the drills tested in this study. The appearance of the worn surfaces of the coated and the uncoated carbide drills all showed gradual wear. The diamond coating flaked off on few isolated locations, which was not a primary limitation on the drill life. The total wear volume, for both coating and substrate, on each of the drills is presented in Figure 3-24. The wear volume was quite linear with the hole number for all drills. The wear volume for the coatings and the carbide substrate on the coated drills were calculated separately based on the cutting edge profile, which enable us to calculate the relative wear rates of coatings comparing with uncoated carbide drill, as presented in Equation (3-1),

$$C = \frac{V_c}{V_u - V_s} \qquad (3-1)$$

where C is the relative wear rate of coating on the coated drill comparing with the uncoated carbide drill, V_u is the wear volume of uncoated drill, V_c is the wear volume of coating on coated drill and V_s is the wear volume of carbide substrate on coated drill.

The wear measurement results are presented in Table 3-3. It is evident that the diamond coated drill was superior to all other drills, as the wear volume was only about one tenth of the uncoated drill. The other coated drills exhibited higher wear rate than the uncoated drill. Since the total wear rate of the BAM, nano-composite and AlTiN coating was higher than that of the substrate itself, it can be concluded that these coatings did not protect the drill from tool wear.

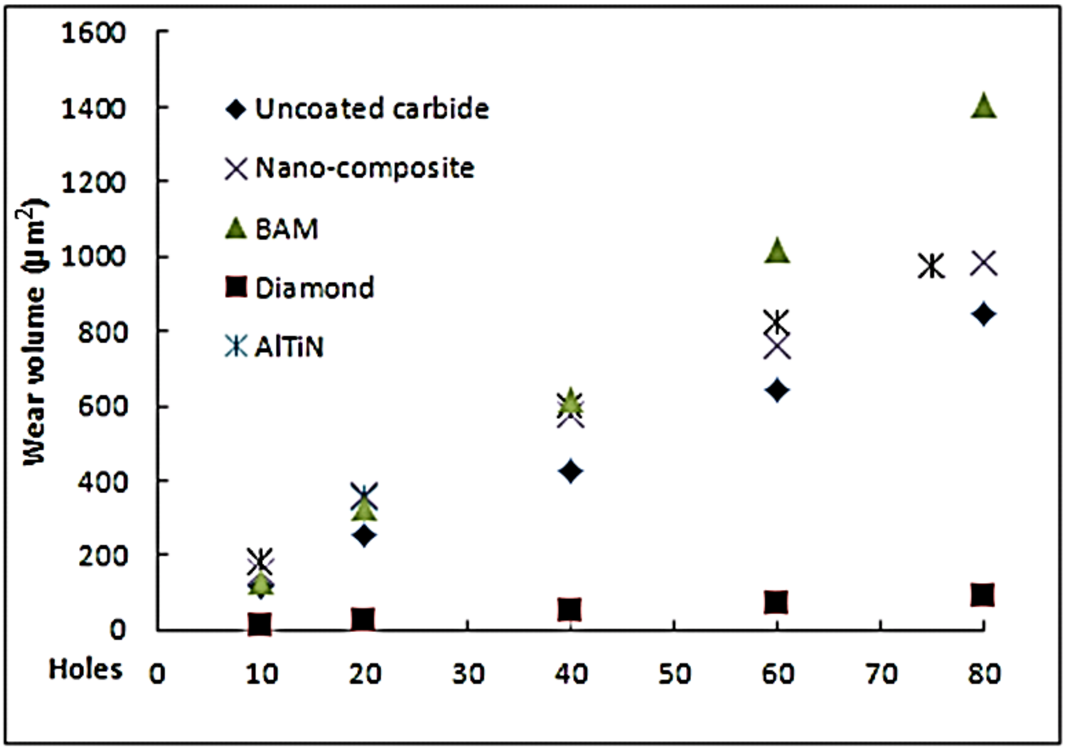

Figure 3-24, Total wear volume of the drills vs. hole numbers

Table 3-3, Wear volume on the substrate and the coatings at 60 holes

Wear vol. (µm²)	Total	Substrate	Coating	Relative wear rate of coatings
Uncoated	641	641	0	1
Diamond	71	0	71	0.111
BAM	1015	516	499	3.992
Composite	761	493	268	1.811
AlTiN	824	419	405	1.820

In the wear process in CFRP drilling, the carbon fibers are cut by the cutting edge of the tool. The broken carbon fibers abrade the cutting edge of the drills. This process may generate abrasive wear or sliding wear. The wear mechanism that dominates the process was depends on the way that wear debris were generated. If the wear debris was mainly generated by the work material cutting the tool material by plastic deformation the abrasive wear mechanism will be the dominated wear mechanism. If the wear debris was mainly generated by micro-fracture, or dislodging of tool material particles by fatigue, chemical reaction or adhesion the sliding wear mechanism will be the dominated wear mechanism.

Abrasive wear is produced by a hard particle or protuberance plowing a groove in a softer surface, which results in the removal of material from the softer surface. Since the abrasive wear rate depends directly on the penetration depth beneath the softer wear surface, the hardness ratio between abrasives and tool is a decisive parameter in predicting the abrasive wear rates on the tool.

The 2-body abrasive wear equations usually applied in the situation that abrasives are harder than the tool material. The 3-body abrasive wear equations include the situation that abrasives are softer than tool material, are presented in Chapter 1.2.2. The 3-body abrasive wear is dramatically reduced when the hardness ratio between the tool material and the abrasive exceeds 1.25.

Based on the hardness of the coatings and the carbide substrate, the relative abrasive wear rates on the uncoated, the diamond coated and the AlTiN coated drills, predicted by Equation (1-3), are shown in Table 3-4. As discussed, the primary wear mechanism in CFRP drilling is likely abrasive wear or sliding wear. In Table 3-4 the relative wear rates from the drilling experiments shown in the last column are compared with the relative abrasive wear rates in the third column on Table 3-4.

Table 3-4, Abrasive wear rate and sliding wear rate of the coatings [24]

	Hard-ness at 25°C (GPa)	Relative abrasive wear rate from the theory[30]	Relative sliding wear rate from tribo-meter test (dry)	Relative sliding wear rate from tribo-meter test (oil)	Relative wear rate from CFRP drilling
Uncoated carbide	26	1	1	1	1
Diamond	70	0.007	0.106	0.088	0.111
BAM	43	0.078	5.689	5.230	3.992
Composite	45	0.037	1.953	2.634	1.811
AlTiN	40	0.113	2.042	2.433	1.820

As shown in Table 3-4, the predicted abrasive wear rates on the coatings are much lower than those on the uncoated carbide due to the higher hardness of the coatings. Therefore, abrasive wear cannot be considered as the main wear mechanism. In CFRP machining, with high speed steel tools, abrasive wear has been reported as a dominating wear mechanism [91]. However, the WC/Co and the other hard coatings have much higher hardness than the high speed steel tools, which greatly reduced the abrasive wear.

Sliding wear refers to the wear resulting from sliding between two surfaces without the formation of significant wear debris by cutting, which is a typical trait of abrasive wear [22, 92]. Sliding wear is considered to be the combination of various wear mechanisms such as adhesion, delamination, oxidation and fatigue [22]. Many possible wear modes of sliding wear have been reported exist for uncoated carbide [52], diamond coating [93-95], and AlTiN coating [96]. It should be noted that the abrasion from the dislodged hard particles from the tool material generates tool wear. The amount of the dislodged hard particles generated during sliding is different depending on the cutting tool material. The resistance of the tool material dislodging into wear debris is typically considered as one of the sliding wear resistances.

Because sliding wear occurs in multiple modes, one tool material can have substantially different wear resistance depending on the sliding wear mode(s) present. The tool wear modes in CFRP machining are dominated by fatigue-induced micro-fracture and grain dislodging, oxidation and the abrasion by wear debris. To correlate sliding wear with tool wear in the CFRP machining, the wear mode in sliding wear test needs to be the same wear mode in CFRP machining. The important conditions of CFRP machining, which related with the tool wear mode, is defined as,

(1) The CFRP did not contain any inclusions that were harder than the tool material.

(2) The mechanical loading on the cutting tool fluctuated due to the property difference between the carbon fiber and plastic matrix.

(3) The temperature in CFRP machining was relatively low.

(4) Chemical reaction between CFRP and the coated and uncoated carbide cutting tools materials did not occur.

(5) The mist coolant used in the drilling experiment cannot reach the intimate tool-work material contact area. Thus, this area is considered as dry machining.

Despite of numerous investigations, the inherent complexity of the sliding wear has prevented the development of a commonly accepted equation and cannot be directly predicted based on simple material properties. Instead, a series of ball-on-disk tribo-meter tests is implemented for sliding wear test. Thus, we have been conducted on a CSM tribometer between a WC/6%Co ball and the tool materials used in the CFRP drilling experiment. Although the tribo-test conditions and the CFRP drilling conditions were substantially different, the tribo-tests satisfy at least the five specified conditions given above.

The experiment parameters in the tribo-meter included a load of 10N and a disk speed of 2.5m/s over 10000 cycles. After the test, the wear tracks of each coating were measured using a DEKTAK D6M surface profiler. The wear volume of the sample was evaluated according to the cross-sectional area of the wear track multiplied by the length of the wear track. The wear rate was computed from the total wear volume divided by the total sliding distance. Finally, the relative wear rates from the tribo-meter tests were included in the last column of Table 3-4.

The relative sliding wear rate for the tribo-meter tests in Table 3-4 indicated that the wear rate of the diamond coating was approximately 10% of that of the uncoated carbide while the wear rate of the AlTiN coating was nearly twice that of the uncoated carbide. The wear rates from the tribo-meter tests correlated well with the results from the CFRP drilling experiments. The coating with the better wear resistance in the tribo-test also performed better in the CFRP drilling. The tribo-test results reported by other authors using similar conditions (wear during contact with a softer pin or ball) also showed that the diamond coating had better wear resistance than the uncoated carbide during sliding contact [97-99] while the AlTiN coating had a poor wear resistance [90], even lower than the uncoated carbide [96]. Despite of the variations in the relative wear rates of various materials, the rank of the wear resistance of the materials was relatively consistent. This verified our assumption that the wear mode in tribo-meter tests, which are carried out under certain specified conditions, may show the same wear mode as in CFRP drilling. Therefore, the economical tribo-test can be used to evaluate prospective tool materials before carrying out expensive CFRP drilling experiments. For example, in Chapter 4, the TiCN coating showed about 5 times better wear resistance than the uncoated carbide in the tribo-meter tests. This would make the TiCN coating a suitable candidate for drilling CFRP. Unfortunately, no reports on the tool life of TiCN coatings in CFRP drilling were found in the literature. However, it has been reported that for milling of carbon fiber composite, a TiCN coated carbide mill bit had 3 times more tool life than an uncoated carbide mill bit [100]. In addition, the soft CrN coating with poor abrasive wear and erosion wear resistance [101] yields relatively good (tribo-meter) sliding wear resistance [102]. It was reported that the CrN coated carbide drill has showed excellent 850 holes in Ti/CFRP/Ti drilling [103], and 4 times more tool life compared to the uncoated carbide drill in machining wood [104]. These related evidences showed strong support of our hypothesis that tribo-meter testing may be used to rank prospective tool materials. It also gave us confidence that the right coating material may substantially increase the tool life in CFRP machining.

However, it still needs to be noted that certain conditions, such as load and speed in the tribo-meter tests, were quite different from the conditions in the drilling experiment. The tribo-meter results may show some difference if these conditions are changed. Thus, further studies may be needed to design and run the tribo-meter tests in conditions that reliably approach the actual drilling conditions.

3.8. Summary of tool wear in drilling of CFRP

The performances of uncoated, BAM coated, diamond coated, nano-composite coated and AlTiN coated carbide (WC-Co) drills when drilling CFRP were investigated in terms of tool wear and drilling forces.

The edge rounding wear was the main wear type in all types of the drills used. A hypothesis was developed to explain the edge rounding wear in CFRP machining. Due to the fracture-based chip formation of CFRP, the stagnation zone at the cutting edge, which normally prevents the edge wear in metal machining, does not exist. Wear accelerates to result in the edge rounding wear. The diamond coating significantly reduced the edge rounding wear while the other coatings did not protect the drill during machining.

The tool wear measurements in CFRP drilling experiments did not match the abrasive wear resistance of the drill materials. However, the tribo-meter tests, which followed several specified conditions, such as contact with a softer pin or ball, etc., gave that results correlated well with the drilling tool wear results. Therefore, the tribo-meter test, which cost very little, can be used to test the tool material before carrying the expensive CFRP drilling experiment.

Chapter 4. Sliding wear and friction of Ti-based coatings in tribo-meter test

4.1. Introduction

As described in Chapter 3, the relative tool wear rate in CFRP drilling has been found to correlate with the relative wear rate in the tribo-meter testing under specified conditions. Since the tribo-meter test was much cheaper than the CFRP drilling, various Ti-based coatings have been tested in the tribo-meter test in this study in order to find more suitable candidate coating materials for CFRP drilling.

The Ti-based coatings, which included TiC, TiN, TiCN, and AlTiN, have good abrasive wear resistance and are relatively cheap compared with diamond and Cubic Boron Nitride (CBN) coatings. This explains their popularity as the coatings for cutting tool field. For the substrate material, WC/Co is one of the most widely used cutting tool materials. In manufacturing industries, the tool life of coated and uncoated WC/Co cutting tool were often been compared to evaluate the efficiency of the coatings. This study was aimed at testing the sliding wear resistance and the friction behavior of the Ti-based materials. The wear rate of WC/6%Co has also been tested as an evaluation standard to rank the wear resistance of the Ti-based materials.

4.2. Experiment setup and procedure

The tribo-meter tests were conducted using a ball on disc CSM Instrument tribo-meter. The ball used was a 6.34mm-diameter WC/6% Co ball. Three types of coatings (AlTiN (Al:Ti=3:2), TiN and TiCN) with carbide substrate and two types of cements (TiC/20%WC and WC/6%Co) were used as the disc materials. The AlTiN was acquired from Franhofler USA, Other four types of materials were acquired from Sandvik Inc.

The experiment was carried out under dry, water and oil lubricated conditions. The oil used in this study was a vegetable oil (Unist, Inc., Grand Rapid, Michigan). As described in Chapter 3.7, the dry and oil lubricated conditions are most similar to the conditions in CFRP drilling. The reason that the tribo-test conditions have also included water as a lubricant was to help us to understand the changes in the sliding wear for different conditions.

Other parameters that were fixed in the tribo-meter tests were a load of 10N, a speed of 2.5cm/s, and a wear track length of 6cm. The total sliding cycles for each test was 10000 cycles. The friction coefficients were obtained from the tribo-meter. In addition, the sliding wear volume was acquired from a profiler-meter. The sliding wear rate was calculated by dividing the wear volume by the total sliding distance and load.

4.3. Experiment results and analysis

4.3.1. Sliding wear rate and average friction in tribo-meter test

Table 4-1, The sliding wear rate of materials in tribo-meter test

Disc material	Dry $10e\text{-}7mm^3/Nm$	Water $10e\text{-}7mm^3/Nm$	Oil $10e\text{-}7mm^3/Nm$
TiN	2.26	1.12	1.48
TiC/20%WC	2.46	3.41	1.76
TiCN	0.27	0.08	0.16
AlTiN	2.84	3.19	1.99
WC/6%Co	1.39	1.07	0.99

The sliding wear rate results of TiN, TiCN, AlTiN, TiC/20%WC, and WC/6%Co in dry, water and oil lubricated conditions are shown in Table 4-1. Although the wear rates have some variation among the different lubrication conditions (especially in water lubricated condition), but the rank of relative wear rate does not substantially change. The TiCN coating showed a much lower wear rate compared with uncoated carbide in all three conditions, and at the same times, other Ti-based materials showed a higher wear rate than uncoated carbide in all three lubrication conditions. The friction coefficients data are shown in Figures 4-1.

Hsieh [90] studied the friction and sliding wear of Ti-based materials under dry conditions and concluded that the AlTiN had a higher friction coefficient and thus had a higher wear rate and that the TiCN and TiN had low friction coefficient, thus had a lower wear rate. In manufacturing industries, it is usually believed that the role of friction found in tribo-testing may only have a minor effect in real machining. Thus, the TiCN coating, which had a lower wear rate in the tribo-test due to its low friction, may not work as well as AlTiN coatings for real machining conditions. However, our experimental results do not support the relation between high friction and high wear rate when comparing between the different materials. For instance, for the oil lubricated condition, TiCN, TiN, TiC/20%WC and AlTiN coatings all had stable and low friction, however, the AlTiN coating still had most wear than the other coatings. Specifically, AlTiN coating had more than 10 times the wear of the TiCN coating. Thus, the sliding wear rate may depend much more on other properties than friction. Those properties affect the wear rate in both the tribo-test and machining. Therefore, the sliding wear resistance of the Ti-based coatings in the tribo-test may still be useful to rank the coating materials for machining. However, it is still interesting to understand the cause of the great difference in the friction of the Ti-based materials for the different lubricated conditions during the tribo-test, which is presented in the next section.

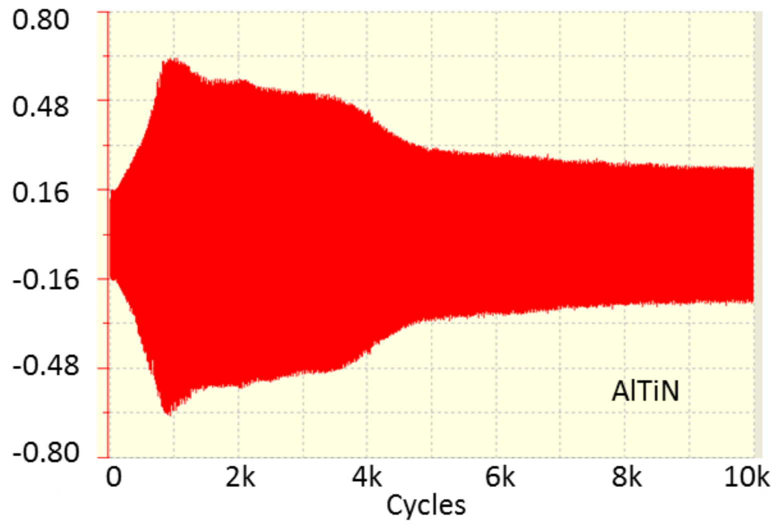

(a) AlTiN-Dry

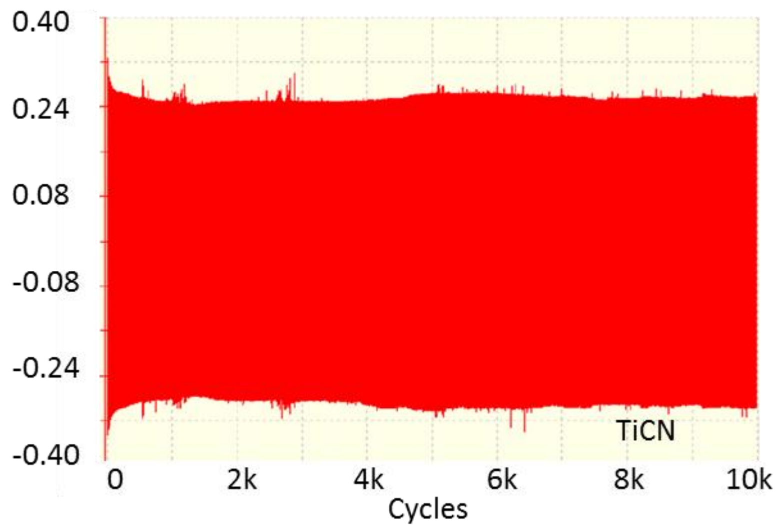

(b) TiCN-Dry

Figure 4-1, Friction of AlTiN, TiC/20% WC, TiN, WC/6%Co and TiCN in dry, water and oil lubrication conditions

Figure 4-1 (cont'd)

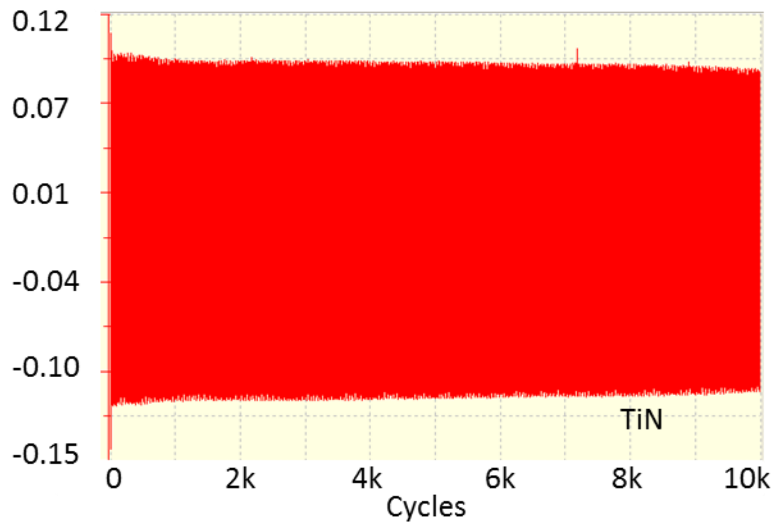

(c) TiN-Dry

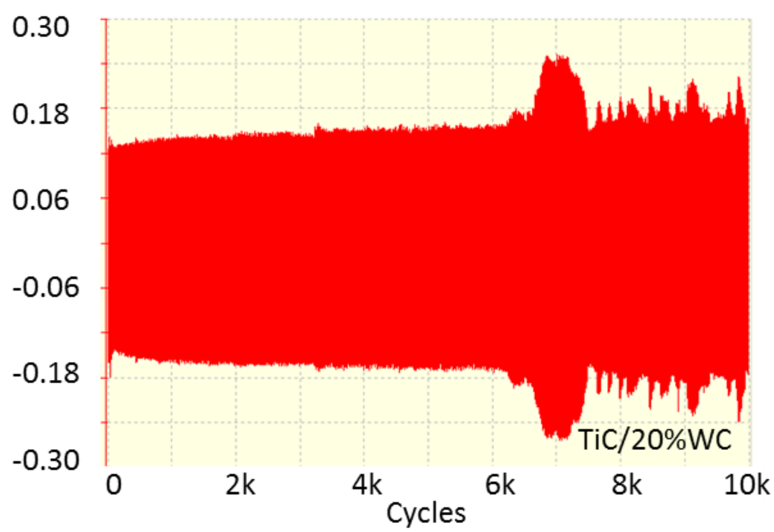

(d) TiC/20%WC-Dry

Figure 4-1 (cont'd)

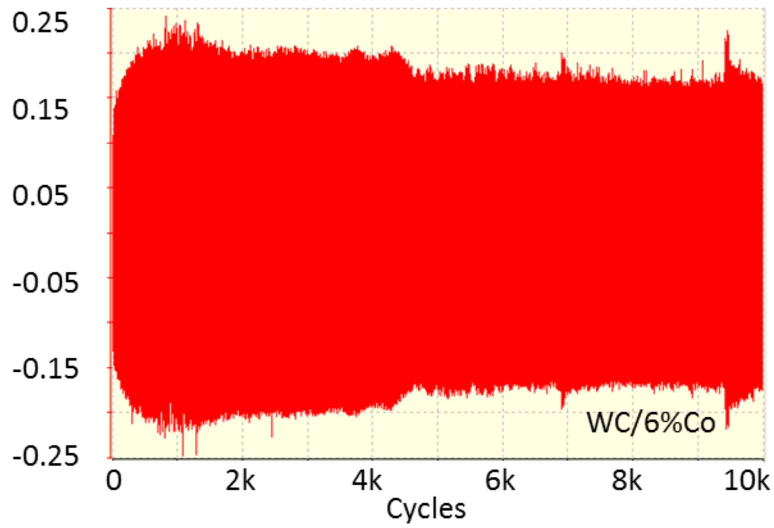

(e) WC/6%Co-Dry

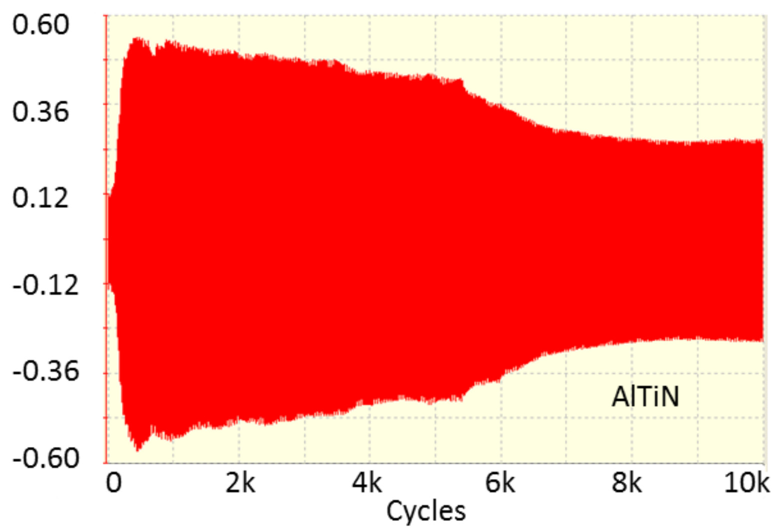

(f) AlTiN-Water

Figure 4-1 (cont'd)

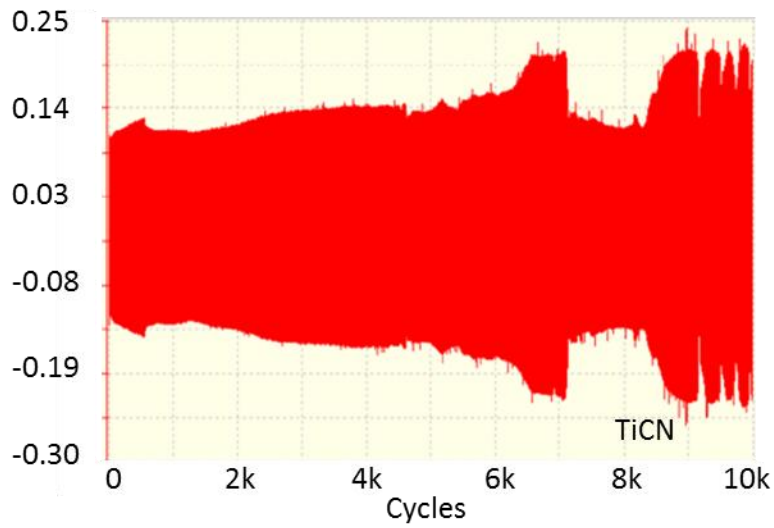

(g) TiCN-Water

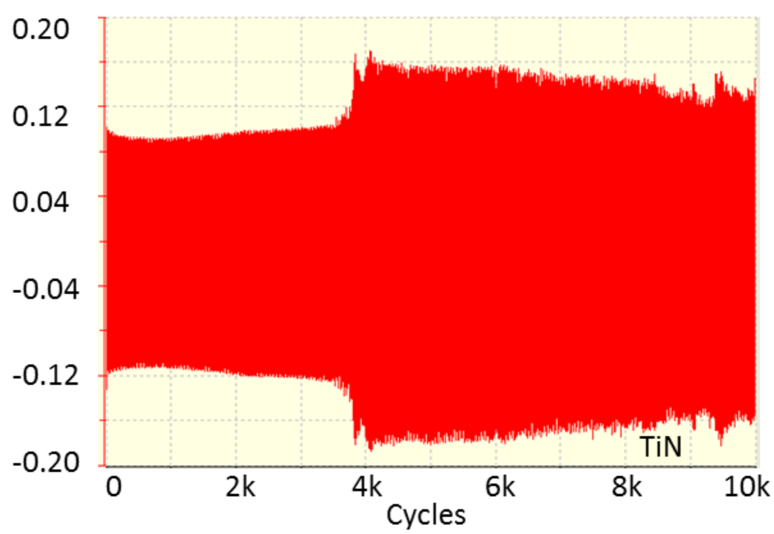

(h) TiN-Water

Figure 4-1 (cont'd)

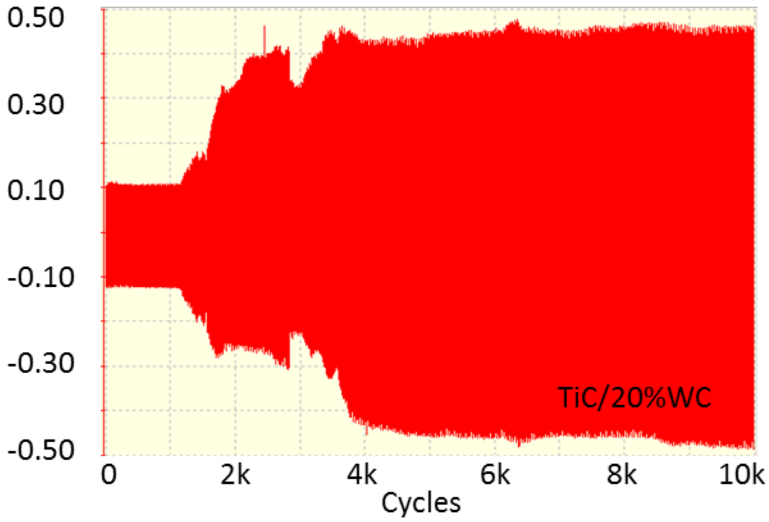

(i) TiC/20%WC-Water

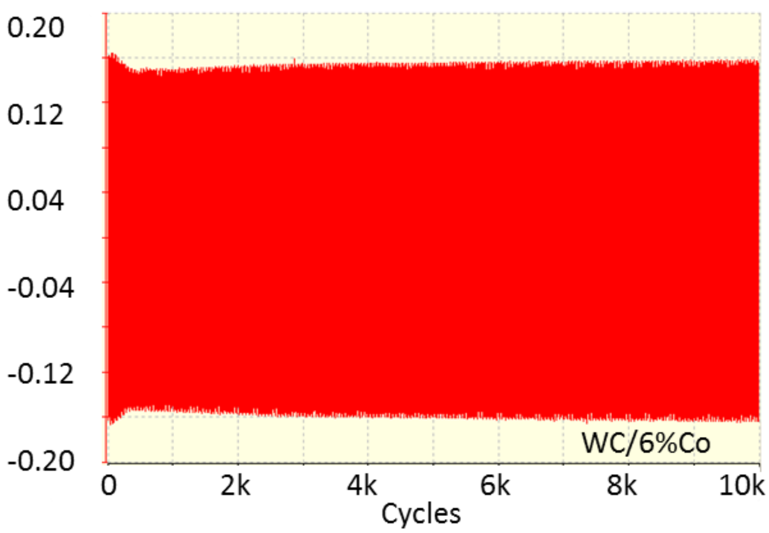

(j) WC/6%Co-Water

Figure 4-1 (cont'd)

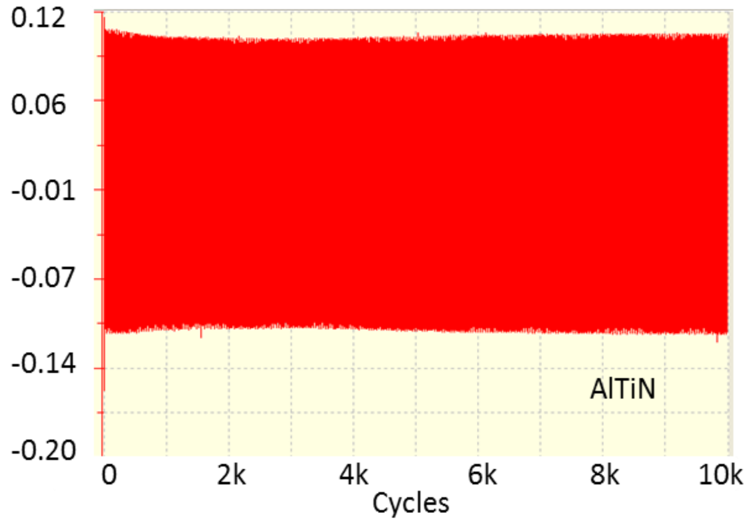

(k) AlTiN-Oil

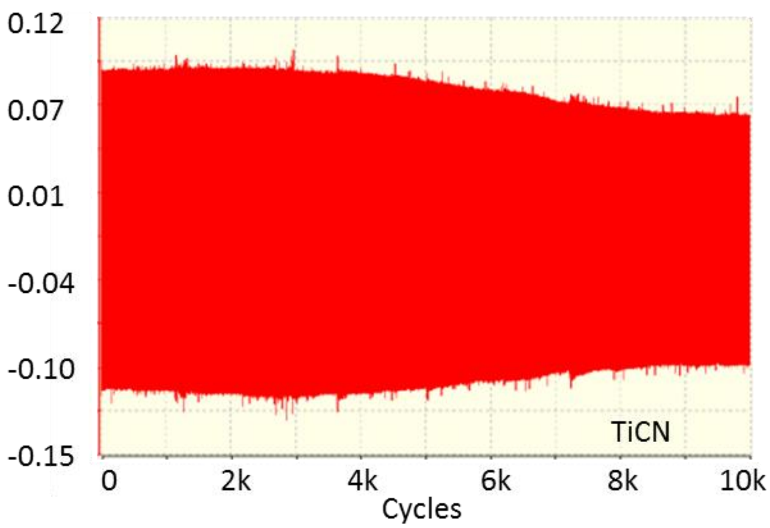

(l) TiCN-Oil

Figure 4-1 (cont’d)

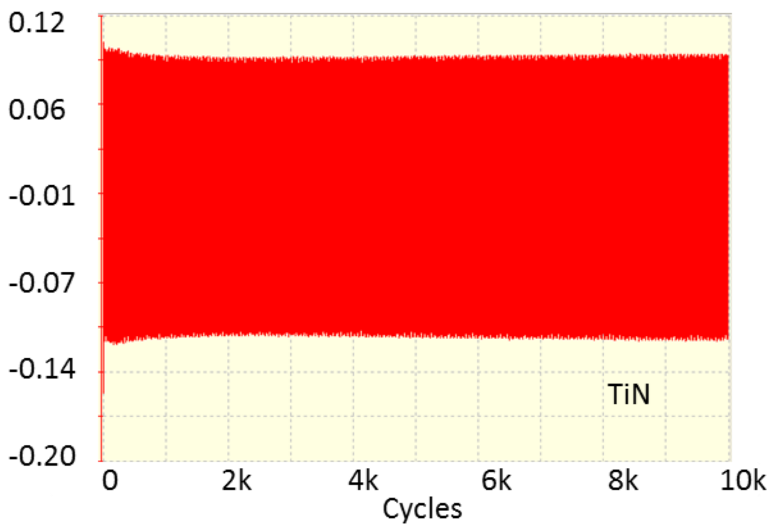

(m)TiN-Oil

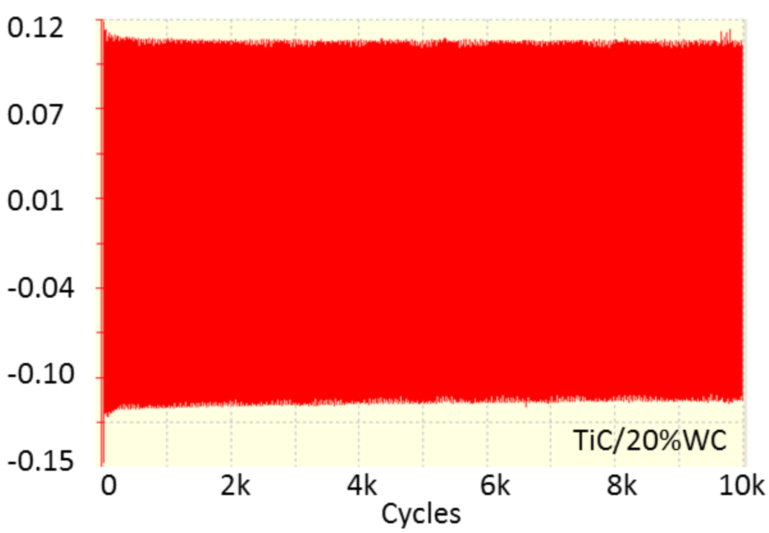

(n) TiC/20%WC-Oil

Figure 4-1 (cont'd)

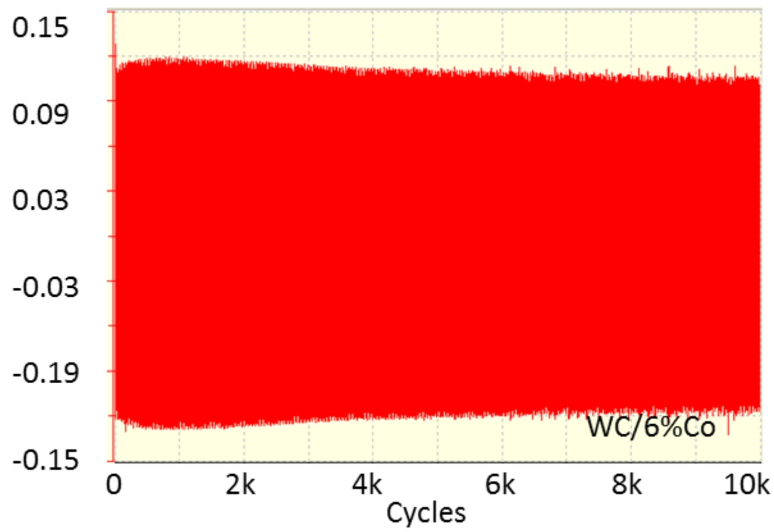

(a) WC/6%Co-Oil

4.3.2. Friction study of the Ti-based materials

In the tribo-meter test, the interlayer formed on the wear track may have greatly changed the friction [105, 106]. SEM images were captured on the wear track of the discs to detect the interlayer formed. The results confirmed the formation of an interlayer on the wear track greatly changed the friction. The interlayer was observed on the AlTiN coatings for the dry and water lubricated conditions, and on the TiC coating for the water lubricated condition (shown in Figures (4-2) ~ (4-4)), while, the stable (large scale) interlayer was not observed for other cases. By comparing the images, the wear track appearance of the AlTiN for the oil lubricated condition and the TiC/20%WC for the dry condition are shown in Figure 4-5 and Figure 4-6.

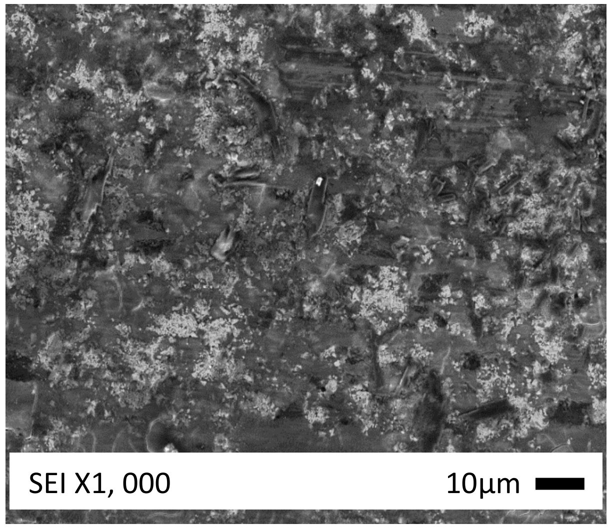

Figure 4-2, Interlayer observed on wear track of AlTiN coating for dry sliding condition

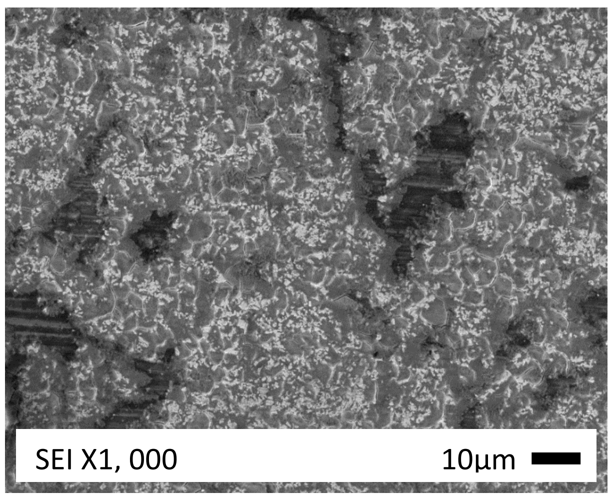

Figure 4-3, Interlayer observed on wear track of AlTiN coating for water lubricated condition

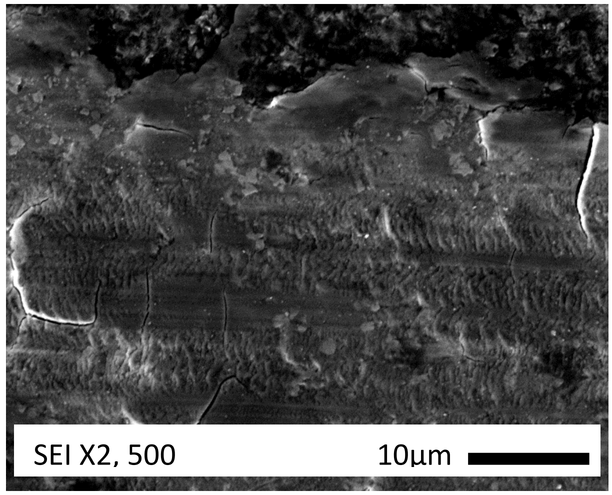

Figure 4-4, Interlayer observed on wear track of TiC/20%WC for water lubricated condition

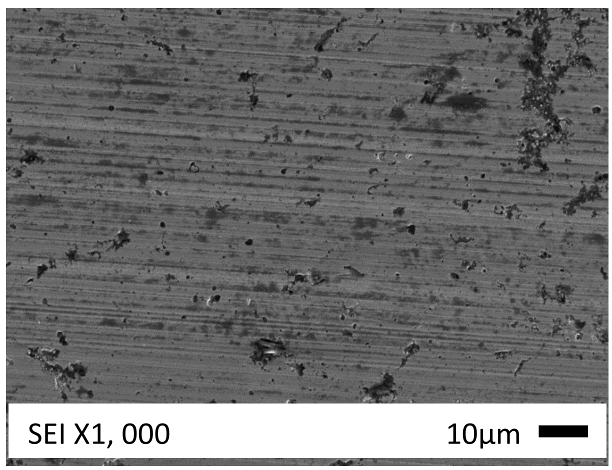

Figure 4-5, Wear track appearance of AlTiN coatings in oil lubricated condition

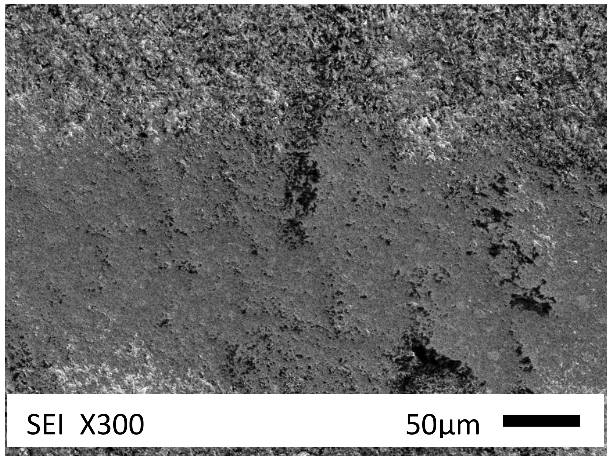

Figure 4-6, Wear track appearance of TiC/20%WC in dry lubricated condition

The friction data in AlTiN-dry, AlTiN-water and TiC/20%WC-water shows that the friction coefficient starts at a very low value. This value nearly equals the friction value for the case with no interlayer as in AlTiN in oil and with TiC/20%WC in dry or oil. However, the friction coefficients gradually increased with increased sliding cycles in the run-in period until it reached a very high value of about 0.5. The water lubricated condition facilitated the steep friction increase for the AlTiN coating compared to the dry condition. The TiC/20%WC coating only had high friction and interlayer formation for the water lubricated condition. Furthermore, for all the other Ti-based materials, there were high fluctuations in the water lubricated condition compared to the other lubricated conditions.

The reason that the water lubricated condition facilitated the friction increase was not very clear. However, one study suggests that the water may absorbed by the metal oxide to form a gel [107] on the surface of wear debris, which are the reactions shown in equation (4-1) and equation (4-2),

$$TiO_2+H_2O = TiO_2 \cdot H_2O \quad \text{gel} \qquad (4\text{-}1)$$

$$Al_2O_3+3H_2O=2Al(OH)_3 \quad \text{gel} \qquad (4\text{-}2)$$

The gel may be more difficult to remove from the wear track than the simple metal oxide due to the high adhesion of the gel, thus facilitating the formation of the interlayer to increase the friction.

4.3.3. Friction behavior of AlTiN

The friction behavior in TiC/20%WC under the water lubricated condition, increases to a relatively high value and remained stable. On the other hand, the friction for AlTiN under dry and water lubricated conditions decreased with the increase in the number of cycles. An additional tribo-test has been carried out on the AlTiN with dry sliding condition, which was stopped when the friction reached 0.5. An SEM picture of the wear track is shown in Figure 4-7.

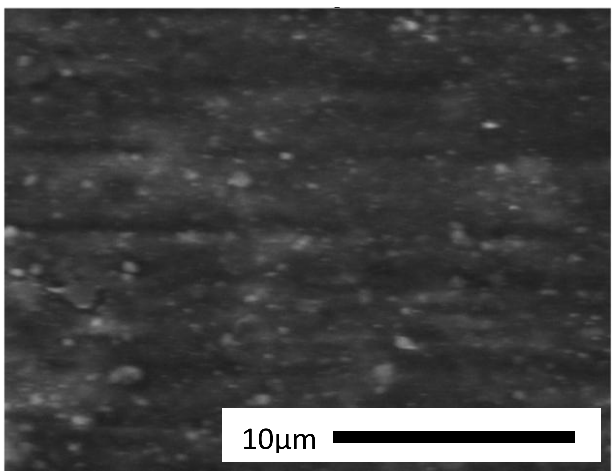

Figure 4-7, Interlayer on the AlTiN at 0.5 friction coefficient

The EDX element mapping showed that the element concentration on the interlayer of AlTiN when the friction reaches 0.5 was mainly Al, Ti, O, W and C, as shown in Table 4-2. Based on the chemical composition, it is believed that the interlayer mainly contain Al_2O_3, TiO_2, WC and WO_2. The high concentration of Carbon in the Table 4-2 is due to the carbon contamination in the EDX process as described in Chapter 2.9, thus, the concentration of Carbon has been excluded from the following considerations.

Table 4-2, The composition of interlayer of AlTiN at 0.5 friction

Element	Weight percent (wt% ± 1%)	Atomic Percentage (at%)
O	28.90	39.99
Al	17.11	14.03
Ti	19.72	9.12
W	15.28	1.84
C	18.99	35.02
Total:	100	100

The composition of the new AlTiN coating is shown in Table 4-3. The atomic percentage of the Al and Ti was very close to 3:2, which is similar as the Al to Ti ratio measured on the interlayer.

Table 4-3, The composition of the new AlTiN surface (exclude Carbon)

Element	Weight percent (wt%± 1%)	Atomic Percentage (at%)
Al	34.28	31.85
Ti	39.14	20.49
N	26.58	47.66
Total:	100	100

The composition of the interlayer on the AlTiN in dry and water lubricated conditions contained much more W and C after 10000 cycles, as shown in Table 4-4 and Table 4-5,

Table 4-4, The composition of interlayer of AlTiN in dry, 10000 cycles (exclude Carbon)

Element	Weight percent (wt% ± 1%)	Atomic Percentage (at%)
O	7.94	40.29
Al	4.74	14.30
Ti	5.64	9.59
W	81.68	35.82
Total:	100	100

Table 4-5, The composition of interlayer of AlTiN in water, 10000 cycles (exclude Carbon)

Element	Weight percent (wt%± 1%)	Atomic Percentage (at%)
O	11.32	46.88
Al	6.32	15.51
Ti	7.74	10.71
W	74.62	26.90
Total:	100	100

From high magnification SEM Figure 4-8 and Figure 4-9, it can be seen that many white grains were embedded on the interlayer of AlTiN in dry and water lubricated conditions after 10000 cycles, while very few of the white grains were observed on the interlayer of TiC/20%WC in water or on the interlayer of AlTiN at 0.5 friction in Figure 4-4 and Figure 4-7.

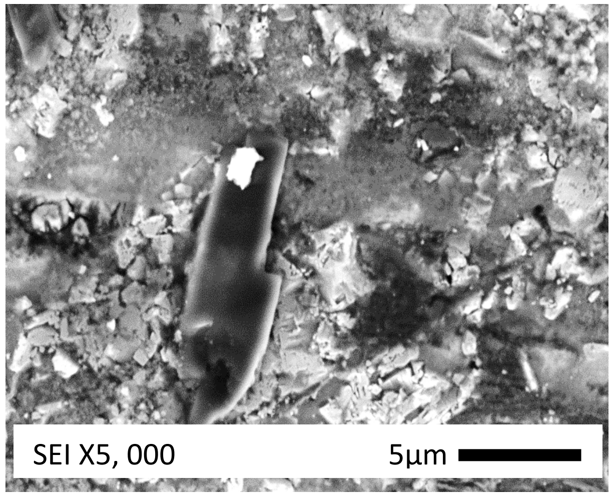

Figure 4-8, Interlayer on the AlTiN in dry lubricated sliding after 10000 cycles

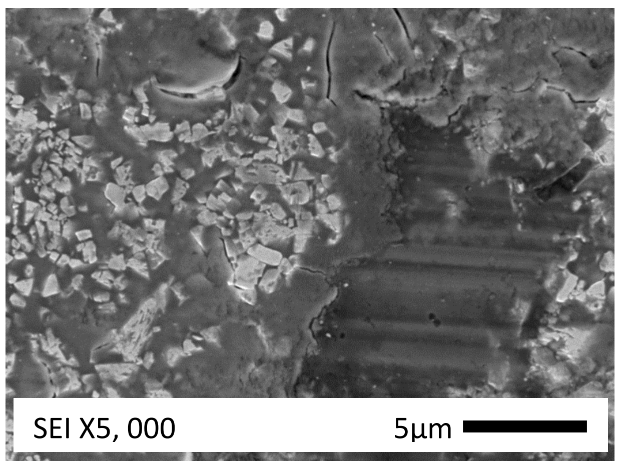

Figure 4-9, Interlayer on the AlTiN in water lubricated sliding after 10000 cycles

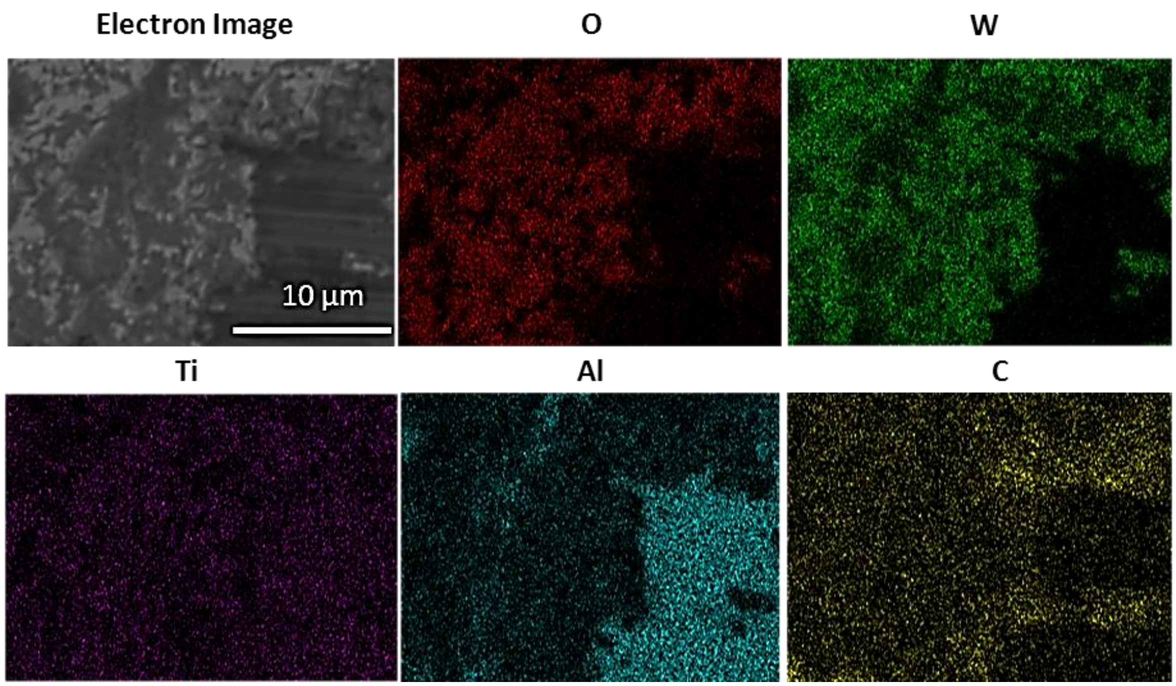

Figure 4-10, EDX figures of the interlayer on the AlTiN

The large white particles on the interlayer were identified as the WC grains from the EDX in Figure 4-10. The gray color interlayer was identified as mainly containing Al, Ti, W, O and C.

Since higher friction was observed when less WC grains were embedded in the interlayer, it was believed that the increase of the WC grains embedded on the interlayer reduced the friction. In Figure 4-1, the friction between the WC/Co-WC/Co pair in dry sliding contact was only about 0.18-0.20. More WC grains embedded on the interlayer may split the load from the interlayer-WC/Co pair to WC-WC/Co pair, thus reduce the friction.

4.4. Summary of sliding wear and friction of Ti-based materials

The friction and sliding wear resistance of the Ti-based materials and uncoated carbide in dry, water and oil lubricated conditions has been presented. The TiCN coating showed much lower wear rate compared with uncoated carbide in all three lubricated conditions, and the other Ti-based materials showed higher wear rates than uncoated carbide in all three lubricated conditions. Although the wear rate of the materials changed with change of the lubricated conditions, the rank of the relative wear rate did not change.

The friction did not dictate the rank of the wear rate in the tribo-test of the different materials. It is believed that the wear rate of each material may depend on other inherent properties other than friction, which will affect the wear rate in both the tribo-test and in machining. Therefore, the wear resistance of the materials in the tribo-test can be correlated to the wear resistance of the coating materials for machining CFRP.

Considering the correlation between tribo-test and CFRP drilling described in Chapter 3.7, the TiCN coating was believed a good candidate for the CFRP drilling.

Chapter 5. Tool wear in Ti-only drilling

5.1. Introduction of Ti drilling

Titanium is a ductile metal with extremely low thermal conductivity. In titanium machining, the cutting temperature is usually very high, promoting the diffusion and dissolution wear mechanisms. For example, in Ti dry turning experiments, the temperature can reach beyond 900°C at high cutting speed, causing the crater wear to increase rapidly, which ultimately causes the failure of the cutting edge.

However, the drilling process of Ti is quite different than the turning of Ti. The average temperature in drilling thin (6.73mm) titanium stack will not be as high as in turning titanium. However, each time the drill engages the Ti stack, the cutting edge suffers a shock, which frequently causes edge chipping.

In the following Ti-drilling experiments, a water soluble lubricant was applied, which considerably reduced the temperature. Therefore, the crater wear is not an important part of the total tool wear compared with the edge chipping and flank wear.

5.2. Experimental procedures

The Ti stack used in the experiments was acquired from The Boeing Company. The titanium alloy on the stack was Ti-6%Al-4%V, which is one of the most commonly used Ti alloys in the aerospace industry. The Ti plate had a total thickness of 6.73 mm. The five types of coated and uncoated drills used in the CFRP drilling experiments were also used in the Ti-only drilling. The Ti drilling experiments was also conducted using the same CNC mill as in the

CFRP drilling. The experimental conditions for the Ti drilling were fixed for all types of drills; RPM of 500 and feed rate of 0.0540 mm/rev. A water soluble cutting coolant was used in the experiment. The mist coolant had a constant flow rate of 16mL/min. The drilling experiments were stopped at 10 holes for the diamond coated and the uncoated drills due to drill failure, and stopped at 40 holes for the AlTiN coated, BAM coated and nano-composite coated drills.

5.3. Experiment results

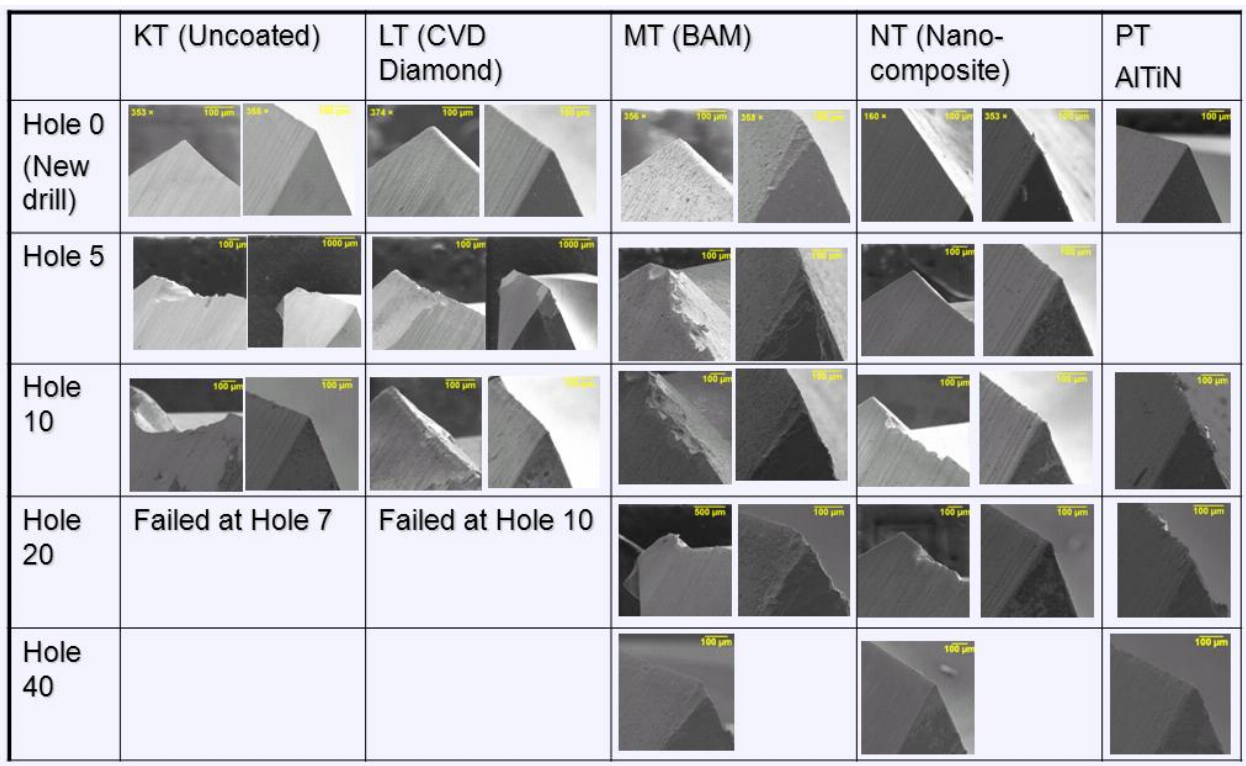

Figure 5-1, SEM images of Ti-only drilling (yellow text in the figure is not meant to be readable)

SEM pictures of the coated and uncoated drills are shown in Figure 5-1. It is clear that the diamond coating was flaked off while the other drills have severe edge chipping.

There are two possible reasons that the diamond coating flaked off in the Ti drilling. First, as shown in Table 5-1, the Coefficient of Thermal Expansion (CTE) of the diamond coating was much lower than the uncoated carbide while the other coatings had a higher CTE than the carbide substrate. As the temperature increased, tensile stress were generated in the diamond coating and compressive stress were generated in the other coatings. Since the tensile strength of brittle materials (such as diamond and ceramics) is much lower than their compressive strength, the diamond coating has a tendency to fracture compared to the other coatings.

Table 5-1, Thermal expansion coefficient for various materials

Materials	CTE (10-6/°C)
WC/Co (6%, 12%)	5.5, 6.2
TiC	7.4
Al2O3	6-7
TiN (TiAlN)	9.35
Diamond	3.1

The second reason that may cause the diamond coating to flake off during drilling is the graphitization of the carbon. A study by Mallika and Komanduri [108] of diamond coating coated onto a carbide substrate, which occurs at temperatures similar to that of the drilling process, showed that the carbon from the diamond diffuses into the cobalt at high temperature. The carbon then comes out of the cobalt and forms the non-adhered graphite phase as the temperature is reduced. A similar phenomenon may be occurring during the drilling of the Ti, since the temperature increases during the drill entry the Ti layer and decreases during the drill exit the Ti layer. In the diamond coating process, usually the surface cobalt on the uncoated carbide will be cleaned as much as possible. However, the high temperature and pressure in the Ti-drilling can lead to the cobalt binder leaching out to the surface from deeper within the tool. Thus the graphitization is very difficult to totally eliminate.

5.4. Drilling forces

The drilling thrust force and torque as a function of hole number are shown in Figure 5.5. The diamond and uncoated carbide drills failed within 10 holes. The thrust force of the BAM coated, nano-composite coated and AlTiN coated drills started at a similar level (<100lbf). However, the thrust force of the BAM coated and nano-composite coated drills increased to 140lbf and 120lbf within the first 10 holes respectively, and only the AlTiN drill remained at a lower thrust force of less than 100lbf.

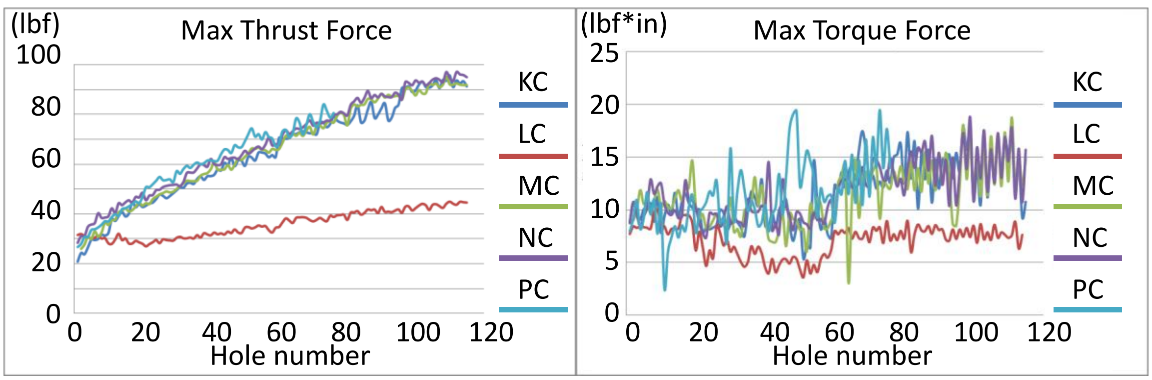

Figure 5-2, Changes in drilling forces versus hole number

As observed from the SEM image seen in Figure 5-1, the BAM coated drills had the most severe edge chipping, and the nano-composite coated drill has the second most severe edge chipping. Both instances occurred mainly within the first 10 holes. In contrast, the AlTiN coated drill had the least edge chipping. In Chapter 5.5, it will be shown that the gradual wear on the coated drills after drilling Ti was very small and also very similar in volume to each other. Therefore, it is believed that the sudden increase in torque during the first 10 holes for the BAM and the nano-composite coated drills was caused mainly by the chipping of the cutting edge rather than by the gradual wear.

Edge chipping is usually considered to be a random process, mostly related to the fracture toughness of the bulk tool material and to the defects in the tool material. Since the bulk material of all the drills is same carbide on this study, the edge chipping on the coated tool may be related more to the defects in each individual drill. However, it is also possible that the residual stresses generated during the coating process may influence the edge chipping.

Unlike CFRP drilling, the maximum torque did not show any substantial increase with the holes numbers. This may be due to the gradual wear occurring during the Ti drilling was much smaller than the gradual wear for the CFRP drilling.

5.5. Tool wear of the drills in Ti drilling

Since edge chipping is a relatively random process, only the gradual wear was measured on the drills. The gradual wear of drills can be seen from the topography profiles shown in Figures (5-3) – (5-6). The diamond coating flaked off within 10 holes, therefore, no profile could be provided for the diamond coated drill.

Based on the profiles, it can be seen that the drills had a relatively large amount of wear volume after the first 10 holes. However, the wear on the drills during the subsequent drilling was extremely small. Even considering the wear volume after the first 10 holes, the total wear volume in Ti-drilling after 40 holes for BAM, nano-composite, AlTiN coated and uncoated carbide drills was less than 1/5th of the wear volume in CFRP-drilling after 40 holes.

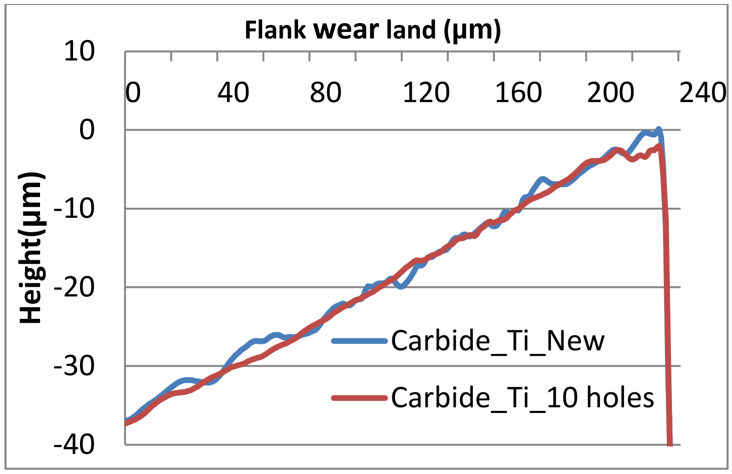

Figure 5-3, The cutting edge profile of uncoated carbide drill for Ti drilling

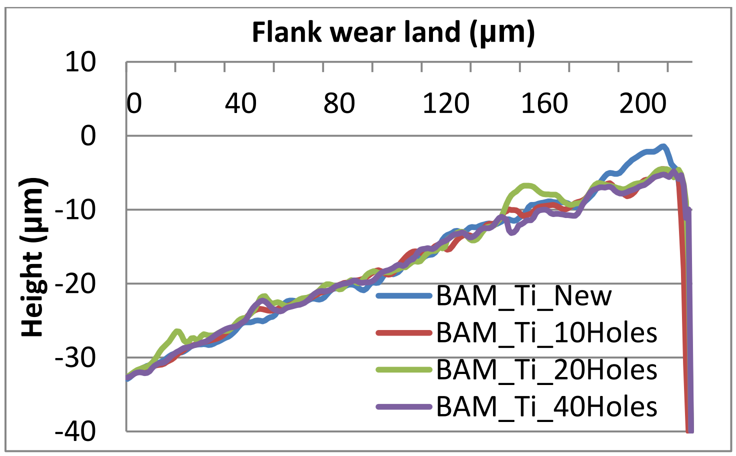

Figure 5-4, The cutting edge profile of BAM coated drill for Ti drilling

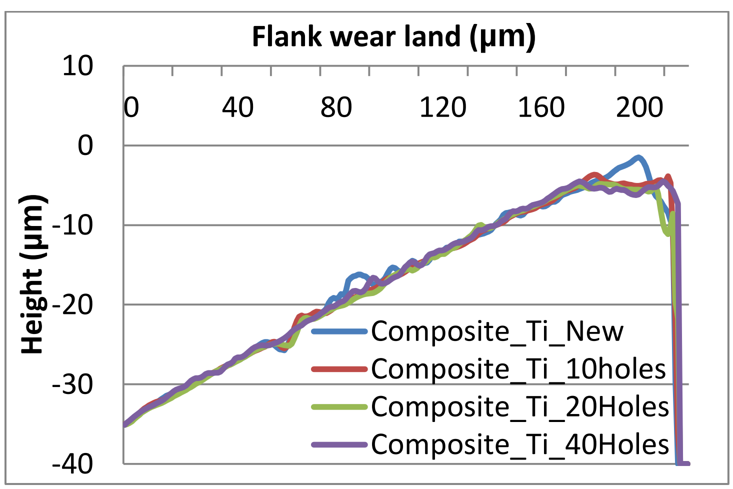

Figure 5-5, The cutting edge profile of nano-composite coated drill for Ti drilling

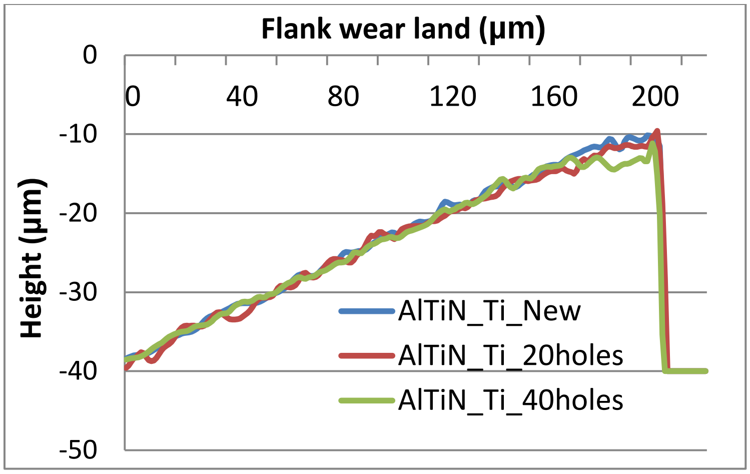

Figure 5-6, The cutting edge profile of AlTiN coated drill for Ti drilling

The relatively large wear volume in the first 10 holes was believed to be due to micro edge chipping. This was caused by the shock of initial contact of the drill with the stack surface, breaking the sharp cutting edge of the drill. After the cutting edge was chipped or became stabilized, the chipping was reduced.

The cutting speed used in our Ti-only drilling is very low at 500 RPM. In addition, with the water soluble lubricant used during drilling, the temperatures during drilling may not have been very high. Thus, the gradual wear generated by diffusion, dissolution and abrasive wear mechanism was very small. The dominate wear mode in the Ti-drilling was edge chipping or the flaking off of the coating.

5.6. Ti adhesion on the drills

The confocal pictures of the drills after the Ti drilling are shown in Figures (5-7) – (5-10). The Ti only adhered in the cutting edge for uncoated carbide drill and BAM coated drill. The width of the adhesion strip on the flank surface was less than 5µm. However, the nano-composite coated drill and AlTiN coated drill have much larger flank surface covered by Ti adhesion. The width of the adhesion strip on the flank surface was about 20μm for nano-composite coated and AlTiN coated drills. This difference may due to the difference of adhesion strength between the Ti and different drills.

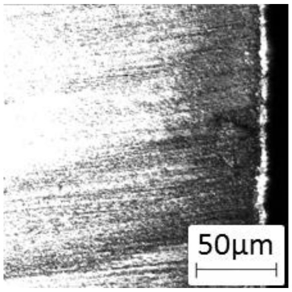

Figure 5-7, Ti adhesion on the uncoated carbide drill, at 10 holes for Ti-only drilling (drill fractured after 10 holes)

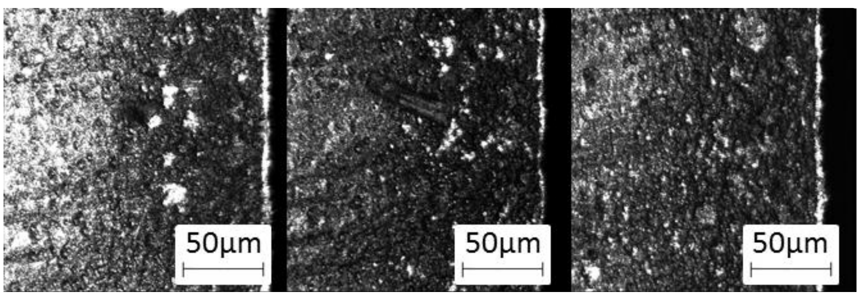

Figure 5-8, Ti adhesion on the BAM coated drill, at 10, 20, 40 holes for Ti-only drilling

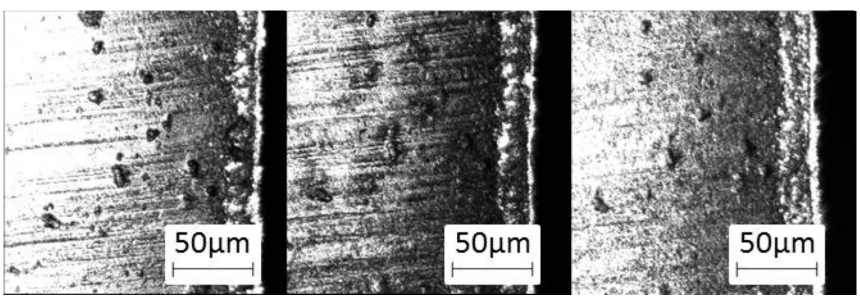

Figure 5-9, Ti adhesion on the nano-composite coated drill, at 10, 20, 40 holes for Ti-only drilling

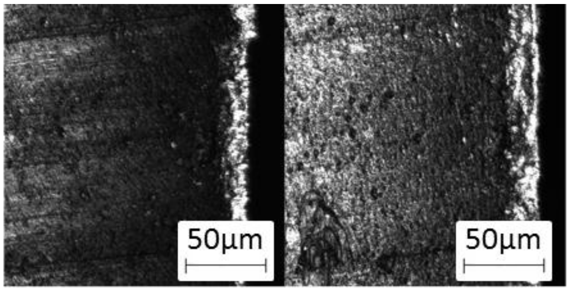

Figure 5-10, Ti adhesion on the AlTiN coated drill, at 20, 40 holes for Ti-only drilling

5.7. Summary of the tool wear in Ti drilling

The tool wear in Ti drilling was mainly due to the edge chipping and coating flaking off. The gradual wear in Ti drilling was much smaller than the gradual wear in CFRP drilling. The thick coating, especially has a CTE lower than substrate, was easier to fracture compared to thin coatings, whose CTEs are higher than the substrate. The graphitization of the diamond coating also prompts the diamond coating flake off.

Chapter 6. Tool wear in CFRP/Ti stack drilling

6.1. Introduction

As introduced in Chapter 3.1, both CFRP and Ti6Al4V (Ti) are promising materials for the aerospace industry. However, both CFRP and Ti are ‘tool killers’. In CFRP machining, the extensive edge rounding wear dulls the cutting edge quickly. The Ti has low thermal conductivity, high hardness and good strength even at elevated temperatures. The maximum temperature in Ti drilling can easily reach more than 600˚C, while turning Ti can cause maximum temperature to exceed 1000˚C. In Ti turning, the dominant tool wear is crater wear, which is generated by the diffusion and dissolution wear mechanisms. In addition, hard inclusions from Ti6Al4V abrade the flank surface, which generates flank wear. The temperature in drilling is not as high as that in turning, which reduces the crater wear. However, the initial impact in the drilling process occurs during the entry into the work material, causing the edge to more easily chip. As described in Chapter 4, edge chipping is the dominant wear in Ti drilling.

In the aerospace industry, a considerable amount of the CFRP/Ti parts to be drilled is on curved surfaces. This causes much of the drilling to be done with hand drills. Thus, CFRP/Ti drilling has relatively high labor cost and in most cases the hole quality is dependent on the worker’s operation. Therefore, changing the drills between the CFRP layer and the Ti layer drilling is not an effective solution. Drilling through the CFRP/Ti stack in one shot can greatly increase the productivity. However, additional problems may occur when the CFRP and the Ti layers with distinct material properties, are stacked together and drilled in one shot. Thus, finding a suitable tool material for CFRP/Ti stack drilling is even more difficult. In this study, five types of drills: diamond coated, BAM coated, nano-composite coated, and AlTiN coated WC-9%Co drills along with an uncoated WC/9%Co drill were used in drilling the CFRP/Ti stack.

6.2. Experiment setup

The CFRP/Ti stack drilling experiments were carried out using the same setup and the same drilling parameters as in the previous CFRP-only and Ti-only drilling studies presented in Sections 3.4 and 5.2. The drilling speed and feed rate in the CFRP layer were 6000rpm and 0.003inch/revolution (0.0762mm/rev). The drilling speed and feed rate in the Ti layer were 500rpm and 0.002inch/rev (0.0508mm/rev). In the previous study, a fire occurred during the CFRP/Ti drilling experiment when drilling was carried out without the use of a coolant. Thus, to avoid further safety concerns, a water soluble coolant was continuously applied during the entire process of the drilling experiments at a constant flow rate at 16mL/min.

The CFRP/Ti stack was fixed on the CNC vertical mill with the CFRP as the top layer and the Ti as the bottom layer. There have not been many studies reporting the results of drilling with Ti as the top layer and CFRP as the bottom layer due to several inherent disadvantages for drilling in this sequence. First, drilling Ti creates exit burrs, which may cause inter-plate damage of the CFRP. Second, the coolant used during drilling has difficulty penetrating the contact area between the tool and the work piece. The Ti burrs was hot, which can damage the entry holes of the CFRP. Third, the CFRP holes may be enlarged on the entry side due to the Ti adhesion and un-removed Ti chips. Lastly, the CFRP has more exit delamination without the presence of the Ti backing.

Therefore, all the CFRP/Ti stack drilling experiments were carried out in the CFRP top/Ti bottom order in this study.

6.3. Wear evolution analysis

The topography of the flank surface of the drills that drilled the CFRP/Ti stack were measured in the same location as were measured in the Ti and the CFRP drilling experiments described in Chapter 3 and Chapter 4 (300um from the end of the cutting edge).

The diamond coating flaked off within 10 holes, which also happened during drilling of the Ti (Chapter 5.3). It is believed that the same reasons described in Chapter 5.3 caused the diamond coating to flake off in the CFRP/Ti drilling. After the diamond coating flaked off, the drilling experiment was continued to finish 20 holes in order to see the influence of the flaked off coating on the overall drilling force. After 60 holes, the other coated and uncoated drills are still in a working condition. These drills performed much better than in the drilling of the Ti.

6.4. Drilling force

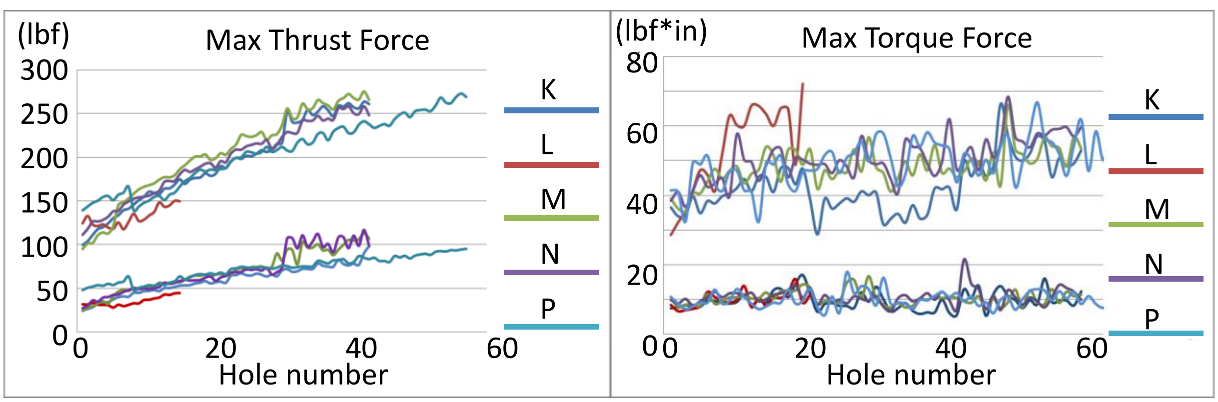

Figure 6-1, The max thrust force and max torque of the drills

The max thrust force and max torque of the drills are shown in Figure 6-1. The torque on the diamond coated drill was greatly increased in drilling the Ti-layer (LS-Ti: Diamond coated drill in Ti layer drilling) after the coating flaked off. However, the torque remained steady when drilling the CFRP layer (LS-CFRP: Diamond coated drill in CFRP layer drilling). This difference was due to the fact that when drilling the Ti layer the torque was generated by the plastic deformation of the Ti, which is very sensitive to the topology of the flank surface. However, in drilling the CFRP layer, the torque was largely contributed by the force necessary to break the carbon fibers at the cutting edge. This was not affected by the topology of the flank surface as much as in drilling Ti layer. The thrust force of the diamond coated drill in drilling both the Ti layer (LS-Ti) and CFRP layer (LS-CFRP) remained nearly steady before the coating flaked off. This was due to the ability of the diamond coating to greatly reduce the edge rounding wear in drilling of the CFRP layer. After the diamond coating had flaked off, the edge rounding wear gradually increased on the carbide substrate, which caused the continuously increasing thrust force.

The other four types of drills showed a similar gradual increase in the thrust force and torque. This increase was mainly due to the edge rounding wear on these drills. The wear volumes were relatively similar. Except for the diamond coated drill, the edge chipping and the flaked off coating rarely occurred on a large scales as it did in the drilling of Ti.

The SEM pictures of the drills after CFRP/Ti stack drilling are shown in Figures 6-2. It can be seen that edge chipping occurred much less in the drilling of the CFRP/Ti stack than in the drilling of the Ti (Figure 5-1). This was believed to be due to the reduced the sharpness of the cutting edge from the edge rounding wear that occurred during the drilling of the CFRP-layer. This edge rounding reduced fracture of the cutting edge.

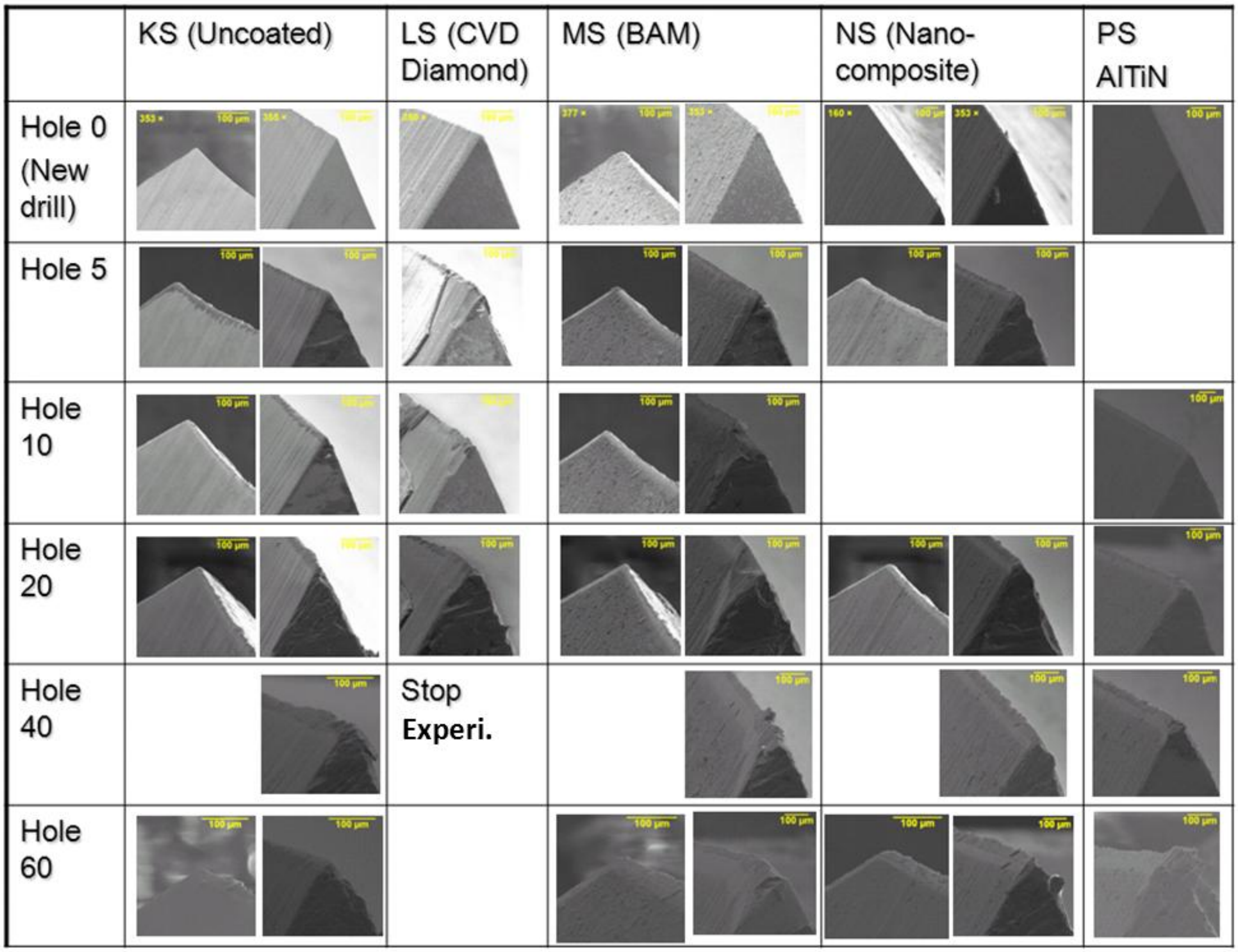

Figure 6-2, The SEM images of the CFRP/Ti stack drilling (yellow text in the figure is not meant to be readable)

The confocal pictures of the drills after the CFRP/Ti stack drilling are shown in Figures (6-3) – (6-6). For a comparison, the confocal pictures of the drills after the Ti drilling are shown in Figures (5-7) – (5-10). It can be seen that there is more Ti adhered on the drill after the CFRP/Ti drilling than after the Ti drilling. And the amount of adhered Ti increased with increasing hole numbers in the drilling of the CFRP/Ti stack but remained constant in the drilling of the Ti. This was due to the edge rounding wear that occurred only in the drilling of the CFRP layer, which dulled the cutting edge. A dull cutting edge had a larger stagnation zone and more Ti adhered on the drill than with a sharper cutting edge for the drilling of the Ti layer. In drilling Ti, the gradual wear grew very slowly, thus the stagnation zone and the adhered layer of Ti did not increase as much as in the drilling of the CFRP/Ti stack.

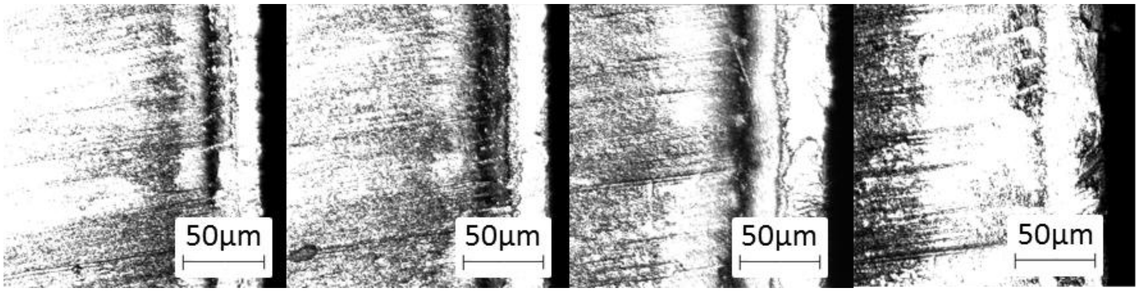

Figure 6-3, Ti adhesion on the uncoated carbide drill, at 10, 20, 40, 60 holes for CFRP/Ti drilling

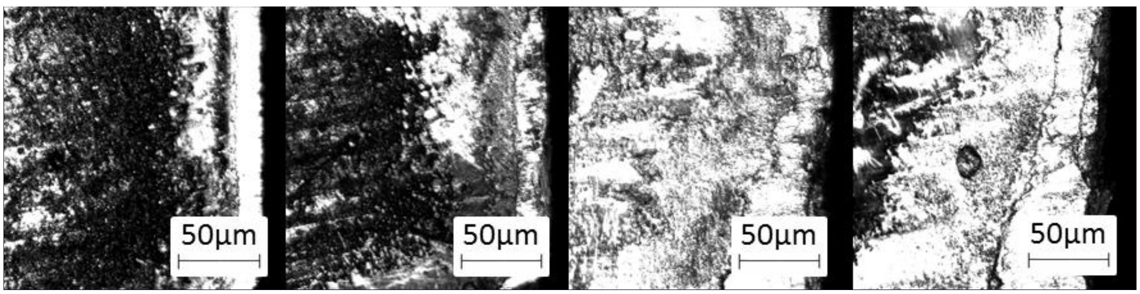

Figure 6-4, Ti adhesion on the BAM coated drill, at 10, 20, 40, 60 holes for CFRP/Ti drilling

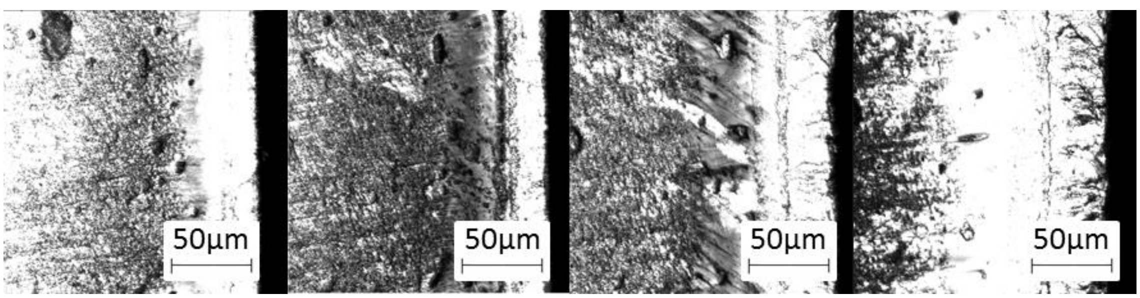

Figure 6-5, Ti adhesion on the nano-composite coated drill, at 10, 20, 40, 60 holes for CFRP/Ti drilling

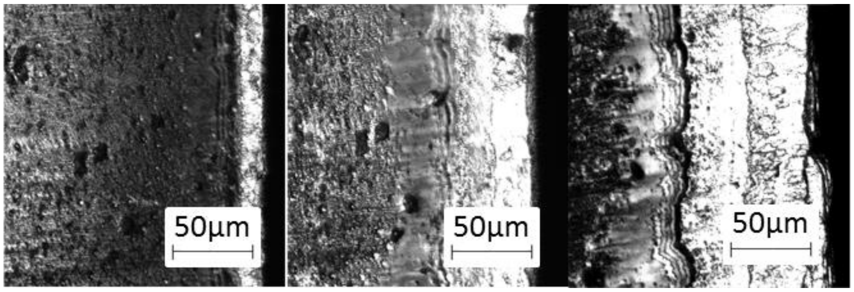

Figure 6-6, Ti adhesion on the AlTiN coated drill, at 20, 40, 60 holes for CFRP/Ti drilling

The profiles of the drills, which have not been etched to remove the adhered Ti from the cutting edge, are shown in Figures (6-7) – (6-10). The tool wear in stack drilling gradually increased with increasing hole number. 10%HF+10%H_2O_2+80%H_2O solution was used to etch the adhered layer of Ti from the uncoated carbide drill after 40 holes. The confocal image and 2D profile of the carbide drill before and after etching are shown in Figure 6-11 and Figure 6-12. It can be seen that the Ti had adhered mainly near the cutting edge of the tool, where the stagnation zone exists. This proved the hypothesis that the Ti adhesion was mainly caused by the Ti trapped in the stagnation zone. Thus, a worn tool, which had a larger stagnation zone, had more Ti adhesion than a new tool.

Unfortunately, the HF acid used to remove the adhered layer of Ti on the uncoated carbide cannot be used for the AlTiN, nano-composite and BAM coated tools due to the damage or even removal of the coatings. Thus the etching was not applied for the AlTiN, nano-composite and BAM coated drills. Instead, a “mechanical cleaning” method has been developed to remove the Ti adhesion without causing any harm to the coatings. This method was based on the abrasive wear mechanism. The abrasive wear rate is greatly dependent on the hardness ratio between the abrasives and tool material. The hardness of carbon fiber is only half that of the carbide tool, however it was more than 3 times harder than the Ti work material. Based on abrasive wear

Equation 1-3, the abrasive wear coefficient caused by CFRP on Ti would is about 500 times higher than on carbide tool. Thus, CFRP can abrade away the Ti adhesion, without causing substantial wear on the carbide tools. In our experiment, after 60 holes of CFRP/Ti stack drilling, one more additional hole on the CFRP layer has been drilled to abrade away the Ti adhesion. The results, seen in Figures (6-13) – (6-16), show that the Ti adhesion has been completely removed from all the drills. The flank surface profiles of the drills after "mechanical etching" are shown in Figures (6-17) – (6-20). An assumption was made that the one additional CFRP hole added to the 60 holes drilled in CFRP/Ti stack does not substantially change the total wear volume of the drills. Thus, use of the tool wear result from this "mechanical etching" was considered to be relatively accurate. The wear volumes of the drills after 60 holes of CFRP/Ti drilling are shown in Table 6-1. The wear volume for the CFRP/Ti stack drilling was quite similar to the sum of the wear volume of the drills after CFRP drilling (Table 3-2) and Ti drilling. In addition, the total wear generated in the CFRP/Ti stack drilling was mostly from the contribution of wear in the CFRP drilling.

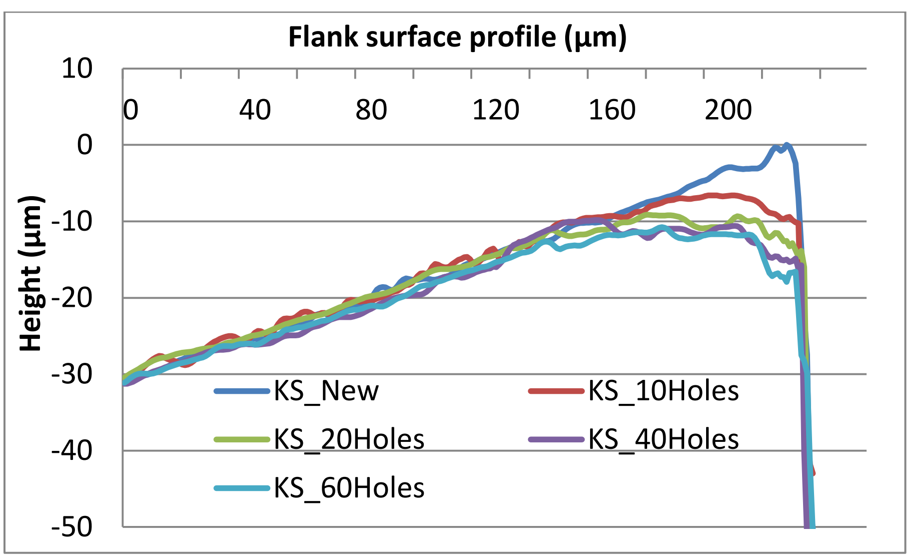

Figure 6-7, Flank surface profiles of the uncoated carbide drill at new, 10 holes, 20 holes, 40 holes and 60 holes for CFRP/Ti drilling

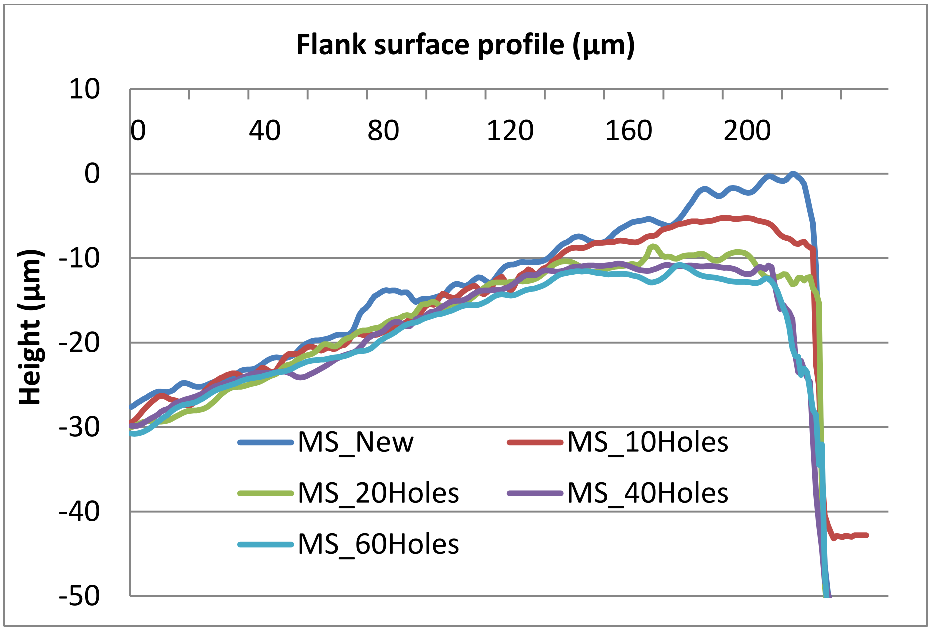

Figure 6-8, Flank surface profiles of the BAM coated drill at new, 10 holes, 20 holes, 40 holes and 60 holes for CFRP/Ti drilling

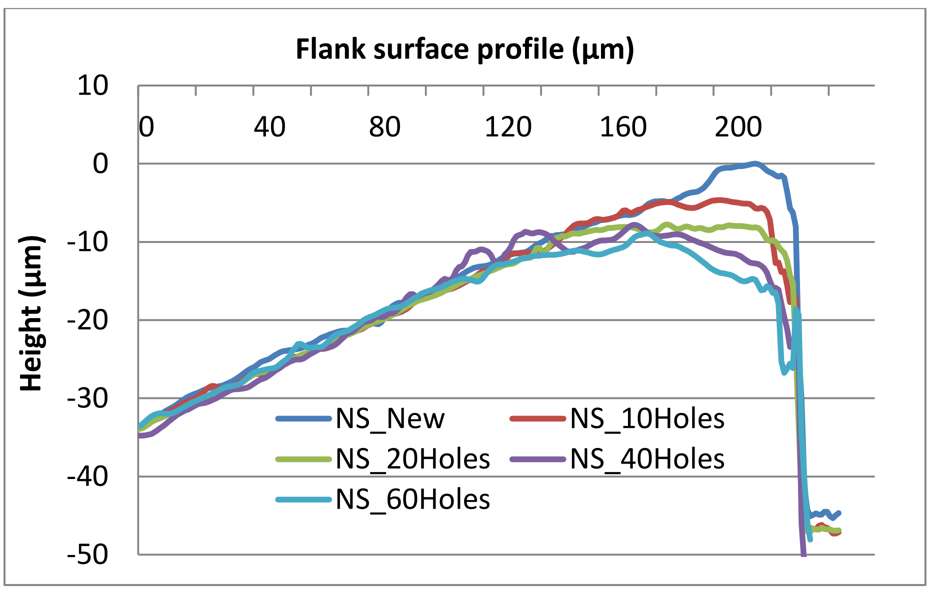

Figure 6-9, Flank surface profiles of the nano-composite coated drill at new, 10 holes, 20 holes, 40 holes and 60 holes for CFRP/Ti drilling

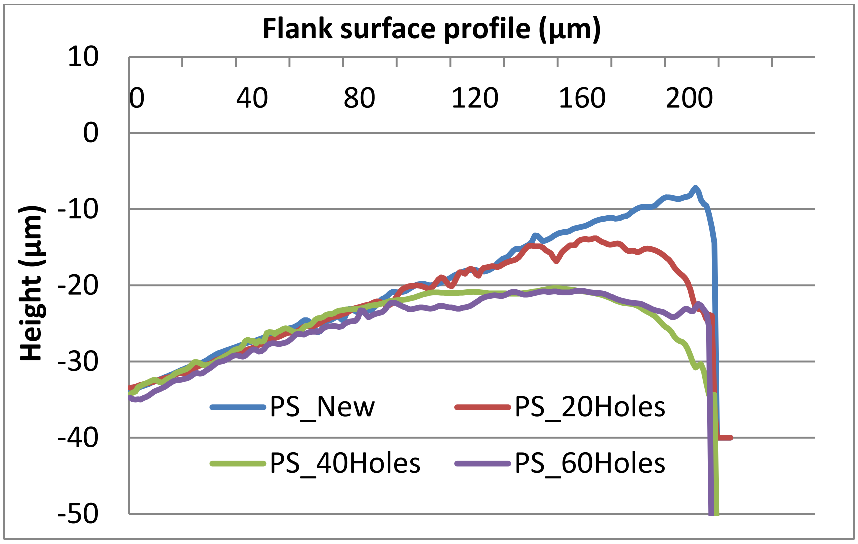

Figure 6-10, Flank surface profiles of the AlTiN coated drill at new, 10 holes, 20 holes, 40 holes and 60 holes for CFRP/Ti drilling

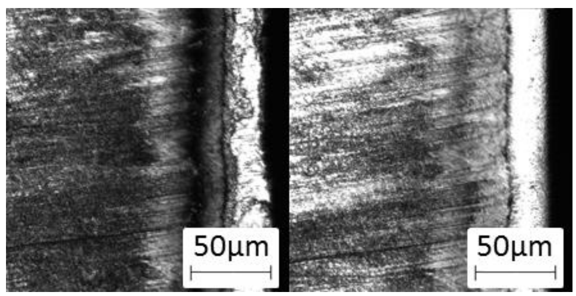

Figure 6-11, Flank surface of uncoated carbide drill before and after chemical etching

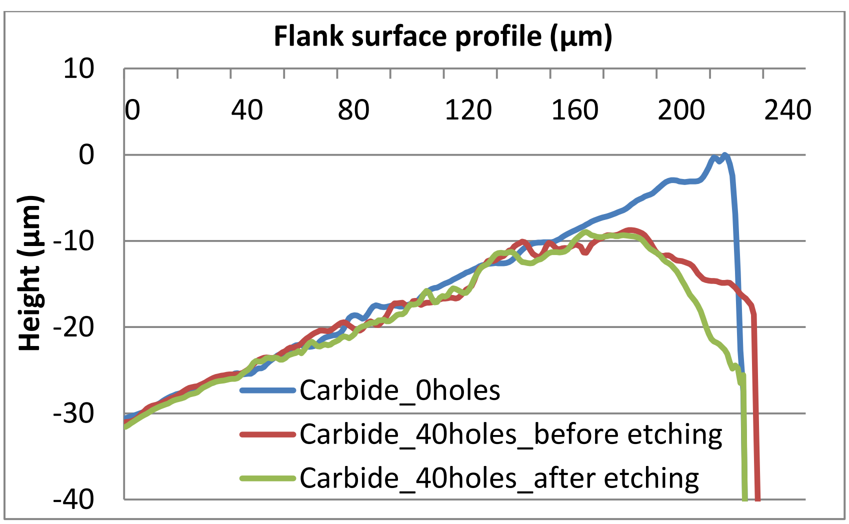

Figure 6-12, Flank surface profile of carbide drill before and after etching

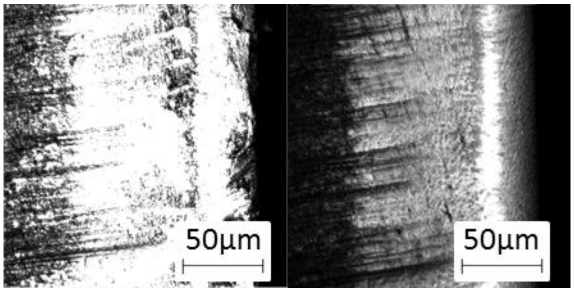

Figure 6-13, Flank surface of uncoated carbide drill before and after mechanical cleaning

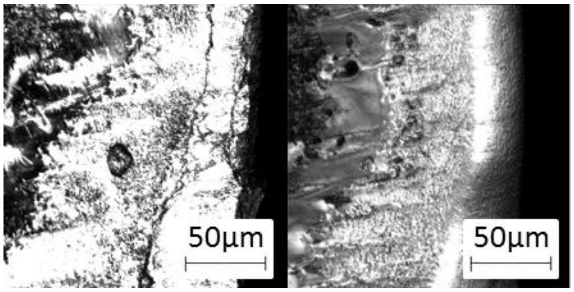

Figure 6-14, Flank surface of BAM coated drill before and after mechanical cleaning

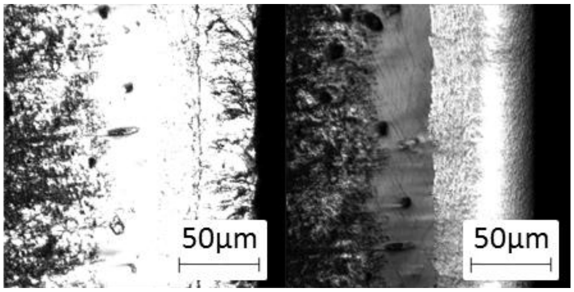

Figure 6-15, Flank surface of nano-composite coated drill before and after mechanical cleaning

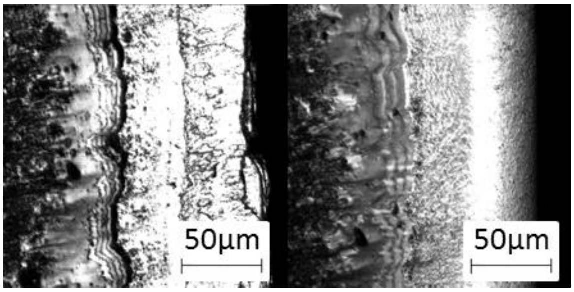

Figure 6-16, Flank surface of AlTiN coated drill before and after mechanical cleaning

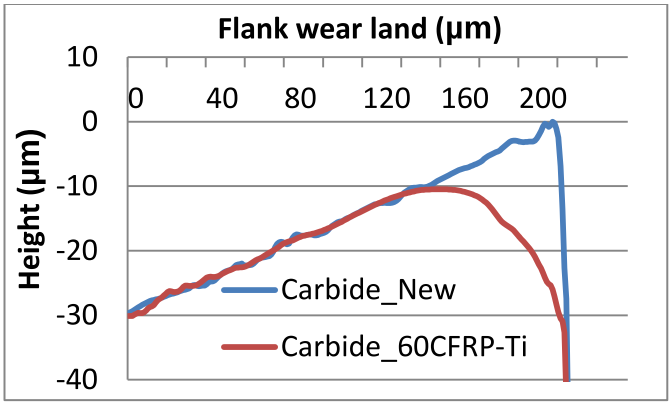

Figure 6-17, Flank surface profiles of the uncoated drill at 60 CFRP/Ti drilling

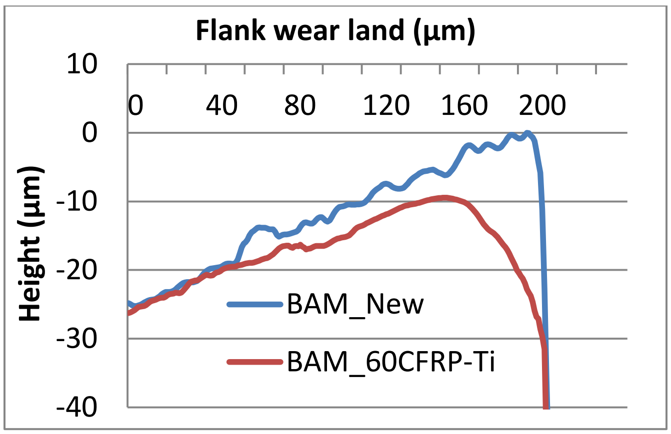

Figure 6-18, Flank surface profiles of the BAM coated drill at 60 CFRP/Ti drilling

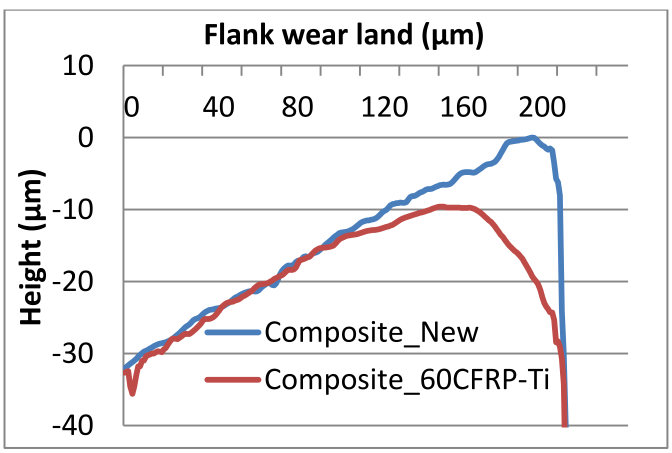

Figure 6-19, Flank surface profiles of the nano-composite coated drill at 60 CFRP/Ti drilling

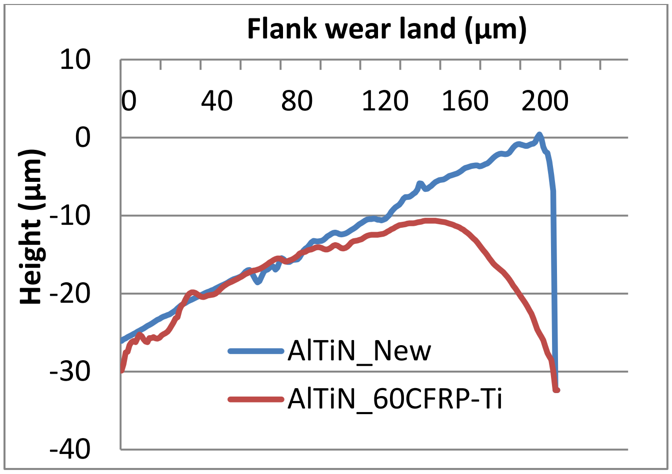

Figure 6-20, Flank surface profiles of the AlTiN coated drill at 60 CFRP/Ti drilling

Table 6-1, The wear volume of the drills in 60 holes CFRP/Ti drilling

Drills	Wear volume (μm^2)
Uncoated	805
BAM	1120
Composite	900
AlTiN	1002

The performance of the coated and uncoated drills based on the cutting force and wear after "mechanical cleaning" showed relatively similar results. None of the coatings tested substantially increased the tool life of the uncoated carbide drill.

6.5. Summary of the tool wear in CFRP/Ti stack drilling

The wear in the drilling of the CFRP/Ti stack was mainly a combination of the edge rounding wear in the drilling of the CFRP and the chipping and coating flake off in the drilling of the Ti layer plus a small amount of adhesion wear caused by the removal of the Ti adhesion in the drilling of the CFRP layer. Since the chemical etching may damage the coatings, a “mechanical cleaning” method has been developed by drilling one additional hole in the CFRP. It has been shown that the “mechanical cleaning” successfully removed the Ti adhesion.

In order to increase the tool life in CFRP/Ti drilling, the most important focus should be to reduce the edge rounding wear in the drilling of the CFRP layer. Also, chipping resistance and coating technology should be improved for the drilling of the Ti layer. In this study, BAM coated, nano-composite coated and AlTiN coated drills were inferior to the uncoated drill, which was mainly because none of these three coatings can reduce the edge rounding wear in the drilling of the CFRP layer. The diamond coating, which greatly reduced the wear in the drilling of the CFRP, flaked off when drilling the Ti or the CFRP/Ti stack due to its extremely low CTE and problems with graphitization. Thus, the diamond coating also cannot improve the tool life in CFRP/Ti stack.

Further study is needed to test coatings that have better resistance to edge rounding wear and chipping and also improved strength of the coating/substrate interface during the drilling of the Ti layer.

Chapter 7. Conclusions and future work

7.1. Conclusions

Tool wear in turning of pure aluminum and drilling of carbon fiber reinforced plastics (CFRP)/titanium (Ti) stacks was investigated due to their importance in modern manufacturing. This study presents a new explanation for tool wear with these work materials based on experimental results.

In dry turning of commercially pure aluminum, carbide grains were directly pulled out from the surface by adhesion. The dislodged carbide grains abraded the tool and generated a small amount of flank wear. The finer grain carbide tool had more flank wear than the coarser grain carbide tool.

The bulk fracture toughness of the coarse grain carbide was higher than the fine grain carbide. Therefore, this provides an explanation of the observed micro chipping on the fine grade carbide but not on the coarse gain grade carbide.

The adhesion between aluminum and cobalt is stronger than that between aluminum and WC. The softer cobalt was preferentially worn down in the machining, which reduced the adhesion strength between aluminum and cutting tool. This has an impact on BUE. The initial volume of the BUE reduced to a certain amount in the machining, and thereafter remained stable as the machining time increased. Higher oxygen concentration was detected in the bottom layer of the BUE which contacts the tool surface. This layer was speculated to contain aluminum oxide, which can increase the adhesion and BUE. It has been found that the high carbon concentration detected on the BUE sample was from carbon contamination rather than from the decomposition of the carbide tool.

The performances of uncoated, BAM coated, diamond coated, nano-composite coated and AlTiN coated carbide (WC-Co) drills when drilling CFRP were investigated in terms of tool wear and drilling forces.

The edge rounding wear was the main wear type in all drills used. A hypothesis was developed to explain the edge rounding wear in CFRP machining. Due to the fracture-based chip formation of CFRP, the stagnation zone at the cutting edge, which normally prevents the edge wear in metal machining, does not exist. Wear accelerates to result in the edge rounding wear. The diamond coating significantly reduced the edge rounding wear while the other coatings did not protect the drill during machining.

The tool wear measurements in CFRP drilling experiments did not match the abrasive wear resistance of the drill materials. However, the tribo-meter tests gave the results correlated well with the wear results after drilling. Therefore, the tribo-meter test, which is more economical, can be used to screen the prospective tool materials before carrying drilling experiment.

The tool wear in Ti drilling was mainly due to the edge chipping and coating flaking off. The gradual wear in Ti drilling was much smaller than the gradual wear in CFRP drilling. The thick coating, especially has a CTE lower than substrate, was easier to fracture compared to a thin coatings, whose CTEs are higher than that of the substrate. The graphitization of the diamond coating also prompts the diamond coating flake off.

The wear in the drilling of the CFRP/Ti stack was mainly a combination of the edge rounding wear in the drilling of the CFRP and the chipping and coating flake off in the drilling of the Ti plus a small amount of adhesion wear caused by the removal of the Ti adhesion in the drilling of the CFRP layer. In order to increase the tool life in CFRP/Ti drilling, the most important focus should be to reduce the edge rounding wear in the drilling of the CFRP layer. Also, chipping resistance and coating technology should be improved for the drilling process of the Ti layer. In this study, the BAM coated, nano-composite coated and AlTiN coated drills were inferior to the uncoated drill, which was mainly because these coatings did not reduce the edge rounding wear in the drilling of the CFRP layer. The diamond coating, which performed best in the drilling of the CFRP, flaked off when drilling the Ti or the CFRP/Ti stack due to its extremely low CTE and the graphitization problem.

7.2. Prospect for future work

Investigation of the sliding wear mechanism of the cutting tool and coatings materials based on the current study continues. In particular, finding better cutting tools and coating materials for sliding wear dominated cutting conditions will be a focus.

Several candidate materials for CFRP machining are TiCN, CrN and AlCrN, due to their great sliding wear resistance in the tribo-meter testing.

REFERENCES

REFERENCES

[1]. Mehrabi M. G. , Ulsoy A. G. and Koren Y. , Reconfigurable manufacturing systems: Key to future manufacturing, Journal of Intelligent Manufacturing, (2000) Volume 11, 403-419.

[2]. Bernhard S., On-line and indirect tool wear monitoring in turning with artificial neural networks: A review of more than a decade of research, Mechanical Systems and Signal Processing, (2002) Volume 16, Issue 4, 487-546.

[3]. Choudhury S.K., Bartarya G., Role of temperature and surface finish in predicting tool wear using neural network and design of experiments, International Journal of Machine Tools and Manufacture, Volume 43, Issue 7, May 2003, 747-753.

[4]. Kramer B.M., Bruce M., Patrick K., Computational design of wear coatings, Journal of Vacuum Science & Technology A: Vacuum, Surfaces, and Films, (1985) Volume 3, Issue 6, 2439-2444 .

[5]. Kramer B.M., A comprehensive tool wear model, Annals of the CIRP, (1986) Volume 35, Issue 1, 67-70.

[6]. Prengel H.G., Pfouts W.R., Santhanam A.T., State of the art in hard coatings for carbide cutting tools, Surface and Coating Technology, (1998) Volume 102, Issue 3, 183-190.

[7]. Hartung P.D., Kramer B.M., Tool wear in titanium machining, CIRP Annals-Manufacturing Technology, (1982) Volume 31, Issue 1, 75-80.

[8]. Rivero A., Aramendi G., Herranz S., Lopez de Lacalle L.N., An experimental investigation of the effect of coatings and cutting parameters on the dry drilling performance of aluminium alloys, Int J Adv Manuf Technol (2006) 28: 1–11.

[9]. List G., Nouari M., Gehin D., Gomez S., Manaud J.P., Petitcorps Y., Girot F., Wear behaviour of cemented carbide tools in dry machining of aluminium alloy, Wear 259 (2005) 1177–1189.

[10]. Sakuma K, Seto M, Taniguchi M and Yokoo Y, Tool wear in cutting carbon-fiber-reinforced plastics: The effect of physical properties of tool materials, Bulletin of JSME Vol.28, No.245 November (1985) 2781-2788.

[11]. Faraz A, Biemann D, Weinert K, Cutting edge rounding: An innovative tool wear criterion in drilling CFRP composite laminates, International Journal of Machine tools &

Manufacture 49 (2009) 1185-1196.

[12]. Park K.H., Beal A., Kim D., Kwon P., Lantrip J., Tool wear in drilling of composite/titanium stacks using carbide and polycrystalline diamond tools, Wear 271 (2011) 2826-2835.

[13]. Organization for Economic Cooperation and Development (OECD), Glossary of Terms and Definitions in the Field of Friction, Wear and Lubrication, Paris, 1969.

[14]. Loladze T.N., Adhesion and diffusion wear in metal cutting Mechanical Engineering Division, in: Proceedings of the 42nd Annual Convention, Calcutta, West Bengal, 1962, p. 108–141.

[15]. Wong T.K.P., Dissolution wear: Decomposition of tool material, and concentration profile into chip, Thesis (Ph. D.) Michigan State University, 2004.

[16]. Groover M.P., Fundamentals of modern manufacturing, John wiley& Sons,Inc, 1999.

[17]. Rabinowicz E., The Least Wear, Wear, 100 (1984) 533-541.

[18]. Archard J. F. and Hirst W., The wear of metals under unlubricated conditions, Proc. R. Soc. London, Ser. A, 236 (1956) 397 - 410.

[19]. Rabinowicz E., Friction and Wear of Materials, Wiley, New York, 1965, Table 6.6.

[20]. Rabinowicz E., Friction and wear properties of rhenium, Wear, 10 (1967) 313 - 318.

[21]. Christenson H.K., Adhesion and surface energy of mica in air and water, Journal of Phys. Chem. 1993, 97, 12034-12041.

[22]. Rigney D.A., Chen L.H. and Naylor M.G.S., Wear processes in sliding systems, Wear, 100 (1984) 195-219.

[23]. Moore M.A., A review of two-body abrasive wear, Wear, (1974) 27, 1-17.

[24]. Rabinowicz E., Abrasive wear resistance as a materials test, Lubrication Engineering, (1977) 33(7), 378-381.

[25]. Nouari M., Molinari A., Experiment verification of a diffusion tool wear model using a 42CrMo4 steel with an uncoated cemented tungsten carbide at various cutting speeds. Wear, 259(2005) 1151-1159.

[26]. Machado A.R. and Wallbank J., Machining of titanium and its alloys – a review, Proc. of the Inst. Mech. Eng. Vol. 204 part B, J. Eng. Manufacture, I IMECHE, London, England, 53-60.

[27]. Machado A.R., Machining of Ti6Al4V and Inconel 901 with a High pressure coolant system, PhD Thesis, University of Warwick, Coventry, England, September, p 288.

[28]. List G., Nouari M., G' ehin D., Gomez S., Manaud J.P., Le Petitcorps Y., Girot F., Wear behavior of cemented carbide tools in dry machining of aluminium alloy, Wear 259 (2005)1177-1189.

[29]. Anderson C.A., Milan G., Silva M.B., Machado A.R., Some observations on wear and damages in cemented carbide tools, J. of the Braz. Soc. Of Mech. Sci. & Eng, (2006) Vol.28, No.3, 269-277.

[30]. Hamade R.F., Ismail F., A case for aggressive drilling of aluminum, Journal of Materials Processing Technology 166 (2005) 86–97.

[31]. Nouari M., List G., Girot F., Coupard D., Experimental analysis and optimization of tool wear in dry machining of aluminum alloys, Wear (2003) Volume 255, 1359-1368.

[32]. Roy P., Sarangi S.K., Ghosh A., Chattopadhyay A.K., Machinability study of pure aluminum and Al-12% Si alloys against uncoated and coated carbide inserts, Int. Journal of Refractory Metals & Hard Materials 27 (2009) 535-544.

[33]. Chattopadhyay A.K., Roy P., Ghosh A., Sarangi S.K., Wettability and machinability study of pure aluminium towards uncoated and coated carbide cutting tool inserts, Surface & Coatings Technology 203 (2009) 941–951.

[34]. Hu J., Chou Y. K., Characterizations of cutting tool flank wear-land contact, Wear 263 (2007) 1454–1458.

[35]. Rowe G. W. and Smart E. F., The importance of oxygen in dry machining of metal on a lathe, Br. J. Appl. Phys.,14, (1963) 924-926.

[36]. Williams J. A., Phd Thesis, Cambridge Univ.1975.

[37]. Iwata K., Aihara J. and Okushima K., On the mechanism of built-up edge formation in cutting, Annals of the CIRP **19** (1971), 323–330.

[38]. Stephen V. Pepper, Effect of adsorbed films on friction of Al2O3-metal systems, Journal of applied physics, Vol.47 No.6 June (1976) 2579-2584.

[39]. Stephen V. Pepper, Shear strength of metal-sapphire contacts, Journal of applied physics, Vol.47 No.3 June (1976) 801-808.

[40]. Doyle E. D., Hornet J. G., and Tabor D., Frictional interactions between chip and rake face in continuous chip formation, Proc. R. Soc. Lond. A. 366, (1979) 173-183.

[41]. Takeyama H. and Ono T., Basic investigation of built-up-edge, Transactions of the ASME, Journal of Engineering for Industry 90 (1968), 335–342.

[42]. Williams J.E. and Rollason E.C., Metallurgical and practical machining parameters affecting built-up-edge formation in metal cutting, Journal of the Institute of Metals 98 (1970), 144–153.

[43]. Nakajima K., Ohgo K., Awano T., Formation of a built-up edge during cutting, Wear, 11 (1968) 369-379.

[44]. Lee L.H., Fundamentals of adhesion, Plenum Press (1991), 46-47.

[45]. J. Olortegui-Yume, P. Kwon, Crater wear patterns analysis on multi- layer coated carbides using the wavelet transform, Wear, 268 (2010) 493–504.

[46]. Nabhani F., Wear mechanisms of ultra-hard cutting tools materials, Journal of Materials Processing Technology, 115 (2001) 402-412.

[47]. John S.S. and John P.N., Study of the bond between gold alloys and porcelain, International and American Associations for Dental Research, (1962)Vol. 41, No 6, 1424-1437.

[48]. Jia K. and Fischer T.E., Abrasion resistance of nanostructured and conventional cemented carbides, Wear, 200 (1996) 206-214.

[49]. Masuda M, Kuroshima Y, Chujo Y, Failure of tungsten carbide-cobalt alloy tools in machining of carbon materials, Wear, 169 (1993) 135-140.

[50]. Shetty D.K., Indentation fracture of WC-Co cermets, Journal of Materials Science, 20 (1 985) 1873-1882.

[51]. Ingelstrom N., The fracture toughness of cemented tungsten carbides, Engineering Fracture Mechanics, 1974, Vol. 6, 597-607.

[52]. Jia K, Fischer TE, Sliding wear of conventional and nanostructured cemented carbides, Wear 1997 volumes 203-204, 310-318.

[53]. Gupta NK, Iqbal MA, and Sekhon GS, Effect of projectile nose shape, impact velocity and target thickness on deformation behavior of aluminum plates. International Journal of Solids and Structures, 44 (2007) 3411-3439.

[54]. H. Yoshimura, T. Moriwaki, N. Ohmae, T. Nakai, T. Shibasaka, H. Kinoshita, M. Matsui and M. Shimizu, Study on near dry machining of aluminum alloys, JSME International Journal, Series C, Vol.49, 1, (2006) 83-89.

[55]. Christian J.S., Comments on the solubility of carbon in molten aluminum, Metallurgical

Transactions, A, Vol 20A (1989) 191.

[56]. T.C. Isabell, P.E. Fischione, C. Keefe, M.U. Guruz, and V.P. Dravid, Plasma Cleaning and Its Applications for Electron Microscopy, Microsc. Microanal. 5 (1999), 126–135.

[57]. S. Janbroers, T.R. de Kruijff, Q. Xu, P.J. Kooyman, H.W. Zandbergen, Preparation of carbon-free TEM microgrids by metal sputtering, Ultramicroscopy 109 (2009) 1105-1109.

[58]. B. Roop, Cleaning of aluminum after machining with coolants, Argonne National Laboratory LS-172

[59]. X. Xiao, L.C. Lev, M.J. Lukitsch, Material transfer during machining of aluminum alloys with polycrystalline diamond cutting tools, Journal of Materials Processing Technology,209, (2009),5760-5765.

[60]. D. Chicea, Comment on carbon production in deuterium-metal systems, Tenth International Conference on Cold Fusion, (2003), Cambridge, 475-481.

[61]. L. Reimer, Transmission Electron Microscopy, fourth edition (Berlin: Springer), (1999) 488-490.

[62]. M. Antognozzi, A. Sentimenti, U. Valdre, Microsc. Microanal. Microstruct. 8 (1997) 355.

[63]. C.J. Edgcombe and U. Valdre, Experimental and computational study of field emission characteristics from amorphous carbon single nanotips grown by carbon contamination, Philosophical Magazine B, Vol.82, No.9 (2002) 987-1007.

[64]. Chen W, Some experimental investigations in the drilling of carbon fiber-reinforced plastic (CFRP) composite laminates, Int. J. Mach. Tools Manufact. Vol. 37. No. 8 (1997) 1097-1108.

[65]. Kaw A, Mechanics of Composite Materials. Taylor & Francis Group, (CRC Press, Florida). (1997)

[66]. König W, Wulf C, Grass P, Willerscheid H, Machining of Fiber-reinforced plastics. Annals of the CIRP, 34 (1985) 537–548.

[67]. Hocheng H, Dharan CKH, Delamination during drilling in composite laminates. Transactions of ASME, Journal of Engineering for Industry, 112 (1990) 236–239.

[68]. Groover MP, Fundamental of Modern Manufacturing, John wiley & Sons, Inc, (1999) 102-104.

[69]. Koplev A, Lystrup A and Vorm T, The cutting process, chip, and cutting forces in machining CFRP. Composites 14, (1983), 371-376.

[70]. Arola D, Ramulu M, Wang DH, Chip formation in orthogonal trimming of graphite/epoxy composite. Composites A27 (1996), 121-133.

[71]. Sakuma K and Seto M, Tool wear in cutting glass-fiber reinforced plastics. Bulletin of JSME 26, (1983) 1420-1427.

[72]. Liu D., Zhang C.Y., Wang H.Y., Study of cutting temperature in drilling carbon fibre reinforced plastics (CFRP) , 4th International conference on intelligent information technology application, (2010) 5-8.

[73]. Rawat S, Attia H, Wear mechanisms and tool life management of WC-Co drills during dry high speed drilling of woven carbon fiber composites. Wear 267, (2009) 1022-1030.

[74]. Iliescu D, Gehin D, Gutierrez ME, Girot F, Modeling and tool wear in drilling of CFRP. International journal of machining tools & Manufacture, 50 (2010) 204-213.

[75]. Kim, D., and Ramulu, M., Drilling Process Optimization for Graphite/Bismaleimide-Titanium Alloy Stacks, Composite Structures 63 (2004) 101-114.

[76]. Murphy C, Byrne G and Gilchrist MD, The performance of coated tungsten carbide drills when machining carbon fibre-reinforced epoxy composite materials. Proc Instn Mech Engrs 216, (2002) 143-152.

[77]. Shyhaa, IS, Aspinwalla, DK, Sooa, SL, Bradleyb, S, Drill geometry and operating effects when cutting small diameter holes in CFRP, International Journal of Machine Tools and Manufacture, 49, (2009) 1008–1014.

[78]. Klamecki BE, A review of wood cutting tool wear literature. Holz als Roh-und Werkstoff, 37 (1979) 265-276.

[79]. Waldorf D.J., De Vor R.E., Kapoor S.G., A slip-line field for ploughing during orthogonal cutting, ASME Journal of Manufacturing Science and Engineering 120 (1998) 693-699

[80]. Waldorf D.J., Shearing, ploughing and wear in orthogonal machining, Ph.D. Thesis, University of Illinois at Urbana-Champaign, IL, 1996.

[81]. Kountanya R.K., Endres W.J., A high magnification experimental study of orthogonal cutting with edge-honed radius, in: Proceedings of ASME International Mechanics Engineering Congress and Exposition, IMECE2001/MED-23317, New York (2001), 1-8.

[82]. Yen Y.C., Jain A., Altan T., A finite element analysis of orthogonal machining using different tool edge geometries, Journal of Materials Processing Technology 146 (2004) 72-81.

[83]. Fang N., Slip line modeling of machining with a rounded-edge tool, Part I: New model and theory, Journal of Mechanics and Physics of Solids 51 (2003) 715-742.

[84]. Schmidt J., Mechanical and thermal effects in turn hardened steels, Dissertation of University Hannover (1999)

[85]. Kazuo N., Minoru A., Torahiko K., Machining characteristics of hard materials, *Annals of the CIRP* 37 (1988) 89-92.

[86]. Cook BA, Peters JS, Harringa JL, Russell AM, Enhanced wear resistance in AlMgB14-TiB2 composities. Wear, 271(2011) 640-646.

[87]. Cook BA, Harringa JL, Anderegg J, Russell AM, Qu J, Blau PJ, Higdon C, Elmoursi AA, Analysis of wear mechanisms in low-friction AlMgB14-TiB2 coatings. Surface & Coatings Technology 205 (2010) 2296-2301.

[88]. Cook BA, Harringa JL, Lewis TL, Russell AM, A new class of ultra-hard materials based on AlMgB14. Scripta mater. 42 (2000) 597-602.

[89]. Zhang W.H., Hsieh J.H., Tribological behavior of TiN and CrN coatings sliding against an epoxy molding compound, Surface & Coating Technology 130, (2000) 240-247.

[90]. Hsieh J.H, Tan A.L.K., Zeng X.T., Oxidation and wear behavior of Ti-based thin films, Surface & Coating Technology 201 (2006), 4094-4098.

[91]. Malhotra S.K., Some studies on drilling of fibrous composites, Journal of materials processing technology, vol. 24, December (1990) 291-300.

[92]. Rigney DA, Sliding wear on metals. Ann. Rev. Mater. Sci. 18 (1988) 141-163.

[93]. Seal M, The abrasion of diamond. Proc. R. Soc. Lond. A. 25 (1958) 379-393.

[94]. Seal M, The wear of diamond. Industrial Diamond Review, 25 (1965) 111-116.

[95]. Erdemir A, Halter M, Fenske GR, Zuiker C, Csencsits R, Krauss R, Gruen DM, Friction and wear mechanisms of smooth diamond films during sliding in air and dry nitrogen. Tribology transactions 40 (1997) 667-675.

[96]. Staia MH, D'Alessandria M, Quinto DT, Roudet F, Marsal AM, High-temperature tribological characterization of commercial TiAlN coatings. Institute of Physics Publishing, Journal of physics: condensed matter 18, (2006) 1727-1736.

[97]. Crompton D., Hirst M., Howse M.G.W., The wear of diamond, Proc. R. Soc. Lond. A. 333 (1973) 435-454.

[98]. Blanpain B., Celis J.P., Roos J.R., A comparative study of the fretting wear of hard carbon coatings, Thin solid films, 223 (1993) 65-71

[99]. Mehan R. L., Dry sliding wear of diamond materials, Wear, 78 (1982) 365-383.

[100]. www.garrtool.com

[101]. Deng J., Wu F., Lian Y., Xing Y., Li S., Erosion wear of CrN, TiN, CrAlN, and TiAlN PVD nitride coatings, Int. Journal of Refractory Metals and Hard Materials, 35 (2012) 10-16.

[102]. Mo J.L., Zhu M.H., Tribological oxidation behaviour of PVD hard coatings, Tribology International, Vol.42 (2009) 1758-1764.

[103]. Denis Dowling, Enhancing product performance through the application of nanocoatings, www.ucd.ie/surfaces, page 24.

[104]. Nouveau C., Djouadi M.A., Deces-Petit C., Beer P., Lambertin M., Influence of CrN coatings deposited by magnetron sputtering on tool service life in wood processing, Surface and Coatings Technology, 142-144 (2001) 94-101.

[105]. Xu J., Kato K., Formation of tribochemical layer of ceramics sliding in water and its role for low friction, Wear, 245 (2000) 61-75.

[106]. Luo Q., Hovsepian P. Eh., Transmission electron microscopy and energy dispersive X-ray spectroscopy on the worn surface of nano-structured TiAlN/VN multilayer coating, Thin Solid Films, 497 (2006) 203-209.

[107]. Wang Q., Zhou F., Wang X., Chen K., Wang M., Qian T., Li Y., Comparison of tribological properties of CrN, TiCN and TiAlN coatings sliding against SiC balls in water, Applied Surface Science, 257 (2011) 7813–7820.

[108]. Diamond coatings on cemented tungsten carbide tools by low-pressure microwave CVD, Wear 224 (1999) 245-266.